Investigating the biogeochemistry of the Mozambique Channel thermocline using an optimum multiparameter analysis approach

Eesaa Harris

Dissertation presented for the degree of Master of

Science in the Department of Oceanography

University of Cape Town

February 2022

Supervisors:
Dr. Sarah Fawcett
Tanya Marshall

Plagiarism Declaration

I know the meaning of plagiarism and declare that all of the work in the dissertation, save for that which is properly acknowledged, is my own.

Signed by candidate

……

Eesaa Harris

28 February 2022

Date

Abstract

The ocean's thermocline represents the transition zone between the surface and deep ocean. Its formation is linked to vertical and horizontal diffusion, and it constitutes part of the ocean's wind-driven circulation, playing a critical role in the lateral advection and vertical supply of nutrients. In the Indian Ocean, the topography, winds, and inter-ocean exchange make the basin's thermocline unique. Particularly complex thermocline circulation occurs in the Mozambique Channel, the highly dynamic region between the coast of southeastern Africa and Madagascar, owing to the confluence of tropical and subtropical regimes in the southwestern Indian Ocean. Our current understanding of the Mozambique Channel thermocline is largely derived from hydrographical analyses (i.e., conservative property relationships such as temperature-salinity), which do not resolve the influence of mesoscale features such eddies on the regional biogeochemistry. Additionally, the Mozambique Channel is one of the three source regions to the Agulhas Current, such that its biogeochemistry may influence the waters of this western boundary current. Here, the thermocline array approach within the *optimum multiparameter* (OMP) analysis framework was used to determine the contributions of different source waters to the thermocline across four transects sampled in the southwestern Indian Ocean, one at either end of the Mozambique Channel and two across the upper Agulhas Current. Three thermocline source regions proximate to the Mozambique Channel were identified (equatorial, tropical and subtropical) and used to initialise the OMP analysis. This localised approach was validated by the low standard deviations (average <20%) associated with perturbing the model parameters in a Monte Carlo analysis and the low residuals (average <5%) associated with the model solution, allowing for an evaluation of relative biogeochemical changes across the region. A decline in the upper thermocline nutrient concentrations between the source regions and the transects can be explained by mixing with nutrient-deplete surface waters. By contrast, an increase in the nutrient concentrations of the thermocline evinces *in situ* remineralization, presumably following primary productivity in Mozambique Channel surface waters. The presence of tropical waters across the two Agulhas transects confirms a supply of tropical nutrients to the current, with the coincidence of significant tropical water contributions (up to 60%) and mesoscale eddies suggesting that these features represent a mechanism by which tropical thermocline water is supplied to the Agulhas Current region. A rise in the thermocline nitrate-to-phosphate ratios across the Agulhas transects

but not in the Mozambique Channel transects indicates that nitrogen is added to the Agulhas Current region by local N_2 fixation occurring in the subtropical waters south of the Mozambique Channel (25°S). This finding contradicts recent suggestions that the channel itself is a hotspot for N_2 fixation. The fact that the OMP analysis applied at the regional scale captures the complexity and heterogeneity of the southwest Indian Ocean indicates that this approach can be used to quantitatively assess thermocline contributions to shallow nutrient cycling in hydrodynamically complex regions.

Acknowledgements

- Firstly, I would like to thank the Almighty Allah for all His blessings and favours He has bestowed upon me; to be able to attend this prestigious institution and to be able to pursue my passions and passions in this worldly life.
- This thesis would not have been possible without the guidance and support of my supervisor Dr Sarah E. Fawcett. Similarly, I would like to thank my co-supervisor and colleague Tanya Marshall for her contributions. Both were integral in the undertaking of this research project.
- I am immensely grateful to the National Research Foundation (NRF) and the University of Cape Town Postgraduate Funding Office (PGFO) for funding my Masters degree.
- To the UCT Department of Oceanography, I am grateful for the opportunities afforded to me throughout my undergraduate studies as well as my Honours year. To the lecturers and fellow students within the department, I am grateful for your friendship and willingness to support me throughout my studies.
- A big thank you to the Fawketieri research group and the UCT Marine Biogeochemistry Lab (both of UCT) for the support, both academically and socially, during a very challenging Masters period.
- Lastly, I would like to thank my parents, for allowing me to pursue my dreams whilst supporting me both materially and emotionally, and for raising me to become the person I am today.

Contents

1. Introduction

Physical oceanography and biogeochemistry are often treated as separate fields in the marine sciences, yet they are intrinsically linked. Of particular significance to both physical and biogeochemical oceanographers is the ocean's thermocline, the layer of strong temperature, density and nutrient gradients that occupies the waters beneath the seasonal mixed layer. Hydrographically, the thermocline forms the transition zone between the wind-driven upper ocean and the thermohaline-driven deep ocean, with elements of both systems influencing the thermocline circulation and its renewal. Thermocline ventilation generally occurs in the mid-to-high latitudes, where processes such as Ekman pumping and deep wintertime convection are responsible for the subduction of surface waters that ultimately form thermocline waters (Stommel, 1979; Williams *et al*., 1995). Following its subduction, the thermocline) constitutes the primary source of nutrients to the overlying surface waters and is simultaneously altered by the biogeochemical processes occurring in these surface waters as well as in the thermocline itself.

The Indian Ocean thermocline is unique as a consequence of the distinct monsoonal regimes, the northern latitudinal (i.e., continental) boundary at ~30ºN, and a strong tropical front linked to the inter-basin connection to the Pacific Ocean at the Indonesian Archipelago (You, 1997). This complexity has led to disagreement among numerous studies conducted in the mid-to-late 20th century as to the definition of Indian Ocean thermocline waters in terms of their physical properties and source regions (Sverdrup *et al*., 1942; Mamayev, 1975; Emery & Meincke, 1986; You & Tomczak, 1993). The Indian Ocean thermocline is influenced by overlapping biogeochemical processes such as enhanced surface productivity in response to the monsoonal system (McCreary *et al*., 1996), subtropical N_2 fixation (Harms *et al*., 2019), and anoxic conditions in the Arabian Sea water column that favour denitrification (Naqvi *et al*., 2006; Ward *et al*., 2009). The imprint(s) of these biogeochemical processes provides a means of identifying the Indian Ocean thermocline, as well as local modifications thereof.

The complexities with respect to thermocline circulation and dynamics in the Indian Ocean are further compounded in the Mozambique Channel and upper Agulhas Current to the southwest of the basin. Eddy features dominate the channel, and the flow is inconsistent and subject to interseasonal and interannual variability (Di Marco *et al*., 2002; Schouten *et al*., 2003; Ulgren *et*

al., 2012), while the Agulhas Current, also dominated by mesoscale features, transports tropical and subtropical waters with distinct properties alongside one another (Beal *et al*., 2006). Defining water masses by way of temperature-salinity relationships, in conjunction with non-conservative properties (e.g., oxygen, nutrient concentrations), has to-date been the principal approach for understanding the regional hydrography (Di Marco *et al*., 2002; Donohue & Toole, 2003; Beal *et al*., 2006; Swart *et al*., 2010). Furthermore, contemporary studies focussing on the biogeochemical characteristics of the Mozambique Channel and the Agulhas Current are lacking, with those that do exist concerned largely with phytoplankton community composition and/or size distribution (e.g., Kolasinski *et al*., 2012; Barlow *et al*., 2014, 2020; Lamont *et al*., 2018).

Regional thermocline hydrography and biogeochemistry can be understood via analysis of the contributing water masses. The respective distributions of these water masses can be related to known physical features (e.g., eddies, currents, and slope interactions), while biogeochemical processes can be inferred from relative changes in non-conservative properties. However, a qualitative diagnosis of the water masses contributing to the thermocline in a particular region may over-simplify their characteristics, leading to erroneous water mass descriptions. A quantitative solution exists in the form of *optimum multiparameter* (OMP) *analysis*, a type of linear regression analysis that computes the relative contributions of different water masses at a particular depth and location using their source-water properties. Pioneered by Tomczak & Large (1989), this method has been applied to various ocean regions, with objectives ranging from understanding the variability in thermocline circulation (e.g., You & Tomczak, 1993; You, 1997; Poole & Tomczak, 1999) to understanding ventilation regions and processes (e.g., Karstensen & Tomczak, 1997; Karstensen & Quadfasel, 2002). The subsequent incorporation of biogeochemistry into the OMP framework by Karstensen & Tomczak (1998) (termed *extended* OMP analyses) represented a major development, allowing for the inclusion of non-conservative properties as inputs (e.g., oxygen (O_2) and macronutrients such as nitrate (NO_3^-) and phosphate (PO_4^{3-})) and the subsequent diagnosis of biogeochemical changes along flow paths (Karstensen & Tomczak, 1998; Hupe & Karstensen, 2000).

The ability to quantitatively partition source waters in a particular region is a powerful tool for understanding changes in local hydrography and biogeochemistry. However, the *traditional* and *extended* OMP analyses applied to the thermocline have certain shortcomings, such as allowing

for diapycnal mixing. This assumption is likely valid for large-scale regions and features but does not hold for the near-surface layers that are characterised by strong stratification. Jenkins *et al*. (2015) modified the earlier isopycnal-based approaches (e.g., You & Tomczak, 1993; Karstensen & Tomczak, 1997) to account for this issue by discretizing the thermocline along fine density increments, which has been shown to work well when the source waters are located relatively near to the region of interest (Peters *et al*., 2018 (a), (b)). For example, Peters *et al*. (2018 (b)) demonstrated the utility of the *thermocline array* model by running the OMP analysis across a highly discretized thermocline and using the output to diagnose the relative importance of in situ remineralization versus local transport from adjacent coastal waters in supplying nitrate to the thermocline and intermediate waters of the central and eastern South Pacific.

The confluence of various hydrographic and biogeochemical regimes in the western Indian Ocean yields an environment that is both complex and multifaceted, and as such, requires innovative approaches to better understand the regional thermocline and the related biogeochemical features and processes. In this study, the OMP analysis was applied to the thermoclines of the Mozambique Channel and upper Agulhas Current in order to quantify and characterize the source waters to the southwestern Indian Ocean Specifically, the research questions addressed in this thesis include:

(a) What are the source regions to the Mozambique Channel and upper Agulhas Current?

(b) How are these sources distributed across the Mozambique Channel and upper Agulhas Current?

(c) How do physical features (e.g., eddies, currents) influence the source water distributions?

(d) What biogeochemical features and/or processes can be inferred from the OMP results?

This investigation begins in Chapter 2 with an overview of the hydrographical and biogeochemical features of the Indian Ocean, and more specifically the Mozambique Channel and upper Agulhas Current System, followed by a description of the OMP analysis approach. The methods are described in detail in Chapter 3, including setting up the OMP analysis and data acquisition, with the results presented in Chapter 4. Finally, in Chapter 5, the appropriateness of the OMP analysis for addressing the research objectives is discussed, along with the implications of the results in the context of general circulation, eddy features, and biogeochemical processes.

2. Literature Review

2.1. Western Indian Ocean upper ocean circulation

Of the world's five major oceans, the Indian Ocean is larger only than the Arctic, with a northern latitudinal extent of 30°N. The northern boundary is set by the Asian continent, although connections do exist to the marginal seas of the Red Sea and Persian Gulf. The southern boundary is marked by the Antarctic Circumpolar Current (ACC) at approximately 40-45°S. The eastern boundary exists as a low latitude inter-basin connection at the Indonesian Archipelago, with the waters transported from the Pacific to the Indian Ocean referred to as Indonesian Throughflow (ITF) (Talley *et al*., 2011) . Continuous flow towards the eastern Indian Ocean is the result of higher sea level pressure across the western Pacific (Wyrtki, 1971; You & Tomczak, 1993). The western boundary is set by the African continent, with the southern termination of the landmass at approximately 34°S allowing for the south-westward extension of the western boundary Agulhas Current toward the South Atlantic Ocean. The waters of Agulhas Current and the adjacent subtropical gyre 'leak' into the subtropical South Atlantic via rings and filaments (Schouten *et al*., 2000; Van Aken *et al*., 2003), thereby linking the Indian and Atlantic Ocean basins (De Ruijter *et al*., 1999).

At the basin-scale, upper ocean dynamics are dominated by the subtropical gyre in the South Indian Ocean and the monsoonal system in the North Indian Ocean, with a distinct separation between these regimes imposed by the broad, westward-flowing South Equatorial Current (SEC) at 10-20°S (Fig. 2.1 (a)) (Talley *et al*., 2011; Vianello *et al*., 2017). The seasonally reversing monsoons influence circulation north of the SEC, with the largest effects observed along the western boundary. During the Southwest monsoon (May-August), circulation in the western tropical North Indian Ocean (~0-20°N, 40-80°E) is predominantly eastwards, forming a seasonal wind-driven anticyclonic gyre (Fig. 2.2 (b)) (Talley *et al*., 2011). Furthermore, the south-westerly winds cause offshore Ekman transport and upwelling of cool surface waters along the Somali and Arabian coastlines. These upwelled waters are rich in nutrients and thus stimulate surface ocean productivity in the region (Currie *et al*., 1973; Schott, 1983; Talley *et al*., 2011). During the Northeast monsoon (November-March), a westward flow emerges in the western tropical North Indian Ocean, which is termed the Northwest Monsoon Current. At the same time, a complete

reversal of the Somali Current is observed, and the regional circulation becomes weaker and disorderly (Fig. 2.2 (a)) (Talley *et al*., 2011). The inter-monsoonal periods are characterised by a relaxation of the winds, with the fall period (August-September) associated with stratified conditions and the spring period with remnants of wintertime convective mixing (Banse, 1987; McCreary *et al*., 1996).

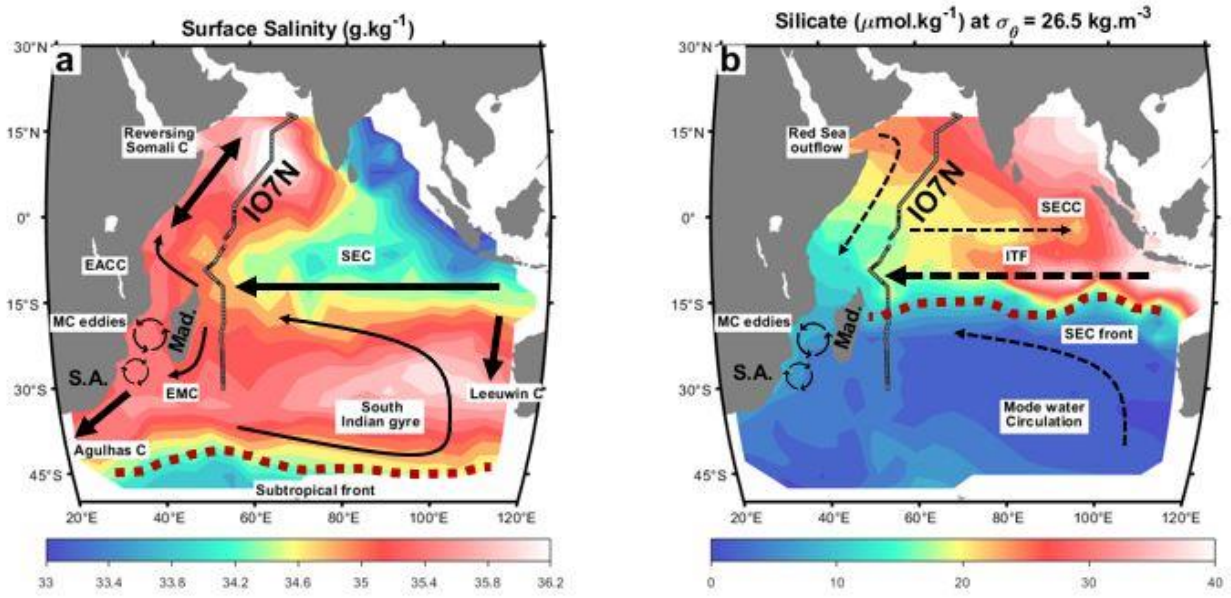

Figure 2.1 Map of (a) surface salinity (g.kg^{-1}) with major currents and surface circulation features indicated by solid black arrows and (b) silicate (μmol.kg^{-1}) at σ_θ = 26.5 kg.m^{-3}, with thermocline circulation features indicated by dashed black arrows. Major fronts are shown by the red dashed lines. The abbreviations are South Equatorial Current (SEC), East African Coastal Current (EACC), Mozambique Channel (MC), East Madagascar Current (EMC), Indonesian Throughflow (ITF) and South Equatorial Counter Current (SECC). The IO7N transect is labelled as a point of reference (see Methods). Data obtained from the *WOCE Indian Ocean* database.

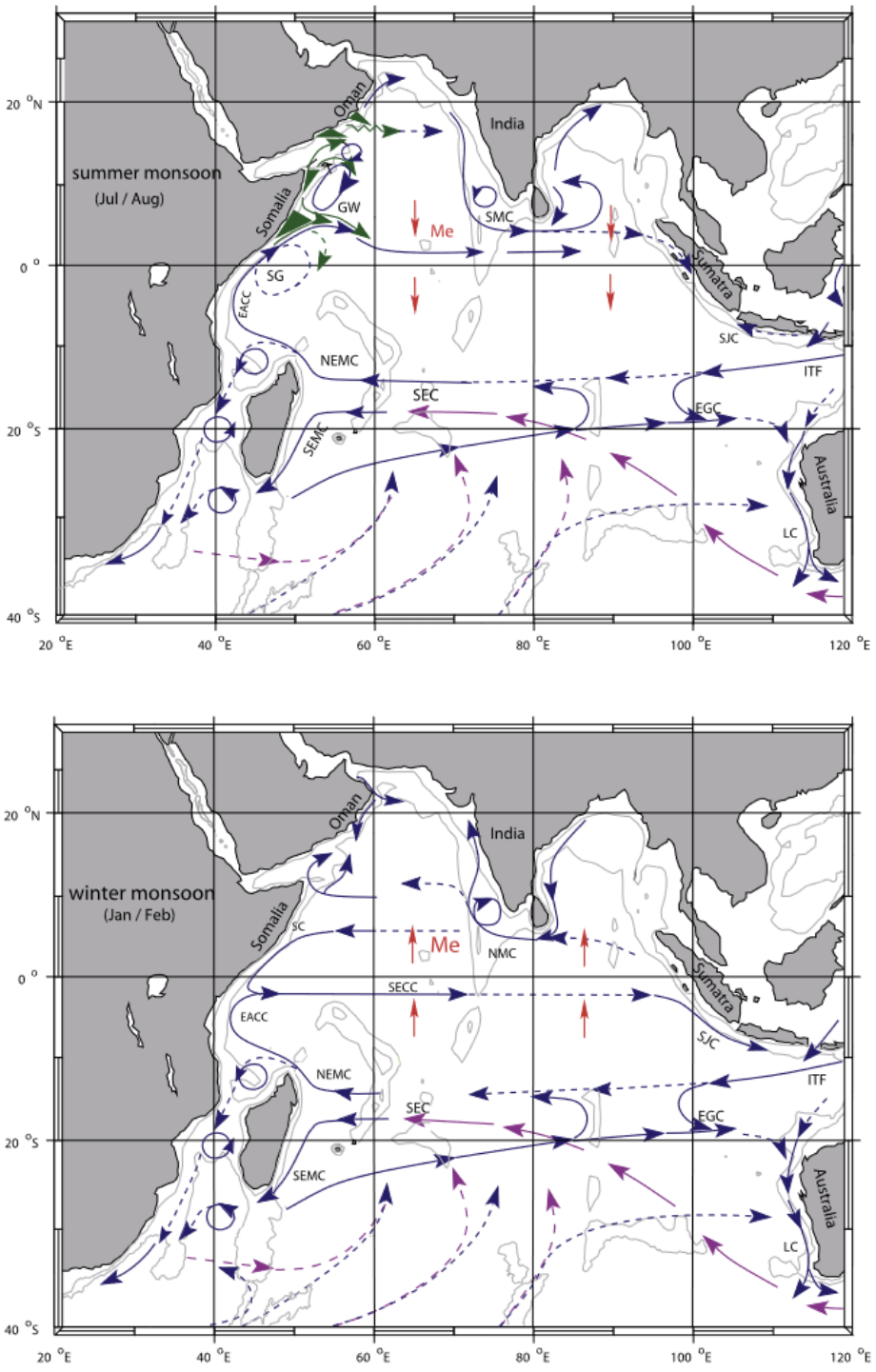

Figure 2.2 Schematic of the major surface currents within the Indian Ocean during the summer monsoon (top) and winter monsoon (bottom). The currents depicted are: South Equatorial Current (SEC), South Equatorial Countercurrent (SECC), Northeast and Southeast Madagascar Current (NEMC and SEMC), East African Coastal Current (EACC), Somali Current (SC), Southern Gyre (SG) and Great Whirl (GW), Southwest and Northeast Monsoon Currents (SMC and NMC, South Java Current (SJC), East Gyral Current (EGC), and Leeuwin Current (LC). The subsurface return flow of the gyre are shown in magenta. [source: Schott *et al.*, 2019]

The subtropical gyre system of the South Indian Ocean includes the westward flow of the SEC at the northern boundary, the southward flow of the East Madagascar Current (EMC) and Agulhas Current at the western boundary, the eastward flow of the South Indian Current at the southern boundary and both the southward flow of the Leeuwin Current and north-westward flow of the Flinders Current at the eastern boundary. The negative wind stress curl drives the anticyclonic gyre circulation. These ocean-atmosphere dynamics lead to Ekman pumping and thus a downwelling regime, which depresses the isopycnals and related nutriclines, resulting in oligotrophic conditions across the southern Indian Ocean (Grundlingh *et al*., 1991; Williams & Follows, 1998; Donohue & Toole, 2003). The meeting of warm, nutrient-rich waters from the northern basin with relatively cool, nutrient-poor waters from the southern basin at the SEC (10-15°S) creates an intense meridional gradient, the strongest biogeochemical gradient in the global ocean (Talley *et al*., 2011). Cross-equatorial transport is thus limited, with the western boundary being the dominant region of (primarily northwards) exchange (You & Tomczak, 1993; Talley *et al*., 2011).

2.2. Western Indian Ocean water masses

2.2.1. Surface waters

The surface waters (σ_θ <24.5 kg.m^{-3}) of the northern and equatorial Indian Ocean are some of the warmest in the world, a consequence of the westward extension of the Pacific warm pool, the lack of an eastern cold tongue due to ephemeral trade winds, and typically cloud-free atmospheric conditions allowing for greater net heating during the northern hemisphere summer (Loschigg & Webster, 2000; Talley *et al*., 2011). While there has historically been much debate as to how these warm surface waters between 10°S and 10°N should be classified (e.g., Sverdrup, 1942; Mamayev, 1975; Emery & Meincke, 1986), they can be broadly defined as *Equatorial Surface Water* (ESW). Within the northwestern Indian Ocean, ESW has a relatively small salinity range of 35.1-35.3 g.kg^{-1} (Fig. 2.3 (b)) (Talley *et al*., 2011).

Low surface salinities (~34.7 g.kg^{-1}) characteristic of *Tropical Surface Water* (TSW) are observed between 10°S and 20°S within the westward flowing SEC, a consequence of high precipitation along the Intertropical Convergence Zone and the contribution of fresh ITF water (Fig. 2.3 (b)) (Talley *et al*., 2011). Finally, the salinity maximum of >35.5 g.kg^{-1} observed within the South Indian subtropical gyre, a consequence of net evaporation in the region, is indicative of *Subtropical Surface Water* (STSW; not displayed on Fig. 2.3 (b)).

2.2.2. Upper thermocline waters

The immediate subsurface layers (i.e., the upper thermocline) are connected to the surface by both physical and biogeochemical processes. A subsurface salinity maximum at σ_θ = ~25.5 kg.m^{-3} (with σ_θ used to denote potential density) is observed north of the SEC front and termed *Persian Gulf Water* (PGW) by Talley *et al*. (2011). These waters are associated with a relative oxygen minimum of <120 µmol.kg^{-1} (Fig. 2.3 (c)), which results from organic matter respiration following elevated productivity associated with the monsoon-induced upwelling off the East African and Arabian coastlines (Olson *et al*., 1993).

Within the southern Indian Ocean, *Subtropical Underwater* (STUW) at σ_θ = ~26.0 kg.m^{-3} is associated with the subduction processes occurring in the subtropical gyre. With its subsurface

salinity and oxygen maxima (~35.7 g.kg^{-1} and ~180 µmol.kg^{-1}, respectively; Fig. 2.3 (b-c)), STUW is restricted to the area north of the surface salinity maximum at ~25°S (Donohue & Toole, 2003; Talley *et al*., 2011).

2.2.3. Permanent thermocline waters

The permanent thermocline is generally defined as the shallowest subsurface layer not under the influence of seasonal variability due to a lack of direct connection to the surface ocean (Woods, 1985; You, 1997). Mechanisms that initially ventilate the permanent thermocline include Ekman pumping, which occurs in the subtropical gyres, and wintertime deep convection at the higher latitudes. Early work undertaken by Sverdrup *et al*. (1942) identified three water masses within the Indian Ocean permanent thermocline. These include *Red Sea Water* (RSW; which is discussed as an intermediate water mass in section 2.2.4), originating in the evaporation-dominated Red Sea basin, *Indian Central Water* (ICW) formed by subduction in the southern Indian Ocean, and *Indian Equatorial Water* (IEW). Subsequent authors (e.g., You & Tomczak, 1993) have argued that IEW is actually a mixture of water masses originating in the northern and southern Indian as well as the Pacific Oceans. In any case, the water masses ventilating the permanent thermocline of the western Indian Ocean form south of 20°S (You & Tomczak, 1993). Associated with subduction processes occurring within the subtropical gyre, the linear T-S relationship of *Indian Central Water* (ICW) dominates the southern Indian Ocean pycnocline, encompassing a large range in salinity of between 34.5 and 35.7 g.kg^{-1} (Fig. 2.3 (b)).

Mode waters are layers of vertically homogeneous (in terms of temperature and salinity) water formed as a result of deep winter mixing (Hanawa & Talley, 2001). They appear as pycnostads in the thermocline and can be found well outside their formation regions. The mode waters of the Indian Ocean are indistinguishable from ICW in terms of salinity but can be identified by their high oxygen concentration (>225 µmol.kg^{-1}) and low potential vorticity (<50×10^{-14} cm^{-1}.s^{-1}) (McCarthy & Talley, 1999; Talley *et al*., 2011). *Subtropical Mode Water* (STMW) forms north of the Agulhas Return Current at σ_θ = ~26 kg.m^{-3}, while *Subantarctic Mode Water* (SAMW) is more pervasive and forms along the Subantarctic Front (50-60°S) within a density range of σ_θ = 26.5-26.8 kg.m^{-3} (McCarthy & Talley, 1999; Hanawa & Talley, 2001). A derivative of this water mass is *Southeast Indian Subantarctic Mode Water* (SEISAMW), which forms from the deep mixed

layers that characterize the southeast sector of the Indian Ocean at densities of σ_θ = 26.8-26.9 kg.m^{-3} (Hanawa & Talley, 2001). These high-oxygen mode waters extend equatorwards to the SEC front, with a slightly elevated oxygen signal still apparent along the East African boundary to the Arabian Sea (Talley *et al*., 2011).

2.2.4. Intermediate and deep waters

Antarctic Intermediate Water (AAIW) is the dominant intermediate water mass in the southern Indian Ocean. It is characterized by a salinity minimum (core value of ~34.5 g.kg^{-1}) within the 27.0-27.3 kg.m^{-3} potential density range that lies at approximately ~1000 m in the southern Indian Ocean and shoals to ~600 m along the SEC frontal region (Talley *et al*., 2011). AAIW is observed along the equator and western Arabian Sea as a weakened salinity minimum that is transported along the western boundary in the northward-flowing East African Coastal Current (EACC) and Somali Current (Talley *et al*., 2011). Within the SEC frontal region, an additional intermediate water mass also characterized by a (relative) salinity minimum (core value of ~34.8 g.kg^{-1}) is transported westwards. Termed *Indonesian Intermediate Water* (IIW), this water mass occurs at similar depths and densities to AAIW (27.0-27.7 kg.m^{-3}) but is distinguishable therefrom by higher nutrient concentrations that accumulate during water mass aging (Wyrtki, 1971; You & Tomczak, 1993, Talley *et al*., 2011).

High salinity *Red Sea Water* (RSW) leaves the Red Sea at Bab el Mandeb with a salinity of 40 g.kg^{-1} and enters the Gulf of Aden at a density of 27.6 kg.m^{-3} (Talley *et al*., 2011), becoming diluted as it spreads into the Arabian Sea and southwards along the western Indian Ocean boundary (Beal *et al*., 2000). The RSW core situated at 27.2-27.4 kg.m^{-3} (similar to fresh AAIW) is transported through the Mozambique Channel (Roman & Lutjeharms, 2009) and subsequently incorporated into the Agulhas Current (Di Marco *et al*., 2002; Donohue & Toole, 2003; Roman & Lutjeharms, 2007).

There are no surface regions of deep water formation in the Indian Ocean. Therefore, deep waters either originate in the Atlantic and Southern Oceans or are formed at depth. *North Atlantic Deep Water* (NADW), which forms in the Subarctic North Atlantic, enters the Indian basin along the western boundary. (Van Aken *et al*., 2003) while *Circumpolar Deep Water* (CDW), which outcrops in the Southern Ocean, enters the Indian basin along the ACC front (Van Aken *et al*.,

2003; Talley *et al*., 2011). *Indian Deep Water* (IDW) is formed in the Indian Ocean at depth from diffusion and deep upwelling of southerly-sourced bottom waters and as such, is characterized by low oxygen and high nutrient concentrations, which reflect its older age (Talley *et al*., 2011).

Table 2.1 Summary of the western Indian Ocean water masses

Water mass	Abbreviation	Density
	Surface	
Tropical Surface Water	TSW	Surface – 24.5 kg.m^{-3}
Subtropical Surface Water	STSW	Surface – 24.5 kg.m^{-3}
Equatorial Surface Water	ESW	Surface – 24.5 kg.m^{-3}
	Upper thermocline	
Subtropical Underwater	STUW	~26 kg.m^{-3}
Persian Gulf Water	PGW	~26 kg.m^{-3}
	Permanent thermocline	
Indian Central Water	ICW	26-27 kg.m^{-3}
Indian Equatorial Water	IEW	26-27 kg.m^{-3}
Subantarctic Mode Water	SAMW	26.5-26.9 kg.m^{-3}
	Intermediate and deep	
Red Sea Water	RSW	27 -27.7 kg.m^{-3}
Antarctic Intermediate Water	AAIW	27 -27.7 kg.m^{-3}
Indian Deep Water	IDW	27.7 -27.9 kg.m^{-3}
Circumpolar Deep Water	CDW	27.7 -27.9 kg.m^{-3}

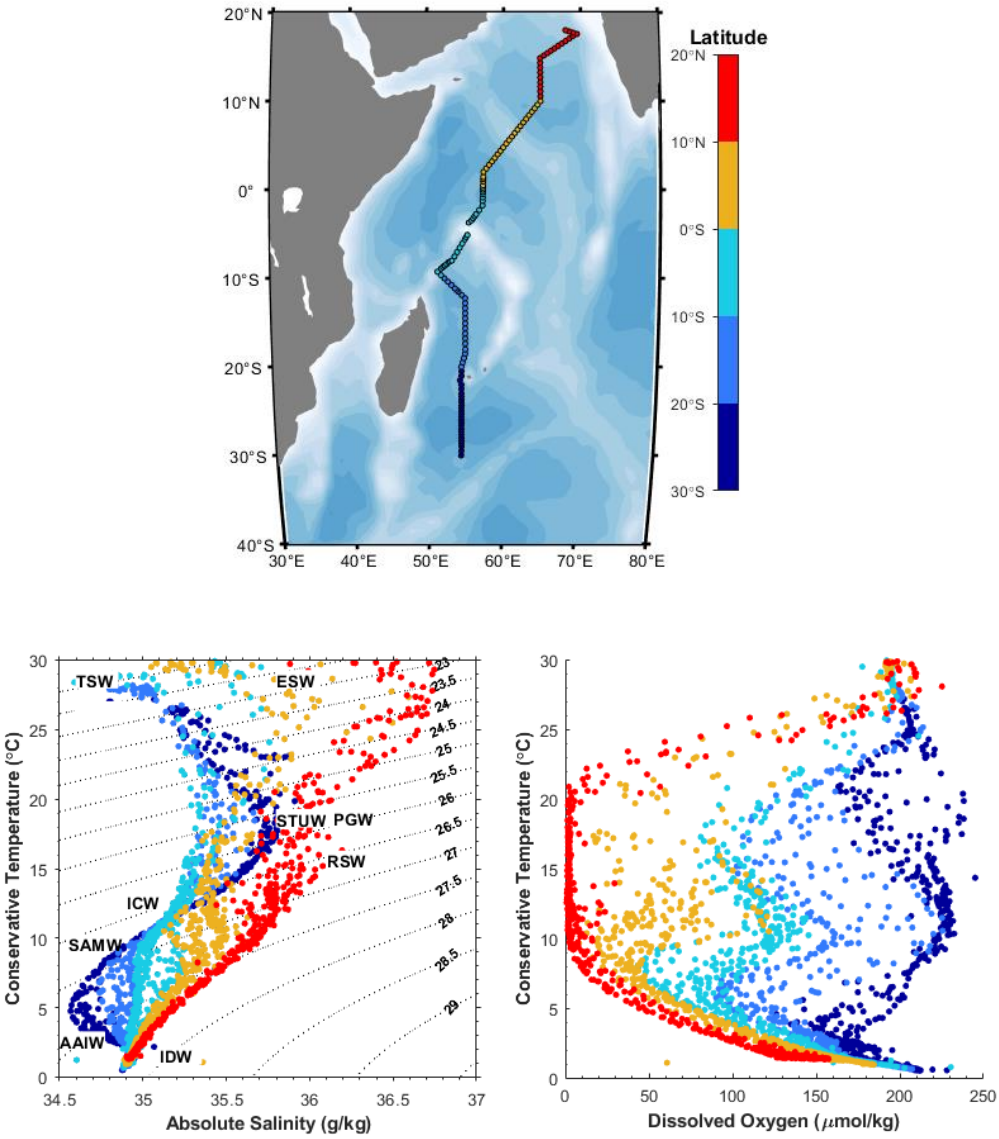

Figure 2.3 WOCE IO7 (a) station locations, (b) potential temperature (°C) versus salinity (g.kg^{-1}) and (c) potential temperature (°C) versus oxygen (μmol.kg^{-1}) across the western Indian Ocean along 60°E. Water masses labelled are: *Tropical Surface Water* (TSW), *Equatorial Surface Water* (ESW), *Persian Gulf Water* (PGW), *Subtropical Underwater* (STUW), *Red Sea Water* (RSW), *Indian Central Water* (ICW), *Subantarctic Mode Water* (SAMW), *Antarctic Intermediate Water* (AAIW), and *Indian Deep Water* (IDW).

2.3. The Mozambique Channel – an overview

The Mozambique Channel lies between the continent of Africa and the island of Madagascar. Its meridional extent is 12°S to 26°S while its zonal extent is approximately 35°E to 45°E. The channel is bordered by shallow continental shelves at both margins and has a cross-channel width ranging from 430 km to 1000 km (Swart *et al*., 2010). The SEC bifurcates upon reaching the

eastern Madagascar landmass at approximately 15°S and 50°E and forms the southward-flowing East Madagascar Current (EMC) and northward-flowing Northeast Madagascar Current (NEMC) (Fig. 2.4) (Swallow *et al*., 1988; Di Marco *et al*., 2001). The NEMC rounds Cape Amber (the northernmost point of Madagascar) and further partitions into a northward and southward component, the former culminating in the EACC, which feeds into the western boundary Somali Current, and the latter entering the northern Mozambique Channel (Di Marco *et al*., 2002; de Ruijter *et al*., 2002).

Numerous studies have noted the discontinuous and variable nature of the net southward flow in the Mozambique Channel (Harris, 1972; Grundlingh, 1985; Di Marco *et al*., 2002) and have proposed the poleward propagation of eddies as an explanation for this observation. de Ruijter *et al*. (2002) conclusively demonstrated the non-existence of a southward-flowing Mozambique Current along the western coast of the channel and highlighted the role of mesoscale eddies in heat and salinity transport. These mesoscale eddies are approximately 300 km in diameter, penetrate the full depth of the water column, and are predominantly anticyclonic with intensification at the surface (Ridderinkhof *et al*., 2001; de Ruijter *et al*., 2002; Swart *et al*., 2010). While no true western boundary current exists in the channel, Swart *et al*. (2010) observed net poleward eddy propagation along the western boundary (which may have been misidentified by Di Marco *et al*. (2002) as a fully formed current) and net equatorial eddy propagation in the centre of the channel. Furthermore, a northward-flowing undercurrent along the western boundary, termed the Mozambique Undercurrent (MUC), was first noted by de Ruijter *et al*. (2002) and further explained by Ullgren *et al*. (2012), and exists as two equatorward-flowing cores below the thermocline.

Net meridional transport estimates for the Mozambique Channel are uncertain, with the various methods applied to-date generally thought to over- or underestimate the volume transport (e.g. Di Marco *et al*., 2002; De Ruijter *et al*., 2002; Donohue & Toole, 2003). The channel is one of three source regions to the Agulhas Current, the others being the EMC and recirculation from the south Indian subgyre embedded within the subtropical gyre (Donohue & Toole, 2003; Nauw *et al*., 2008; Stramma & Lutjeharms 1997). The Agulhas Current is the strongest western boundary current in the southern hemisphere, with an average transport of 70 Sv (1 Sv = 1 000 000 $m^3.s^{-1}$), and ultimately links the Indian Ocean to the Atlantic Ocean (Bryden & Beal, 2001). Therefore,

determining the net meridional transport through the channel and its contribution to the Agulhas Current is central to understanding the regional dynamics more broadly.

2.4. Ocean productivity

2.4.1. The role of phytoplankton

Phytoplankton, single-celled photoautotrophic organisms, are largely responsible for ocean productivity and form the foundation of marine food webs (Field *et al*., 1998; Falkowski *et al*., 1998). Light requirements limit the vertical distribution of phytoplankton, confining them to the sunlit euphotic zones of the world's oceans, while nutrient requirements limit their spatial distributions. By converting inorganic carbon to its organic forms via photosynthesis, phytoplankton provide *organic matter* (OM) to heterotrophs, respiring single- or multicellular organisms including zooplankton, nekton and benthic communities. The OM available to heterotrophs is termed *net primary production* (NPP) and is equivalent to the difference between the total rate of organic carbon production (*gross primary production;* GPP) and the rate of autotrophic respiration. NPP describes the energy available for higher trophic levels within the marine ecosystem and is thus a measure of foundational productivity.

The mechanism of OM formation by phytoplankton and its subsequent export out of surface waters is termed the *biological carbon pump*, which is responsible for the sequestration of atmospheric CO_2 in the deep ocean (Volk & Hoffert, 1985). However, only a small fraction of the OM produced in surface waters is ultimately exported, with most (>85-90% on average) remineralized (i.e., decomposed by heterotrophic bacteria, resulting in the production of CO_2 and inorganic nutrients) within the euphotic zone (Eppley & Peterson, 1979). *Net ecosystem productio*n (NEP) refers to the OM that is exported out of the euphotic zone, equal to GPP minus total respiration by both auto- and heterotrophs (Sigman & Hain, 2012). NEP provides a measure of the amount of atmospheric CO_2 that is sequestered by a particular ocean ecosystem and thus, of the strength of the biological carbon pump.

2.4.2. Biomass and nutrient stoichiometry

Since phytoplankton play a key role in ocean productivity and the biological pump, their nutritional

demands are pivotal in controlling carbon cycling within and between the ocean and atmosphere. The molar ratio of carbon to nitrogen to phosphorus (C:N:P) of 106:16:1, known as the *Redfield ratio*, describes not only the elemental ratio of phytoplankton biomass but also the average concentrations in which phytoplankton use CO_2 and dissolved nutrients (predominantly nitrate and phosphate) (Redfield *et al*., 1963). In addition, NO_3^- and PO_4^{3-} exist in the deep ocean in an approximate molar ratio of 16:1. There is some debate as to whether phytoplankton set the *in situ* nutrient ratios through the remineralization of their biomass or whether phytoplankton nutrient requirements have evolved to match the ambient nutrient ratios in seawater (Redfield *et al*., 1963; Falkowski, 1987; Gruber, 2004; Mahaffey, 2005). Regardless, a link exists between C, N and P, as well as *consumed oxygen* (-[O_2]), with variations in their uptake ratios having the potential to alter ocean productivity and thus influence the carbon cycle (Falkowski, 1997).

The Redfield ratio describes the average stoichiometry of C, N, P, and O_2 consumption and production in the ocean. However, various factors and processes can influence the stoichiometry associated with phytoplankton uptake and remineralization ratios on regional or local scales (Bonachela *et al*., 2013). For instance, DeVries & Deutsch (2014) investigated the global variability in the stoichiometry of respired OM using an ocean circulation model and found a correlation with latitude. For the subtropical gyres in all ocean basins, the ratios of -O_2:P were relatively high (~ -200:1, compared to the global mean of 150:1), which the authors attributed to high light levels and low nutrient concentrations, while in the equatorial regions, -O_2:P was similar to the global mean. Weber & Deutsch (2010) used a similar model to investigate the diversity of phytoplankton N:P requirements, which varied significantly with region and which they concluded can be explained by (1) regional abundances of different phytoplankton groups (and their respective export ratios) and (2) circulation averaging, where ratios greater and less than Redfield are mixed via ocean circulation.

Over sufficiently large spatio-temporal scales, OM remineralization typically adheres to the Redfield ratio (Redfield *et al*., 1963; Anderson & Sarmiento, 1994). Deviations from this average ratio are thus indicative of elemental fractionation by local or regional processes that are not constrained by the same molar ratios (Brea *et al*., 2004). For example, N_2 fixation and denitrification supply and remove N in excess of the expected stoichiometric quantity of P, causing measurable deviations in regional nutrient ratios (Gruber & Sarmiento, 1997; Deutsch *et al*., 2007).

As such, nutrient stoichiometry can be used as a tracer for N loss and gain in a system (Gruber & Sarmiento, 1997; Deutsch et al. 2007; Hansell *et al*., 2007; Flohr *et al*., 2014).

2.5. The marine nitrogen cycle

Biologically available ("fixed") N is the major limiting nutrient across the (sub)tropical ocean (Broeker *et al*., 1982). The N cycle can be divided into two categories; the first, input processes that supply fixed N to the system (N_2 fixation, atmospheric deposition, rivers) and output processes that result in its removal (denitrification and anammox). The second, recycling processes such as assimilation, remineralization, and nitrification, which involve the conversion of fixed N into its various organic and inorganic forms. The marine N cycle is thus complex, as sources, sinks, and recycling involve both biotic and abiotic processes occurring across the air-sea interface and throughout the water column.

2.5.1. Major N input: N_2 fixation

The addition of N to oceanic systems can occur via atmospheric deposition, terrestrial inputs from rivers (Cotrim da Cunha *et al*., 2007), and biologically-mediated *N_2 fixation*. The dominant process supplying fixed N to marine waters is N_2 fixation, which involves the conversion of inert atmospheric *dinitrogen gas* (N_2) to bioavailable *ammonium* (NH_4^+). Specialized plankton (most of them photoautotrophic), termed diazotrophs (*Trichodesmium* spp. being the most commonly observed), possess the nitrogenase enzyme that is capable of breaking the strong triple bond in N_2 and thus fixing N (Capone *et al*., 1997; Deutsch *et al*., 2001). These microorganisms typically inhabit the warm, well-lit, low-nutrient surface waters of the tropical and subtropical oceans and are at times observed as dense near-surface blooms (Carpenter & Capone, 1992). The controls on N_2 fixation are still debated, with the availability of *iron* (Fe) and/or P in excess of N surmised to control the rate and distribution of N_2 fixation (Deutsch *et al*., 2007; Moore *et al*., 2009; Weber & Deutsch, 2014). This process is thought to have a stronger effect on carbon sequestration than the upwelling of "new" nitrate as CO_2 is upwelled simultaneously with the latter (Winn e*t al*., 1995).

The rate and distribution of N_2 fixation in the Indian Ocean is very poorly constrained. The oligotrophic setting and occurrence of excess phosphate across the surface, as well as the low N:P waters deriving from the Arabian Sea, have been suggested to promote N_2 fixation in the South

Indian subtropical gyre (Gruber & Sarmiento, 1997; Harms *et al*., 2019; Grand *et al*., 2015). However, modelling efforts and direct analyses of N_2 fixation in this region are limited by sample coverage, which results in a high level of uncertainty (Landolfi *et al*., 2018). A recent observational study by Karlusich *et al*. (2021) suggests that the Mozambique Channel is a "hotspot" for diazotrophs, with these plankton constituting up to 40% of the phytoplankton community in the larger (20-2000 µm) size-fractionated samples. The implication is that N_2 fixation is a key biogeochemical process occurring within the channel, although direct measurements are required to confirm this.

2.5.2. Major N loss: denitrification

The dominant sink for fixed marine N is the biologically-mediated process of *denitrification*, a metabolic process that replaces aerobic respiration under anoxic conditions. During denitrification, nitrate is reduced to N_2 gas via a series of intermediates (i.e., *nitrite* (NO_2^-), nitric oxide, and nitrous oxide). Specialized heterotrophic bacteria are the primary denitrifying organisms. They are facultative anaerobes that use nitrate as an electron acceptor when O_2 is no longer available. Denitrification therefore occurs in anoxic sediments where diffusion of O_2 from the overlying oxygenated water column is limited, and in the water column where O_2 concentrations are low (<10 µM; Codispoti *et al*., 2005) due to high rates of subsurface OM respiration following elevated productivity in the surface, combined with sluggish circulation (Deutsch *et al*., 2001). Global estimates suggest that sedimentary rather than water-column denitrification is the dominant N loss process in the global ocean (Devol, 1991; Devol, 2008; Eugster & Gruber, 2012).

A secondary route of fixed N loss is anaerobic ammonium oxidation or *anammox* (Mulder *et al*., 1995), which similarly occurs in anoxic environments. In contrast to denitrification, the electron acceptor for anammox is nitrite (as opposed to nitrate), while the bacteria themselves are autotrophic and thus fix CO_2. Nonetheless, the net effect of anammox is as per denitrification, the conversion of fixed N to biologically unavailable N_2 gas.

The Arabian Sea is one of three major water column denitrification zones in the global ocean. Here, N loss occurs within the thermocline/intermediate depth range (100-1000 m) where an intense perennial *oxygen deficient zone* (ODZ) ([O_2] of <5 µmol.kg^{-1}) has been established. The ODZ is a result of elevated primary productivity, driven by monsoon-induced upwelling, and

subsequent remineralization of sinking OM off the Somali and Arabian coastlines (Brock & McClain, 1992; Bauer *et* al., 1991; McCreary *et al*., 1996). Additionally, subsurface waters transported from the semi-enclosed northern Indian Ocean basin hinder advection, which also drives low-oxygen concentrations (Naqvi, 1987; Mantoura *et al*., 1993). Devol *et al*. (2006) estimated N loss in the Arabian Sea to be 41±18 Tg $N.a^{-1}$ from isotopic incubation experiments, which is within the range of other estimates (10-44 Tg $N.a^{-1}$; Naqvi, 1987; Mantoura *et al*., 1993; Codisposti *et al*., 2001), while global estimates range from 60-250 Tg $N.a^{-1}$ (Middelburg *et al*., 1996; Gruber and Sarmiento, 1997). Devol *et al*. (2006) further suggested that denitrification in the region is typically underestimated due to inaccurate stoichiometric assumptions and a failure to account for other N gain and loss processes, highlighting the intricacies associated with understanding denitrification in the region.

2.5.3. Internal cycling of N

Internal N cycling in the marine environment can be broadly divided into three main processes: (1) *nitrogen assimilation*, where inorganic (e.g. ammonium and nitrate) and organic (e.g. urea) N species are incorporated into the OM of phytoplankton, (2) the *remineralization* of that OM back to ammonium by heterotrophic microbes (Gilbert *et al*., 2016), and (3) *nitrification*, the oxidation of ammonium in the presence of O_2 to nitrate by chemoautotrophic microbes (Ferguson *et al*., 2007).

The gradients in nitrate observed in the world's oceans are thus influenced physically by circulation and biogeochemically through internal cycling (Sarmiento & Gruber, 2006). Furthermore, the consistent nature of surface assimilation and subsurface remineralization is implied by the similarity in the average N:P of phytoplankton biomass and the spatial variability in nitrate and phosphate (Takahashi *et* al., 1985; Anderson & Sarmiento, 1994). Thus, in theory, internal cycling processes do not affect the general stoichiometry of nitrate and phosphate.

2.5.4. Tracers of N sources and sinks

Quasi-conservative tracers are useful tools for identifying biogeochemical processes that do not adhere to the classic Redfield ratio and have the additional benefit of illustrating the spatial distribution of these processes (Gruber & Sarmiento, 1997). The tracers N* and P* relate nitrate

and phosphate to their average assimilation/remineralization ratio, r_n (= 16:1), where the equations:

$$N^* = [NO_3^-] - r_n[PO_4^{3-}] + 2.90\ \mu mol.kg^{-1} \quad (2.1a)$$

$$P^* = [PO_4^{3-}] - [NO_3^-]/r_n g \quad (2.1b)$$

describe this relationship, accounting in the case of N* for the global P excess (i.e., the constant, 2.90 μmol.kg^{-1}, which equates to a P excess of ~0.18 μmol.kg^{-1}). Initially utilised by Gruber & Sarmiento (1997) after the idea of Broecker & Peng (1982), N* identifies both N gains (rise in N*) and losses (decline in N*) by removing the effect of non-diazotrophic nutrient assimilation and OM remineralization. Similarly, P* can be used to identify occurrences of P in excess of N and is thus an additional method by which to identify the potential for (i.e., elevated P*) or incidences of (i.e., a decline in P*) N_2 fixation (Deutsch *et al*., 2007).

Gruber & Sarmiento (1997) applied the concept of N* to identify regions of N_2 fixation and denitrification across the global ocean. Their results showed large nitrate deficits (negative N*) occurring within the Arabian Sea ODZ, with this signature being transported outside of the region by advective and diffusive processes. Furthermore, they found positive N* concentrations in the shallows of the tropical and subtropical western Indian Ocean and suggested that these evince the addition of newly fixed N. A later study involving analyses of N isotope ratios came to the same conclusion (Harms *et al*. 2019).

2.6. Indian Ocean biogeochemistry

2.6.1. Southwest Indian Ocean

The downwelling nature of anticyclonic subtropical gyres typically inhibits nutrient supply mechanisms such as Ekman upwelling and eddy-induced mixing, which results in surface low nutrient concentrations and phytoplankton biomass. McClain *et al*. (2004) investigated the biogeochemical variability of subtropical gyres globally and found that the Indian Ocean is unique in that *chlorophyll* concentrations increase with downwelling intensification. The authors linked

this unexpected finding to lateral nutrient supply associated with the seasonal northward migration of the Subtropical Front. Furthermore, the aforementioned study by Harms *et al*., (2019) used measurements of nutrient concentrations and nitrate isotope ratios to suggest that nutrients from the Arabian Sea and Southern Ocean could contribute significantly to the nutrient supply to the Indian subtropical gyre system.

Another unique biogeochemical feature of the southwestern Indian Ocean is the strong hydrographic front that exists within the SEC (10-15°S). The westerly flow of the tropical ITF sets up a strong meridional gradient in both the physical and biogeochemical properties of the region, with a vertical extent that reaches the depth and density levels of the intermediate water masses (>1000m; >27 $kg.m^{-3}$) (Talley *et al*., 2011). North of the front, surface salinities are fresh (<34.8 $g.kg^{-1}$) and the thermocline nutrient concentrations are elevated, with a pronounced rise in silicate (from 0 to ~20 $\mu mol.kg^{-1}$) (Talley *et al*., 2011).

The biogeochemical setting of the Mozambique Channel is complex, as the circulation introduces waters from the tropics and subtropics into the region. Previous studies have noted the generally oligotrophic nature of the region and described the thermocline as subtropical (i.e., deep mixed layers and low surface nutrients, e.g. Di Marco *et al*., 2002; Donohue & Toole, 2003; Swart *et al*., 2010). However, the biogeochemical influence of the tropical SEC that enters the northern end of the channel has not been described in detail, which may add additional complexity (e.g., elevated lateral nutrient supply) to the thermocline.

2.6.2. Physical forcings on Mozambique Channel biogeochemistry

Eddy dynamics can have important and complex implications for ocean biogeochemistry and productivity, particularly when the eddies interact with continental margins. It is generally accepted that there are at least two mechanisms by which eddies may enhance productivity in nutrient-poor environments: (1) “eddy pumping” of nutrient-rich deep water into well-lit surface waters (McGillicuddy *et al*., 1998) and (2) the mainly lateral entrainment of highly productive coastal waters into the nutrient-deplete offshore environment (Batten & Crawford, 2005).

In the Mozambique Channel, southward-propagating anticyclonic eddies along the western

coastline have been reported to have low chlorophyll concentrations at their centres, and surface chlorophyll filaments have been observed to extend from the coast towards the eddy edges; these findings were first reported by Quartly & Srokosz (2004) from satellite ocean colour data. A similar study by Tew-Kai & Marsac (2009) found strong seasonality in the northern and southern sections of the channel, with late winter (August-September) characterized by the highest concentrations of chlorophyll. Both these studies suggest the entrainment of coastal waters into the offshore regions of the channel. A similar conclusion was drawn by Kolasinki *et al*. (2012) from carbon and N isotopic analysis of particulate OM collected from these eddies. Using a combination of *in situ* and satellite data, Roberts *et al*. (2014) investigated eddy dipoles interacting with the Mozambique Channel's western continental slope, which resulted in intense upwelling not only via shoaling of isopycnals but also (and in fact, predominantly) by horizontal divergence at the margins of the eddy dipoles. This study highlighted the effects of mesoscale eddies on the physical properties of the entire water column, including the regional thermocline.

The influence of physical forcings on the biogeochemistry of the Mozambique Channel is both complex and multifaceted. As outlined above, our current understanding is based on inferences of features and processes from qualitative analyses. While valuable, a quantitative approach, such as that facilitated by optimum multiparameter (OMP) analysis, may be more useful for determining the water and nutrient sources to the channel, as well as for describing local and/or regional biogeochemical changes.

2.7. Optimum Multiparameter Analysis

2.7.1. Introduction

In the early 1980s, Tomczak (1981) developed a multiparameter analysis that was an expansion of the universal temperature-salinity analysis (i.e., the two end-member mixing equation) in order to investigate contributions from three or more water masses simultaneously. The analysis assumes non-conservative parameters (variables affected by both physical and biogeochemical processes) to be conservative, with the objective of quantifying the mixing proportions of predefined water types that best describe the hydrographic properties of a disparate water mass. This method was further developed by Tomczak & Large (1989) by including a non-negative constraint on the water mass fractions, expanding on improvements made by Mackas *et al*. (1987) to Tomczak's original

work, and was then termed “optimum multiparameter (OMP) analysis”.

2.7.2. Background

The properties of seawater can be characterised by the types of processes that influence them. Below the surface layer, conservative properties (e.g., temperature and salinity) are only affected by the physical processes of advection and mixing, while non-conservative properties (e.g., oxygen and macronutrient concentrations) are affected by both physical and biogeochemical processes. Furthermore, some non-conservative properties can be redefined as *quasi-conservative* if the regional contextualisation allows for the omission of certain biogeochemical processes – for example, a region without (or with very little) diatom-related production will be characterized by (near-)conservation of silicate concentrations (e.g., You & Tomczak, 1992) – or if regional biogeochemical processes are considered relative to the study domain and thus taken into account (Hupe & Karstensen, 2000).

Following water mass subduction, the surface physical and biogeochemical properties are communicated to the ocean interior via advection and mixing. The unique suite of properties set at formation defines the *water type*, while the mixture of two or more water types gives rise to a *water mass* (Grover *et al*., 2011). As water masses are incorporated into global ocean circulation, they are modified by biogeochemical processes and conventional physical mixing.

2.7.3. Analysis framework

Multiparameter analysis is set up as a linear system of m equations, which yield a solution of m source water type fractions (Tomczak, 1981). The system of m equations is limited by the number of defined constraints, which implies that the number of such parameters, n, must equal the number of source water types, m. Conveniently, n can actually be composed of m-1 parameters as the n^{th} constraint is that of mass conservation.

If we consider the example of two water types and two parameters (temperature and salinity) plus the mass conservation constraint, with characteristic temperatures T_1, T_2 and salinities S_1, S_2, the water type fractions x_1, x_2 can be calculated from a sample with temperature T and salinity S as follows:

$$x_1T_1 + x_2T_2 = T$$

$$x_1S_1 + x_2S_2 = S$$

$$x_1 + x_2 = 1 \tag{2.2}$$

The mass conservation constraint always sums to 1. A negative water type fraction is unrealistic; hence the fractions are forced to be positive ($0 \leq x_i \leq 1$) by incorporating a separate mathematical technique (see Tomczak & Large, 1989). For simplicity, these equations can be expressed as a set of n simultaneous equations with a design matrix **A**, a vector of water type fractions **x**, and the sample values and associated residuals **b**:

$$\mathbf{Ax} = \mathbf{b} \tag{2.3}$$

where the m-1 rows of **A** are the parameters and the m^{th} row is the mass conservation constraint.

Integral to the OMP analysis is the overdetermination of the system of equations, initially formulated by Tomczak & Large (1989). This is achieved by ensuring the number of constraints exceeds the number of water types, $n > m$. Not only does this step improve the accuracy of the calculated water type fractions, but it also allows for the application of multiparameter analysis within the thermocline and across regions with frontal systems, where property gradients are large (Tomczak & Large, 1989). In reality, observational data are subject to error, source properties may fluctuate with time and space, and unidentified water types may be present in a sample region (Grover *et al*., 2011). To account for these uncertainties, OMP analysis utilises a least squares regression.

Biogeochemical effects related to water mass aging (i.e., remineralization) can be included in the OMP analysis (termed the extended OMP analysis), as demonstrated by the likes of Karstensen & Tomczak (1997), Hupe & Karstensen (2000) and Peters *et al*. (2018 (a) and (b)). The extended OMP analysis provides two benefits, the approach (1) accounts for *in situ* changes to water mass properties along flow pathways, and (2) enables non-conservative properties (e.g., nutrients) to be

reclassified as quasi-conservative, which expands the number of parameters (and thus water mass types) that can be included in the OMP analysis

2.7.4. Normalization and weighting

An inherent issue with the OMP analysis is that water mass properties are generally reported in different units, while properties with the same units may exhibit variations across different ranges and analytical precisions (Grover *et al*., 2011). The normalization of both water type and sample data is required to address this issue as it sets each parameter to a mean of zero and a variance of order 1. The normalization is performed 'row-wise' for both the design matrix **A** and sample matrix **b** by the formulation:

$$G_{i\,j} = (\boldsymbol{A}_{i\,j} - \bar{\boldsymbol{A}}_i)/s_i \text{ and } d_i = (\boldsymbol{b}_i - \bar{\boldsymbol{A}}_i)/s_i \tag{2.4}$$

with $\bar{\boldsymbol{A}}_i$ and s_i representing the mean and standard deviation of the design matrix $G_{i\,j}$, respectively.

Similarly, the measurements of the various parameters may not be achieved with the same degree of precision and confidence (Grover *et al*., 2011). Therefore, it is necessary to apply a confidence weighting to account for these differences. Simply put, a weighting matrix **W** consists of diagonal elements that are calculated as the mean and standard deviation of the individual parameters across the various water types:

$$W_{i\,i} = \delta_i / \sigma_i \tag{2.6}$$

where δ_i is the range across all water types and σ_i is the analytical uncertainty associated with variable i.

2.7.5. Thermocline array method

Numerous studies that have utilised OMP analysis define water types as single points in oceanic-property space. This approach assumes the occurrence of diapycnal mixing, which is justified in the case of large-scale applications of the method and/or specific regional hydrography (e.g.

Tomczak & Large, 1989; Poole & Tomczak, 1999; Hupe & Karstensen, 2000). However, the dynamics associated with the thermocline suggest weak diapycnal mixing as a result of stratification (Luyten *et al*., 1983; Ledwell *et al*., 1993). To this end, Jenkins *et al*. (2015) developed the *thermocline array* approach within the OMP analysis, where arrays of properties are defined from source regions across a range of potential density anomalies.

To apply the thermocline array approach, water type properties are interpolated onto a potential density anomaly grid resolved at fine-scale increments (e.g., 0.01 $kg.m^{-3}$ as per Jenkins *et al*. (2015)). These interpolated properties form the 'arrays' of the method. The same property gridding is applied to a given sample. The water mass fractions are then computed along matching potential density anomalies for each array.

The thermocline array method assumes that mixing occurs only along isopycnal surfaces (and not diapycnally) and thus "better" represents thermocline conditions than the single water type point approach that assumes mixing is diapycnal. However, by employing an array of water type properties for the thermocline instead of a point water type, the estimated water mass fractions do not necessarily distinguish between water masses within the sample region, but rather among contributions from each source region.

2.7.6. Historical applications of OMP analysis in the Indian Ocean

Coincidentally, the first application of the OMP analysis (Tomczak & Large 1989) was to the eastern Indian Ocean. The potential for this type of analysis to discern thermocline constituents was demonstrated in this original study as the authors were able to resolve the horizontal and vertical distributions of the water masses in the region and relate them to known circulation features.

Subsequently, the OMP analysis was applied to the Indian Ocean thermocline by You & Tomczak (1993). The approach taken in this study resolved the water mass fractions along three isopycnals and allowed for the tracing of water masses within the stratified thermocline where diapycnal mixing is weak. The study resolved the water mass fractions throughout the Indian Ocean basin, noting the influence of Indo-Pacific waters within the SEC as well as the advection of subtropical

waters into the northern Indian Ocean along its western boundary. While novel, the You & Tomczak (1993) study did not account for the seasonality of Indian Ocean circulation, particularly that of the monsoonal systems. This consideration formed the crux of a later OMP analysis study by You (1997), who took a similar approach in terms of the isopycnal resolution of the water masses, but divided the sample data temporally (i.e., summer versus winter). By way of this method, seasonal changes that result in current weakening and reversals (such as of the Somali Current and Equatorial Countercurrent) were linked to changes in the circulation of water masses resolved in the OMP analysis.

2.7.7. Applications of OMP analysis to investigations of regional biogeochemistry

The utility of OMP analysis for studying regional biogeochemistry was first illustrated by Hupe & Karstensen (2000). In their study of the Arabian Sea, they sought to understand nutrient stoichiometry in the ODZ. By use of the extended OMP method, the authors were able to account for diapycnal mixing of intermediate and deep waters, as well as to estimate remineralization ratios and quantify denitrification in the Arabian Sea. This particular study is a strong example of a localised application of the OMP analysis, as the region is uniquely influenced by local denitrification.

The OMP analysis solution (i.e., water type fractions) can also be applied to source water type biogeochemical properties (e.g., O_2 and nutrients) to determine the expected *background* concentration of these properties at the sample site that would result solely from mixing. Subsequently, differences between the background and measured biogeochemical properties can be quantified and attributed to various biogeochemical processes occurring between the source and sample regions.

Traditionally, to determine the fraction of remineralized nutrients in a system, mean nutrient stoichiometries (i.e., Redfield ratios) are relied upon, with the oxygen production-to-nutrient utilization ratio held constant. However, studies have shown that this ratio is not constant across the global ocean (Takahashi *et al*., 1985; Anderson & Sarmiento, 1994; DeVries & Deutsch 2014). In addition, overestimating the burden of remineralized nutrients is a concern when this pool is computed using the derived parameter of apparent oxygen utilisation (AOU; = $[O_2]_{sat}$ - $[O_2]_{observed}$).

AOU is a measure of biological O_2 respiration that assumes the background O_2 concentration ($[O_2]_{back}$, defined as $[O_2]_{sat}$ in the AOU equation above) in a particular water mass was fully saturated when that water mass was last in contact with the atmosphere (Ito *et al*., 2004). While these assumptions are reasonable for the high latitudes, they can easily be violated in (sub)tropical waters. To avoid overestimating remineralized nutrients, we can instead calculate True Oxygen Utilization (TOU), which was originally defined by Broecker & Peng (1982) as:

$$TOU = [O_2]_{back} - [O_2]_{obs} \quad (2.7)$$

where $[O_2]_{obs}$ is the measured $[O_2]$ in a particular sample. Applying an OMP analysis can yield a more robust estimate of $[O_2]_{back}$ than $[O_2]_{sat}$ because it does not assume oxygen saturation. Peters *et al*. (2018) used this technique to investigate N loss in the Eastern Tropical South Pacific. In this study, the authors quantitatively assessed fixed N loss in the ODZ by calculating the relative changes between the background and observed nutrient concentrations, the former calculated from source water concentrations and water mass fractions. The N deficits computed from the OMP analysis were in better agreement with the estimates of local N_2 production than the deficits calculated by Redfield stoichiometry, highlighting the utility of the approach.

2.8. Thesis scope

The complexities related to circulation and physical forcings in the Mozambique Channel have resulted in conflicting ideas of even the most foundational oceanography in this region, such as the water sources to the thermocline and the relative importance of various biogeochemical processes. Existing literature provides a largely hydrographic characterisation of the Mozambique Channel (e.g., Di Marco *et al*., 2002; Donohue & Toole, 2003; Swart *et al*., 2010). Minimal attention has been paid to local biogeochemical cycling, with the few studies that are inclined towards biogeochemistry focusing largely on phytoplankton community composition (e.g., Kolasinski *et al*., 2012; Barlow *et al*., 2014). Given that the Mozambique Channel is a source region to the Agulhas Current, a quantitative study of its biogeochemistry will assist in evaluating the role that the channel plays in setting the biogeochemical conditions (e.g., nutrient concentrations and ratios) and, by extension, the productivity of the Agulhas Current.

This thesis provides a quantitative assessment of the thermocline water masses in the Mozambique Channel and Agulhas Current, resolved via an OMP analysis. The work described herein has three aims: (1) to identify the two-dimensional distribution of the thermocline sources to the Mozambique Channel and Agulhas Current across four hydrographic transects available through the World Ocean Circulation Expedition (WOCE); (2) to identify local incidences of remineralization and/or other biogeochemical processes by coupling the OMP analysis solution with estimates or measurements of TOU, NO_3^- and PO_4^{-3} concentrations; and (3) to link changes in source water contributions to hydrographic features such as (anti)cyclonic eddies sampled in the WOCE transects and to investigate the biogeochemical implications of such changes in the thermocline.

The thesis begins with a description of the sample data in the western Indian Ocean, along with the methods of collection and analysis. Following this, a brief overview of the general hydrographical and biogeochemical trends in the study region is given. The thermocline array approach within the framework of the OMP analysis is then introduced and the source regions, selected based on contemporary understandings of general circulation and features in the western Indian Ocean, are defined. Finally, the biogeochemical components are incorporated by using the OMP analysis to estimate background concentrations of O_2, nitrate and phosphate, which are then compared to measurements of these parameters in order to infer biogeochemical changes and features.

3. Methods

3.1. Hydrographic data

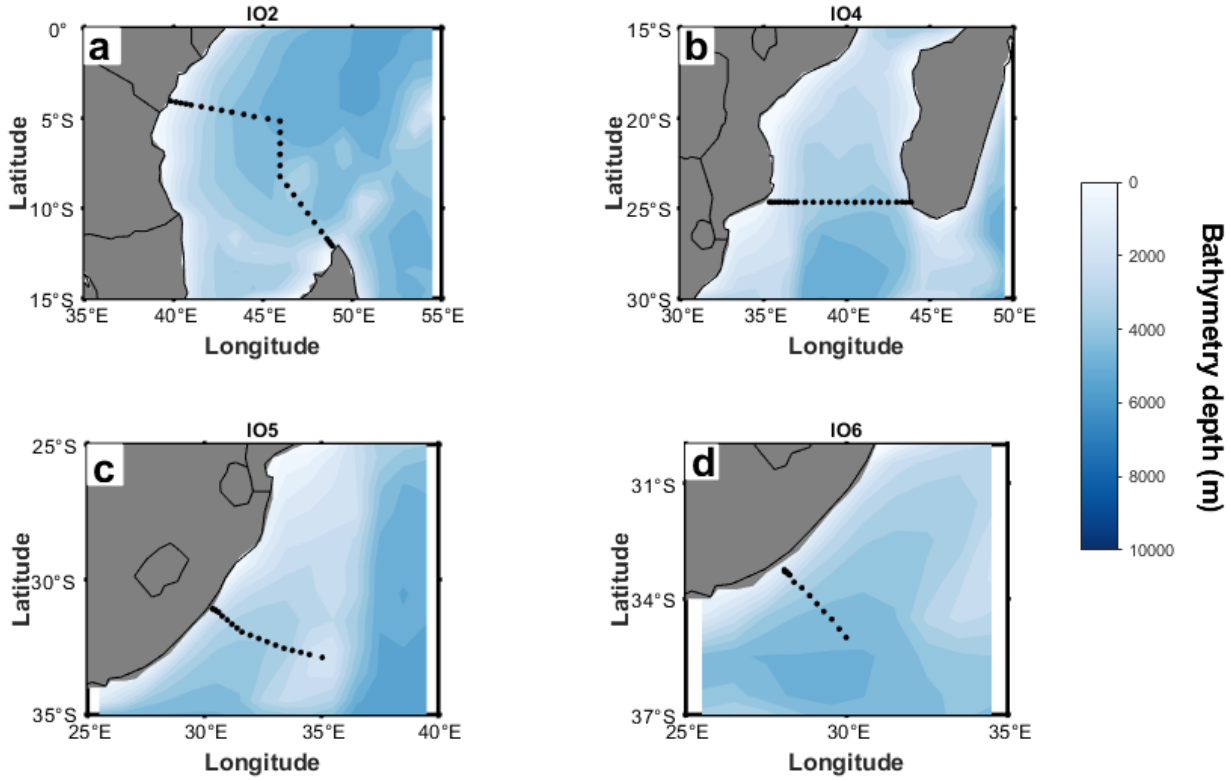

Figure 3.1 Hydrographic transects in the southwestern Indian Ocean from the World Ocean Circulation Experiment (WOCE) database that were used in this study. From north to south, they are (a) IO2, (b) IO4, (c) IO5, and (d) IO6. Bathymetry is shaded in blue.

To investigate the distribution of different water masses in the thermocline of the Mozambique Channel, this study makes use of two World Ocean Circulation Experiment (WOCE) transects that sampled the northern and southern boundaries of the channel (Fig. 3.1). Samples from the northern-boundary transect (hereafter denoted as *IO2*) were collected as part of cruise WHP (WOCE Hydrographic Program) IO2 aboard the *R/V Knorr* that took place from 14–21 January 1996. Sampling occurred between the northern tip of Madagascar near Cape Amber and the East African coast at Mombasa, Kenya, and the transect can be divided into two segments. The eastern segment from Cape Amber to 5.2°S forms an approximately diagonal section, while the western segment between 46°E and the coast of Africa is roughly zonal. Samples from the southern-boundary transect (hereafter denoted as *IO4*) were collected as part of the meridional cruise WHP

leg IO4 at 24.7°S aboard the *R/V Knorr* that took place from 15–19 June 1995, between the southern end of Madagascar and the Mozambican coast (35.4°E-39°E).

The downstream influence of the Mozambique Channel thermocline on the Agulhas Current is also investigated, by including two WOCE transects that sampled the current and the adjacent open ocean (Fig. 3.1). The upper transect (hereafter denoted as *IO5*) was sampled as part of the CLIVAR/CO_2 Repeat Hydrography Program leg IO5 between the southern African coast (31°S 30.3°E) and 31.6°S 31.2°E aboard the *R/V Roger Revelle* on the 24 March 2009. Similarly, the lower transect (hereafter denoted as *IO6*) was sampled as part of the CLIVAR/CO_2 Repeat Hydrography Program leg IO6 between the southern African coast (33.3°S 28°E) and 35°S 30°E aboard the *R/V Roger Revelle* between the 6-10 February 2008. Both transects are roughly diagonal.

The WOCE hydrographic stations are located roughly 55 km apart, with closer spacing near the continental slope. A rosette equipped with conductivity-temperature-depth (CTD) and oxygen sensors was lowered between the surface and seafloor at each station, with the sensors calibrated prior to and following the cruise as recommended by SCOR Working Group 51 (UNESCO, 1988; Muller *et al*., 1994). Water samples were collected at a maximum of 36 depths distributed throughout the water column. Salinity, oxygen, and nutrient concentrations were measured shipboard, with all chemical analyses conducted using recommended WOCE methods (WOCE, 1994). That the datasets were collected years apart does not matter for this study given the residence time of the thermocline (i.e., decades) and the fact that the study focus is mainly on understanding the broad features of the thermocline.

3.2. Optimum multiparameter (OMP) analysis

An optimum multiparameter (OMP) analysis was used to determine the water type fractions present in the thermocline across all four WOCE transects (IO2, IO4, IO5 and IO6). Defining appropriate source water types is integral for obtaining meaningful results from the OMP analysis. Hydrographic and biogeochemical observations from the meridional WOCE IO7N transect were used to isolate the source water types entering the Mozambique Channel (Fig. 2.1). On this largely meridional transect, samples were collected as part of the Global Ocean Ship-Based Hydrographic Investigation Program (GO-SHIP) aboard the NOAAS *Ronald H. Brown* from 23 April to 6 June

2018, between 18°N and 30°S. As the goal of this study was not to identify the water masses in the Mozambique Channel, but rather to diagnose the contribution of waters from the designated source regions to the regional thermocline, the entire thermocline within a source region (often composed of multiple water masses) was used to define a single source water type.

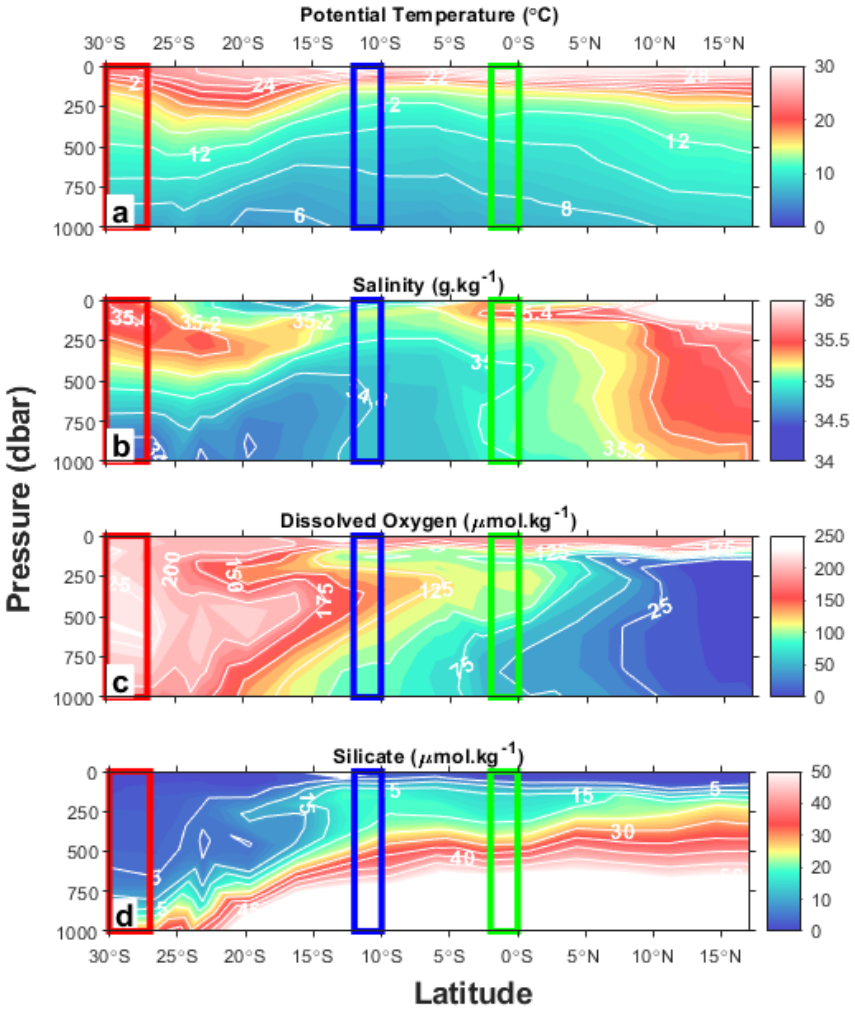

Figure 3.2 Section plots from the IO7N transect between 18°N and 30°S showing (a) potential temperature (in °C), (b) salinity (in g.kg^{-1}), (c) oxygen concentrations (in µmol.kg^{-1}), and (d) silicate concentrations (in µmol.kg^{-1}). Coloured rectangles define the geographical ranges of the source waters: Subtropical (red), Tropical (blue), and Equatorial (green).

Three source regions were ultimately identified: Subtropical, Tropical, and Equatorial. Meridional section plots of temperature, salinity, oxygen, and silicate were used to define the source regions (Figure 3.2 (a-d)). *Subtropical* source waters (27-30°S; red box in Fig. 3.2) are characterised by

high surface salinities, of ~35.8 g.kg^{-1}, at relatively high densities (σ_θ = 25 kg.m^{-3}). The T-S relationship across the entire thermocline range is linear and well constrained (Figure 2.3 (b)), and an oxygen maximum of >200 µmol.kg^{-1} persists between the isopycnals of 26.5-26.9 kg.m^{-3} (Fig. 3.2 (c)). The region is also low in silicate (<10 µmol.kg^{-1}) down to the depths of the intermediate waters (~800 m) (Fig. 3.2 (d)). *Tropica*l source waters (12-10°S; blue box in Fig. 3.2) are generally relatively fresh owing to the contribution of the ITF. Many authors (e.g., Sharma, 1976; Quadfasel & Schott, 1982; You & Tomczak, 1992) describe the waters ascribed here as *Equatorial* source waters (2-0°S; green box in Fig. 3.2) as a mixture of other water masses; however, the near-uniform salinities between 23 and 26 kg.m^{-3} (depths of 250 to 1000 m) suggest that these particularly fresh waters constitute a unique source to the channel (Fig. 3.2 (a-b)). Both the Tropical and Equatorial regions display similar ranges in silicate concentrations (15-20 µmol.kg^{-1}) (Fig. 3.2 (d)), with the latter region hosting slightly higher concentrations on average (Table 3.1). The source region properties are summarised in Table 3.1 and shown on density profiles in Fig. 3.3 (a-d) along with data from transects IO2, IO4, IO5 and IO6.

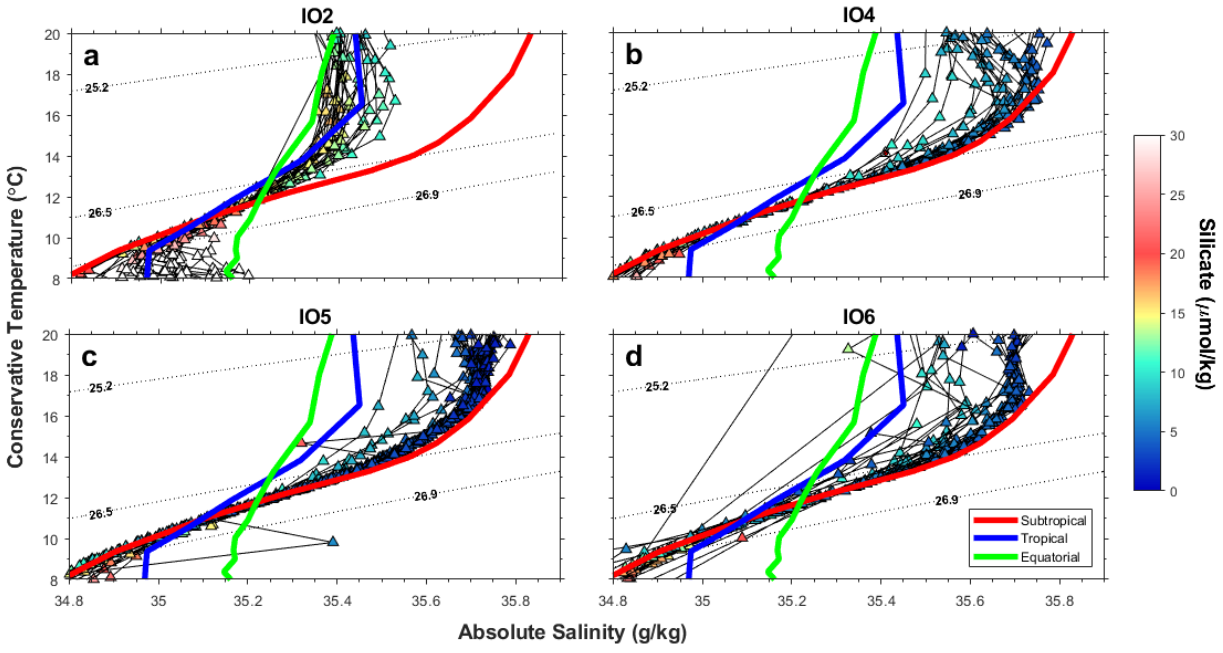

Figure 3.3 Temperature-Salinity (T-S) diagram (in °C and g.kg^{-1}, respectively) of the transects (a) IO2, (b) IO4, (c) IO5, and (d) IO6 overlayed with the T-S properties of the Subtropical (red line), Tropical (blue line), and Equatorial (green line) source regions. Sample data are coloured by silicate concentration (in µmol.kg^{-1}). Density contours for the upper and lower bounds of the OMP analysis (σ_θ = 25.2 kg.m^{-3} and 26.9 kg.m^{-3}), as well as the transition between the upper and permanent thermocline (σ_θ =26.5 kg.m^{-3}) are denoted by the black dots.

Table 3.1 Average upper and permanent thermocline properties for the source regions. Included in the last column are the latitudinal ranges used to constrain the source regions.

Source Waters	Potential Temperature (°C)	Salinity ($g.kg^{-1}$)	Silicate ($\mu mol.kg^{-1}$)	Latitudinal range
Upper thermocline (25.2-26.5 $kg.m^{-3}$)				
Subtropical	17 ± 2	35.6 ± 0.10	3 ± 1	27-30 °S
Tropical	16 ± 2	35.2 ± 0.06	13 ± 2	10-12 °S
Equatorial	16 ± 2	35.1 ± 0.04	17 ± 2	0-2 °S
Permanent thermocline (26.5-26.9 $kg.m^{-3}$)				
Subtropical	11 ± 2	35.0 ± 0.22	6 ± 2	27-30 °S
Tropical	11 ± 1	34.9 ± 0.07	20 ± 3	10-12 °S
Equatorial	12 ± 0.7	35.0 ± 0.02	27 ± 4	0-2 °S

To calculate the source water type values, temperature, salinity, and silicate profiles from within the water type geographical range (Table 3.1) were interpolated onto a density grid with increments of 0.01 $kg.m^{-3}$ between the defined thermocline density range (25.2 - 26.9 $kg.m^{-3}$), and then averaged to produce a mean water type profile. The high resolution density interpolation ensures that the mixing of water types occurs along isopycnal surfaces only (Jenkins *et al*., 2015; Peters *et al*., 2017). Each measurement from IO2, IO4, IO5, and IO6 was matched to the nearest density increment for each source water type property (Jenkins *et al*., 2015; Peters *et al*., 2018 (a) and (b)). The conservative properties used in this study include potential temperature (T) in °C, salinity (S) in $g.kg^{-1}$, and silicate in $\mu mol.kg^{-1}$. The inclusion of silicate as a quasi-conservative tracer is reasonable as diatoms, the primary drivers of changes in silicate concentrations on the timescales of interest here, are not a significantly abundant in the study region or the source regions (Barlow *et al*., 2002; Goncalves-Araujo *et al*., 2012; Barlow *et al*., 2020).

The following equations were used:

$$x_{sub}T_{sub} + x_{trop}T_{trop} + x_{eq}S_{ieq} = T_{obs} + T_R$$

$$x_{sub}S_{sub} + x_{trop}S_{trop} + {}_{eq}S_{eq} = S_{obs} + S_R$$

$$x_{sub}Si_{sub} + x_{trop}Si_{trop} + x_{eq}Si_{eq} = Si_{obs} + Si_R$$

$$x_{sub} + x_{trop} + x_{eq} = 1 + x_R$$

(3.1)

where x_{sub}, $x_{trop,}$ and x_{eq} are the Subtropical, Tropical, and Equatorial source water type fractions respectively, T_n, $S_{n,}$ and Si_n are the potential temperature, salinity, and silicate concentrations of the source water types, T_{obs}, $S_{obs,}$ and Si_{obs} are the potential temperature, salinity, and silicate concentrations measured along the transect, and T_R, S_R, $Si_{R,}$ and x_R are the residuals associated with potential temperature, salinity, silicate concentration, and mass fraction, respectively.

Weighting of the parameters is crucial as it accounts for both the uncertainty of the sample measurement and the source water type (Glover *et al*., 2011). The following weights were calculated using equation 2.6, as described in the literature review: 24, 24, 2, and 24 for potential temperature, salinity, silicate, and mass fraction (with this last parameter assigned the same value as the largest weight), respectively. Thereafter, the best fit solution was found using non-negative least squares optimization, via the "nonneglsq" function in MATLAB's "Optimization Toolbox".

A Monte Carlo analysis was used to quantify the uncertainty in the computed water mass fractions due to the chosen source waters and parameter weights (Jenkins *et al*., 2015; Peters *et al*., 2017 (a) and (b)). Two tests were conducted: the first involved running the OMPA 100 times while perturbing the chosen source waters by a percentage (shown in Table 3.2) of that value at each iteration. The second involved running the OMPA 100 times with the addition of 25% random noise to the weights for each iteration. The water mass fractions were found to be fairly insensitive to both the chosen source water values and the chosen weights, as evidenced by the low standard deviations (average <20%) that were achieved across all transects (Fig. 3.4 and 3.5). This gives us confidence in the OMPA solution and thus the interpretation of those results. Further elaboration related to the distribution of the uncertainties will be presented in the Discussion.

Table 3.2 Perturbation levels for the first Monte Carlo analysis of the source water properties.

End member parameter	Potential temperature	Salinity	Silicate
Perturbation	10%	1%	10%

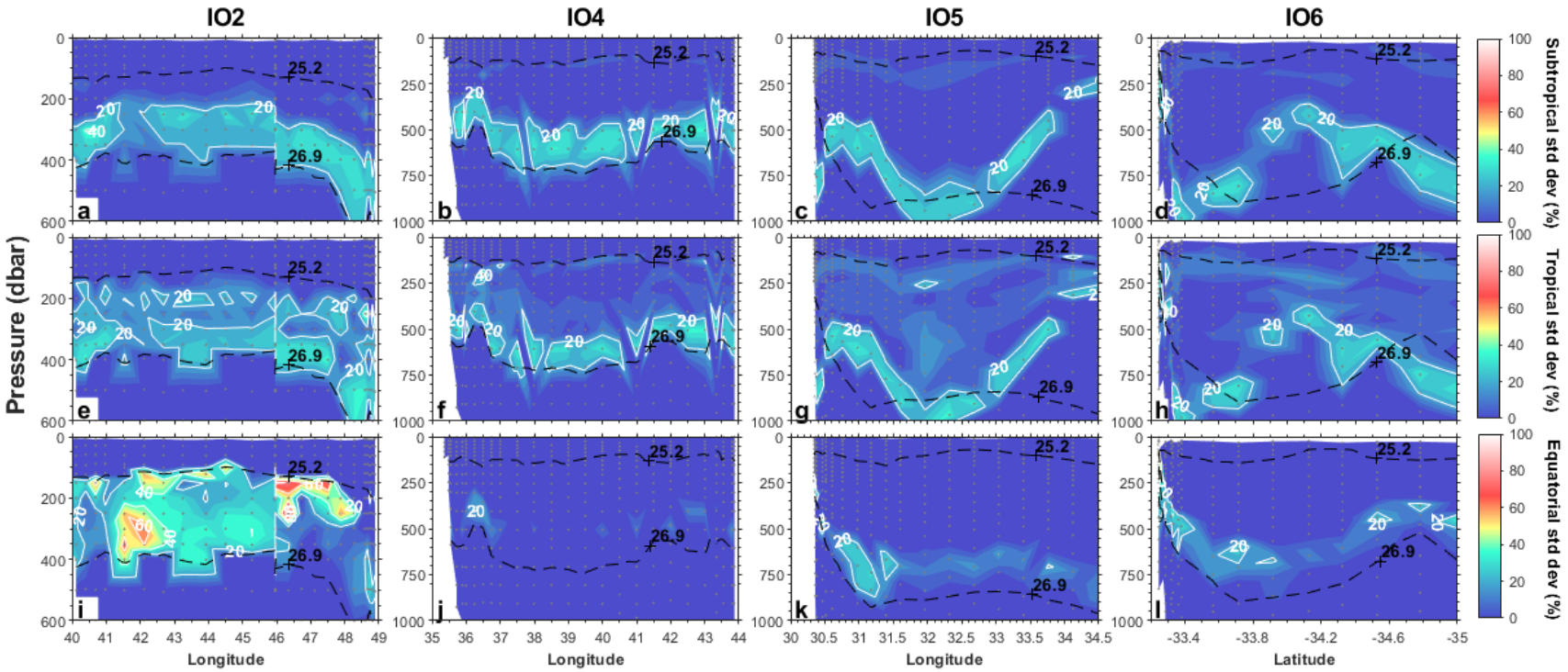

Figure 3.4 Depth sections of the standard deviations associated with each source water fraction (%) for the transects IO2, IO4, IO5, and IO6 (from left to right), for the first Monte Carlo test (perturbation of source water values; see text for details). Isolines for each property are shown in white. Isopycnal surfaces indicating the thermocline range (σ_θ = 25.2-26.9 kg.m^{-3}) are shown by the black dashed lines. Small grey dots indicate the CTD stations. For IO2, the data to the right of the black line at 46°E are from the meridional section of the transect (see Fig. 3.1). Note, the maximum depth for the IO2 transect is 600 m while for IO4, IO5, and IO6, it is 1000 m, and transects IO2, IO4, and IO5 are shown as a function of longitude while IO6 is shown versus latitude.

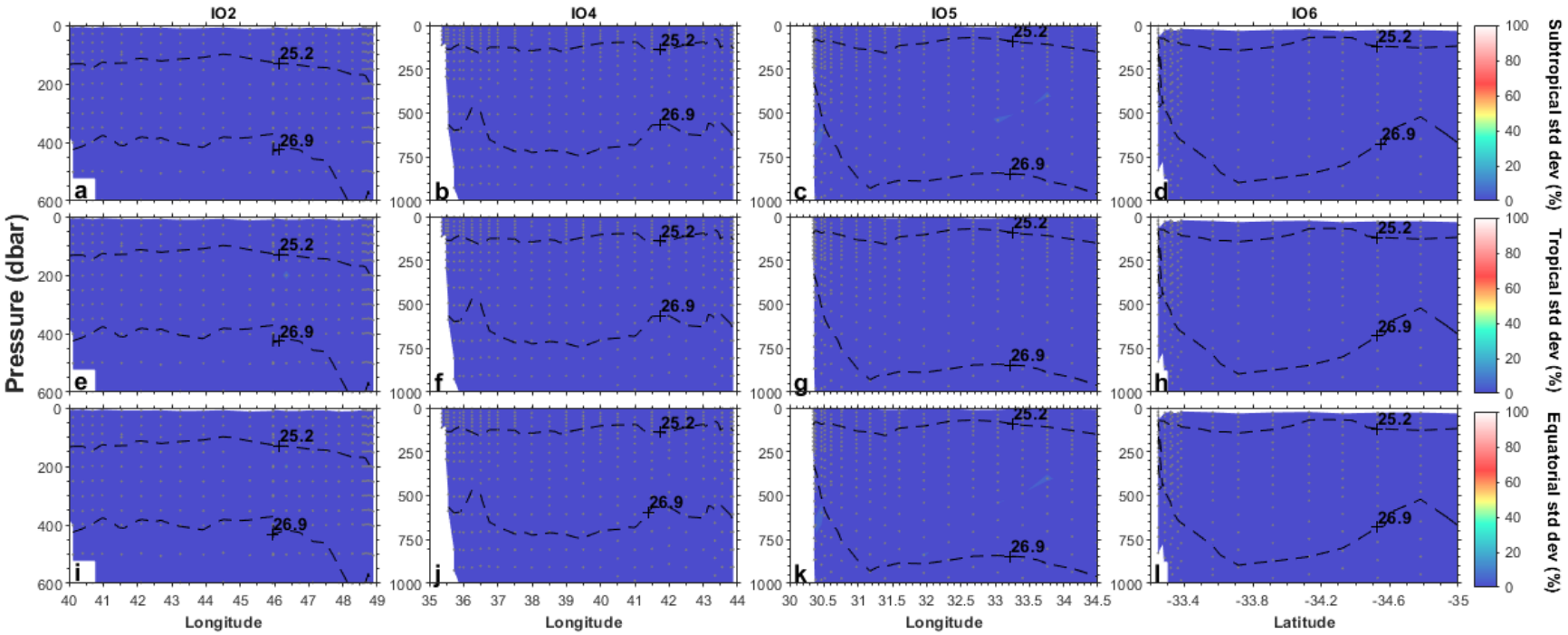

Figure 3.4 Depth sections of the standard deviations associated with each source water fraction (%) for the transects IO2, IO4, IO5, and IO6 (from left to right), for the second Monte Carlo test (perturbation of weights; see text for details). Isolines for each property are shown in white. Isopycnal surfaces indicating the thermocline range (σ_θ = 25.2-26.9 kg.m^{-3}) are shown by the black dashed lines. Small grey dots indicate the CTD stations. For IO2, the data to the right of the black line at 46°E are from the meridional section of the transect (see Fig. 3.1). Note, the maximum depth for the IO2 transect is 600 m while for IO4, IO5, and IO6, it is 1000 m, and transects IO2, IO4, and IO5 are shown as a function of longitude while IO6 is shown versus latitude.

3.3. Application of the OMP analysis to the local biogeochemistry

The results from the OMP analysis were used to investigate biogeochemical processes related to the observed relative changes in nutrient concentrations and ratios in the Mozambique Channel. The OMP analysis allows for the calculation of a background $[O_2]$ that results from the mixing of the source water types:

$$[O_2]_{back} = x_1[O_2]_1 + x_2[O_2]_2 + x_3[O_2]_3 \quad (3.2)$$

where x_n is the water type fraction and $[O_2]_n$ the associated source water type oxygen concentration ($[O_2]$). The source water type $[O_2]$ values were interpolated onto the same density grid as the thermocline array properties and averaged across the designated source regions mentioned above. Thereafter, the TOU described by Broeker & Peng (1982) was determined. TOU gives an indication of the intensity of remineralization in the water column, with positive values indicating the consumption of $[O_2]$ between the sampled and source regions. TOU is useful for evaluating $[O_2]$ changes within water masses that have not recently equilibrated with the surface and hence already carry a signature of remineralization within the source region. Negative values of TOU may be a sign of upwelling, mixing, or unaccounted-for source water types.

Similar to the expression for background $[O_2]$ given above, the background $[NO_3^-]$ and $[PO_4^{3-}]$ can be calculated from the water type fractions:

$$[NO_3^-]_{back} = x_1[NO_3^-]_1 + x_2[NO_3^-]_2 + x_3[NO_3^-]_3$$

$$[PO_4^{3-}]_{back} = x_1[PO_4^{3-}]_1 + x_2[PO_4^{3-}]_2 + x_3[PO_4^{3-}]_3 \quad (3.4)$$

where x_n is the water type fraction and $[NO_3^-]_n$ the associated source water type $[NO_3^-]$ (same for $[PO_4^{3-}]$). Thus, the concentration differences between the source and sampled regions for both nutrients can be calculated by subtracting the background from the observed concentrations:

$$[NO_3^-]_{diff} = [NO_3^-]_{obs} - [NO_3^-]_{back}$$

$$[PO_4^{3-}]_{diff} = [PO_4^{3-}]_{obs} - [PO_4^{3-}]_{back}$$

(3.5)

where $[NO_3^-]_{diff}$ is the difference between sample and source $[NO_3^-]$, $[NO_3^-]_{obs}$ is the observed $[NO_3^-]$ value, and $[NO_3^-]_{back}$ is the background $[NO_3^-]$ calculated from the water type fractions (same for $[PO_4^{3-}]$). These estimates of $[NO_3^-]$diff and $[PO_4^{3-}]$diff will be interpreted in terms of the thermocline distribution from the respective source regions, known circulation and flow pathways, as well as physical forcings associated with mesoscale dynamics.

Two final steps are (1) to calculate the fraction of the difference in the nutrient concentrations relative to the observed concentrations:

$$Frac.[NO_3^-]_{diff} = [NO_3^-]_{diff} / [NO_3^-]_{obs}$$

$$Frac.[PO_4^{3-}]_{diff} = [PO_4^{3-}]_{diff} / [PO_4^{3-}]_{obs}$$

(3.6)

and (2) to estimate the ratio in which $[NO_3^-]$ and $[PO_4^{-3}]$ are added to the thermocline in the sample region:

$$[N:P]_{diff} = [NO_3^-]_{diff} / [PO_4^{3-}]_{diff}$$

(3.7)

4. Results

4.1. Temperature, salinity, and oxygen concentrations in the southwest Indian Ocean

The highest surface temperatures were observed across the IO2 transect, in excess of 30°C (Fig. 4.1 (a)). Along the meridional section of IO2 near the Madagascan coast (46-49°E), the permanent thermocline (σ_θ = 26.5-26.9 kg.m^{-3}) was depressed from 400 m to 600 m for the σ_θ = 26.9 kg.m^{-3} isopycnal. The thermal gradient was less pronounced across IO4 where surface temperatures only reached 25°C, resulting in the thermocline occupying a larger depth range of 100-700 m (Fig. 4.1 (b)). Mesoscale features were evident in the shoaling of isotherms (and other variables (Fig. 4.1 (f and j)) at 36°E and 42°E along IO4 and were most apparent in the σ_θ = 26.9 kg.m^{-3} isopycnal. IO5 and IO6 displayed similar thermal trends; the thermocline occupied the 100-800 m depth interval, and a sharp shoaling of the isotherms occurred near the southern African coast (Fig. 4.1 (c-d)). For IO5, the σ_θ = 26.9 kg.m^{-3} isopycnal shoaled from ~800 m at 31°E to 300 m at 30.5°E, while for IO6, it shoaled from ~800 m at 33.6°S to 100 m at 33.2°S. A mesoscale feature was apparent along IO5 in the shoaling of the mid-thermocline isotherms at 31.25°E (Fig. 4.1 (c)) and along IO6 in the subsurface isotherms at 34.8°S (Fig. 4.1 (d)).

Salinity within the thermocline decreased fairly consistently with depth across all transects (Fig. 4.1 (e-h)). For IO2 near the northern Madagascar coast (46-49°E), relatively low surface salinities of <35 g.kg^{-1} were observed compared to the rest of the transect (Fig. 4.1 (e)). Similarly, two low salinity features (<34.8 g.kg^{-1}) were evident beneath the thermocline (~500 m), one directly below the eastern low-salinity surface feature and the other along the east African coast (40.5°E). The salinity distributions across transects IO4, IO5, and IO6 were relatively similar, with a salinity maximum of >35.5 g.kg^{-1} occurring in the near surface/shallow thermocline and a salinity minimum of <34.6 g.kg^{-1} evident within the sub-thermocline (Fig 4.1 (f-h)). However, this salinity minimum was less pronounced and more disjointed across IO4 (Fig. 4.1 (f)). The surface salinities across IO5 and IO6 were less consistent, with fresher signals (<35.4 g.kg^{-1}) observed near the African coast (30.5°E and 33.2°S, respectively) and values of up to 35.8 g.kg^{-1} apparent across the southern half of the transect. For IO5, a peak in subsurface salinities occurred at the same longitude as the shoaling of the mid-thermocline isotherms described above (31.25°E) (Fig. 4.1 (g)).

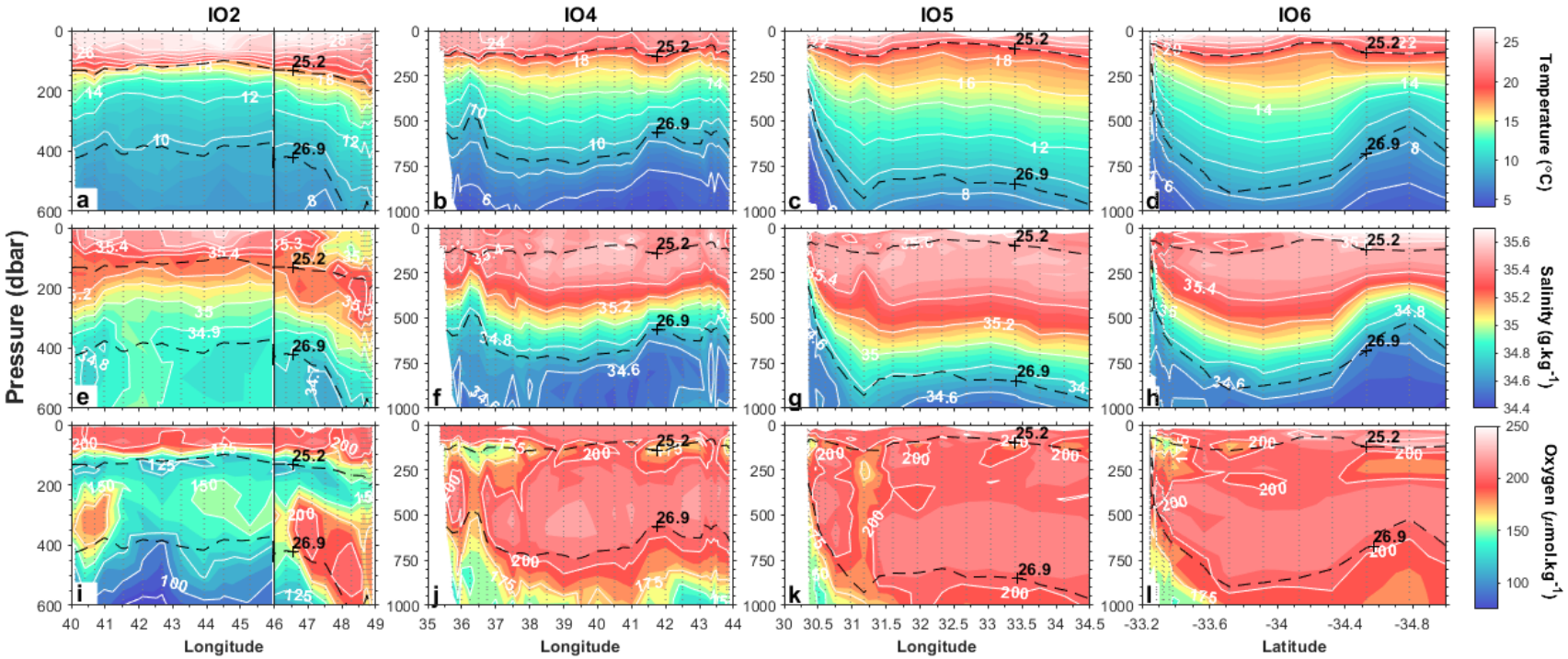

Figure 4.1 Depth sections of temperature (a-d), salinity (e-h), and oxygen concentrations ($[O_2]$) (i-l) for the transects IO2, IO4, IO5, and IO6 (from left to right). Isolines for each property are shown in white. Isopycnal surfaces indicating the thermocline range (σ_θ = 25.2-26.9 kg.m^{-3}) are shown by the black dashed lines. Small grey dots indicate the CTD stations. For IO2, the data to the right of the black line at 46°E are from the meridional section of the transect (see Fig. 3.1). Note, the maximum depth for the IO2 transect is 600 m while for IO4, IO5, and IO6, it is 1000 m, and transects IO2, IO4, and IO5 are shown as a function of longitude while IO6 is shown versus latitude.

The oxygen concentration distributions across all transects displayed similar patterns within the surface and thermocline waters (Fig. 4.2 (i-l)); an oxygen minimum (75-150 μmol.kg^{-1}) was observed in the upper thermocline (σ_θ = 25.2-26.5 kg.m^{-3}), sandwiched between two oxygen maximums, one in surface waters (>200 μmol.kg^{-1}) and the other in the permanent thermocline (~175 μmol.kg^{-1}). Oxygen concentrations across IO2 contrasted those of IO4, IO5, and IO6, with generally lower values measured in the thermocline and sub-thermocline (150 to 100 μmol.kg^{-1}) (Fig. 4.1 (i)). Here, the upper thermocline oxygen minimum was the most intense (<125 versus 175 μmol.kg^{-1} on average across IO4, IO5, and IO6) and the permanent thermocline, which overlaid low oxygen (75 to <125 μmol.kg-1) intermediate waters, was characterized by elevated horizontal variability owing to two oxygen maximums (>175 μmol.kg^{-1}) occurring at either end of the transect (i.e., at the northern Madagascan and east African coasts). Across IO4, the mesoscale features characterized by shoaling isopycnals at 36.5°E and 42°E (hereafter, upwelling features) were associated with lower upper thermocline oxygen concentrations than in the adjacent waters (<175 μmol.kg^{-1} versus ~200 μmol.kg^{-1}), and in the case of the feature at 36.5°E, lower oxygen concentrations were apparent over the entire thermocline depth range (Fig. 4.1 (j)). Across IO5, there were two localised oxygen minimums (<175 μmol.kg^{-1}), one at the coast (30.4°E) and another at 31.25°E (Fig. 4.1 (k)), with the latter coincident with an upward kink in both temperature and salinity (Fig. 4.1 (c and g)). Similarly low oxygen concentrations were observed at the African coast in IO6, and an additional low oxygen feature (~175 μmol.kg^{-1}) was observed in the offshore upper thermocline at 34.8°S (i.e., associated with an upwelling feature; Fig. 4.1 (l)).

4.2. Silicate [$Si(OH)_4$], nitrate [NO_3^-], and phosphate [PO_4^{3-}] concentrations in the southwest Indian Ocean

Since the dominant trends in the concentrations of the macronutrients - silicate, nitrate and phosphate - were similar for a given transect, they are described together for each transect. The distributions at the lower thermocline boundary closely followed the σ_θ = 26.9 kg.m^{-3} isopycnal in its peaks and depressions. Silicate occurred in low concentrations throughout the thermocline (0-15 μmol.kg^{-1}) (Fig 4.2 (a-d)), with thermocline silicate across IO2 that was noticeably higher than for the other transects (>10 μmol.kg^{-1}) and horizontally heterogeneous, with incidences of low silicate (~5 μmol.kg^{-1}) occurring coincident with the aforementioned oxygen maxima (Fig 4.2 (i)). Similar low concentration features were observed in the nitrate (<15 μmol.kg^{-1}) and phosphate (<1

μmol.kg^{-1}) concentrations measured for IO2 (Fig 4.2 (e) and (i)).

Across IO4, the upwelling features at 36°E and 42°E appeared to inject nutrients into the thermocline (Fig 4.2 (b), (f), and (g)). Sub-thermocline silicate, nitrate, and phosphate concentrations (20 μmol.kg^{-1}, 20 μmol.kg$^{-1,}$ and 1.5 μmol.kg^{-1}, respectively) were observed in the subsurface, especially coincident with the feature at 36°E, as was observed for temperature, salinity, and oxygen (Fig. 4.1 (b), (f), and (j)). A similar feature was observed in IO5 at 31.25°E as a slight peak in the concentrations of silicate (7.5 μmol.kg^{-1}), nitrate (15 μmol.kg^{-1}), and phosphate (0.75 μmol.kg^{-1}); however, this feature does not appear to have affected the lower bounds of the thermocline (Fig 4.2 (c), (g), and (k)). East of this feature (31.7°E), a substantial decrease in the concentrations of all the nutrients was observed, with the change in silicate being the most pronounced (declining to <2.5 μmol.kg^{-1} at the base of the thermocline). For IO6, the offshore upwelling feature at 34.8°S was also associated with higher thermocline silicate (7.5 μmol.kg^{-1}), nitrate (15 μmol.kg^{-1}), and phosphate (0.75 μmol.kg^{-1}), but differed from the feature in IO5 by extending to the sub-thermocline (Fig 4.2 (d), (h), and (l)). Both of the Agulhas transects (IO5 and IO6) were associated with higher subsurface nutrients along the southern African coast, with the concentrations of silicate, nitrate and phosphate reaching 20 μmol.kg^{-1}, 20 μmol.kg$^{-1,}$ and 1.5 μmol.kg^{-1}, respectively.

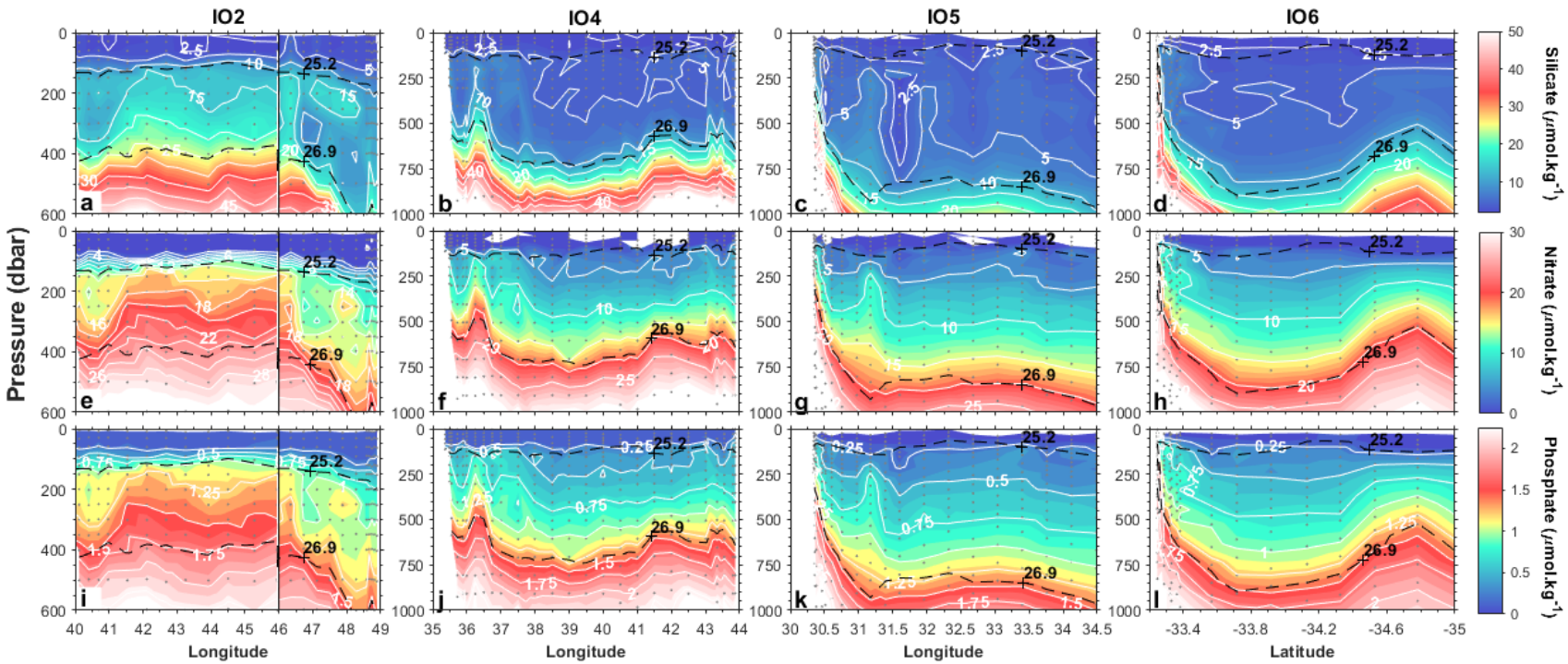

Figure 4.2 Depth sections of silicate (a-d), nitrate (e-h), and phosphate concentrations (i-l) for the transects IO2, IO4, IO5, and IO6 (left to right). Contours of each property are shown in white. Isopycnal surfaces indicating the thermocline range (σ_θ = 25.2-26.9 kg.m^{-3}) are contoured in black dashed lines. Small grey dots indicate the sampling resolution. For IO2, the black line at 46°E denotes the point at which the meridional section of the transect ends; to the right of this line is the zonal section (see Fig. 3.1 (b)). Note, the maximum depth for all IO2 transects is 600 m while for IO4, IO5, and IO6, it is 1000 m and transects IO2, IO4, and IO5 are zonal while IO6 is meridional.

4.3. OMP analysis of the thermocline

Across IO2, Subtropical source waters were confined to the permanent thermocline, with incidences of up to 80% observed near the northern Madagascan coast (46-49°S) and up to 60% along the east African coast (40-42°E) (Fig. 4.3 (a)). These features coincided with the high oxygen and low silicate features described above. Subtropical source waters dominated the thermocline across the IO4, IO5, and IO6 transects (Fig. 4.3 (b-d)). Here, low Subtropical contributions (from 0-40%) occurred coincident with mesoscale features. More specifically, lower Subtropical contributions (of <60%) were observed in the upper thermocline at 36.5°E in the IO4 transect where a mesoscale upwelling feature was evident (Fig. 4.3 (b)). This decrease in the Subtropical fraction to ≤60% is apparent in the scatter figure at σ_θ = ~26.5 kg.m^{-3} (Fig. 4.4 (b)). Across IO5, the Subtropical contribution declined to ~50% approximately between 200-600 m at 31.25°E. The scatter plot for IO5 shows a local maximum in the Subtropical fraction at σ_θ = 26 kg.m^{-3}, followed by a decrease at σ_θ = ~26.5 kg.m^{-3}, and then an increase to 100% between σ_θ = ~26.6 kg.m^{-3} and the lower thermocline boundary (Fig. 4.4 (c)). For IO6, the Subtropical contribution declined between 100 and 250 m at 33.25°S and at 250 m at 34.8°S (Fig. 4.3 (c-d)), with similar trends apparent in the scatter figure, albeit less cohesive (Fig. 4.4 (d)).

Across IO2, Tropical source waters dominated the upper thermocline (up to 70%) and the permanent thermocline (up to 50%) in the central region of the transect (42-46°E) (Fig. 4.3 (e)). Across IO4, IO5, and IO6, Tropical fractions of up to 100% were observed in the upper- and mid-thermocline (Fig. 4.3 (f-h)) coincident with the aforementioned reductions in the Subtropical source-water fractions and the location of the mesoscale features (Fig. 4.4 (b-d)). The scatter trends described for the Subtropical source water were inversely related to the Tropical source water contributions (Fig. 4.4). For IO4, the Tropical fraction increased to a maximum of 40% at σ_θ = ~26.5 kg.m^{-3} followed by a decrease to ~0-10% within the permanent thermocline (Fig. 4.4 (b)). Transects IO5 and IO6 displayed similar trends; Tropical source waters were at a minimum of ~10% at σ_θ = 26 kg.m^{-3}, then increased, to 30% for IO5 and 60% for IO6, at σ_θ = ~26.5 kg.m^{-3}, with little to no contribution within the permanent thermocline (Fig. 4.4 (c-d)). For IO5 specifically, an increase of up to 40% was observed at 31.25°E, the same longitude at which the Subtropical contribution decreased (Fig. 4.3 (g)).

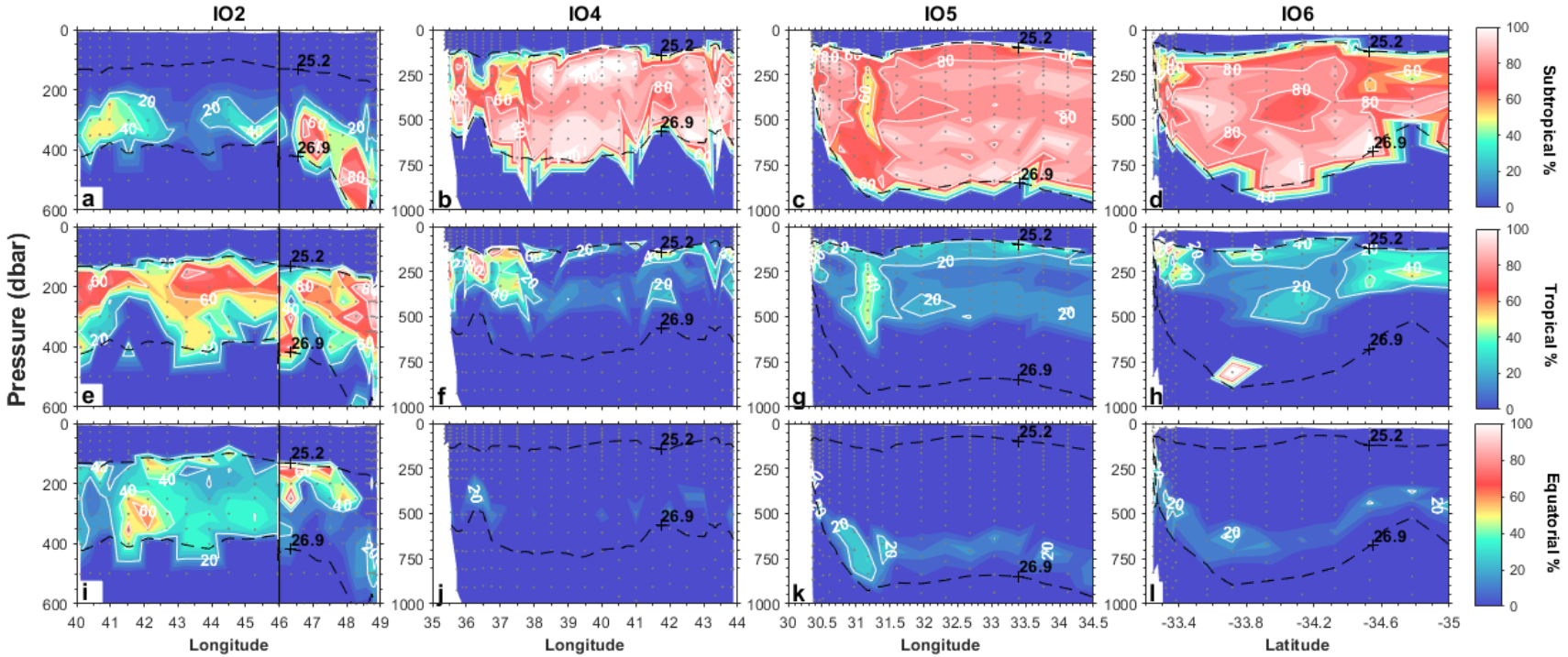

Figure 4.3 Percentages of the Subtropical (a-d), Tropical (e-h), and Equatorial (i-l) source waters diagnosed in the thermocline of the transects IO2, IO4, IO5, and IO6 (from left to right). Contours of source water percentages are shown in white. Isopycnals surfaces indicating the thermocline range (σ_θ = 25.2-26.9 kg.m^{-3}) are shown by the black dashed lines. Small grey dots indicate the sampling resolution. For IO2, the black line at 46°E denotes the point at which the meridional section of the transect ends; to the right of this line is the zonal section (see Fig. 3.1 (b)). Note, the maximum depth for all IO2 transects is 600 m while for IO4, IO5, and IO6, it is 1000 m and transects IO2, IO4, and IO5 are zonal while IO6 is meridional.

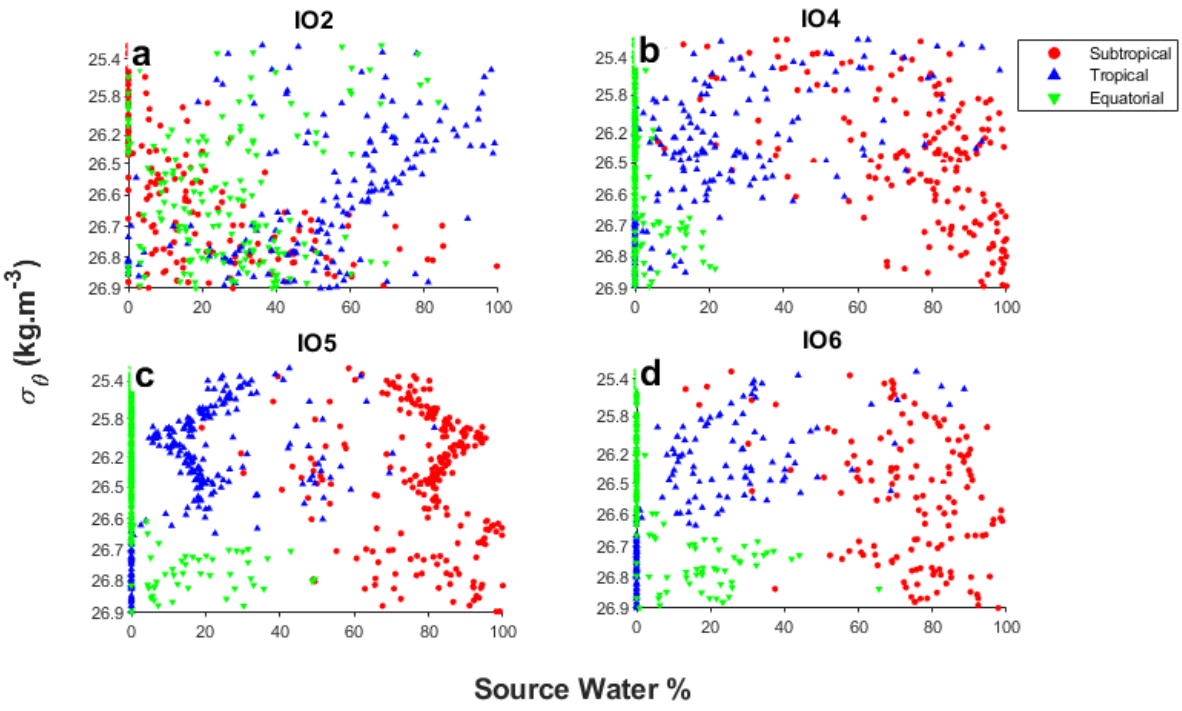

Figure 4.4 Density profiles of the Subtropical, Tropical, and Equatorial source waters as percentage contributions to samples in the thermocline (σ_θ = 25.2-26.9 kg.m^{-3}) for the transects IO2 (a), IO4 (b), IO5 (c), and IO6 (d).

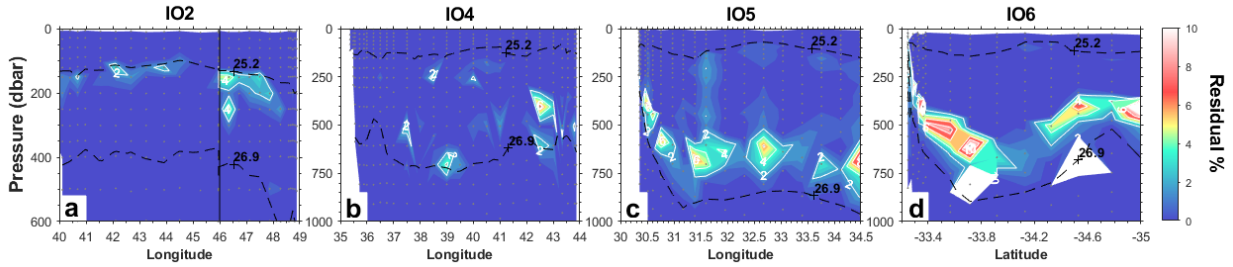

Figure 4.5 Residuals (as percentages) from the OMP analysis for the transects IO2 (a), IO4 (b), IO5 (c), and IO6 (d). Note that the colour bar shows 0-10% only. Contours of residuals are shown in white. Isopycnals surfaces indicating the thermocline range (σ_θ = 25.2-26.9 kg.m^{-3}) are contoured by the black dashed lines. Small grey dots indicate the sampling resolution. For IO2, the black line at 46°E denotes the point at which the meridional section of the transect ends; to the right of this line is the zonal section (see Fig. 3.1 (b)). Note, the maximum depth for all IO2 transects is 600 m while for IO4, IO5, and IO6, it is 1000 m and transects IO2, IO4, and IO5 are zonal while IO6 is meridional.

Equatorial source waters were the least represented (Fig. 4.3 (i-l) and Fig. 4.4) in the study region, with IO2 being the only transect with fractions >20% and contributions distributed across the transect (Fig. 4.3 (i)). Here, two cores of up to 70% Equatorial waters were observed; one in the upper thermocline between 46-48°E (coincident with an oxygen minimum: Fig. 4.1 (i)), and another in the permanent thermocline between 41-43°E. Across IO4, IO5, and IO6, only low

Equatorial contributions, of ≤20%, were observed (Fig. 4.3 (j-l)). For IO4, this contribution was apparent in the permanent thermocline at 36.5°E, associated with the upwelling of the σ_θ = 26.9 kg.m^{-3} isopycnal. Across IO5 and IO6, Equatorial contributions ≤20% were observed near the southern African coast coincident with the shoaling of isopycnals and above the lower thermocline boundary (Fig. 4.3 (k-l) and Fig. 4.4 (c) and (d) at σ_θ = 26.75-26.9 kg.m^{-3}).

4.4. Residuals and error from the OMP analysis

The residuals for the source water fractions across all transects did not exceed 10% (Fig. 4.5). More specifically, the residuals across IO2, IO4, and IO5 were very low, reaching a maximum of 5% (Fig. 4.5 (a-c)). Overall, the distribution of the residuals did not correlate with any physical or biogeochemical features, although higher residuals appear to coincide with increased Equatorial source water fractions across IO5 and IO6 (Fig 4.3 (i-j)), particularly at the upper and lower thermocline boundaries. The residuals across IO6 were notably higher (up to 10%) than for the other transects, predominantly within the permanent thermocline but also within the upper thermocline along the southern African coast (Fig. 4.5 (d)). Again, incidences of higher residuals appear to be linked to the Equatorial source water distributions, with prominent features evident between 33.4-33.8 and at 34.5 °S.

As mentioned in the Methods section, the water mass fractions were found to be fairly insensitive to both the chosen source water values and the chosen weights, as evidenced by the low standard deviations (average <20%) that were achieved across all transects (Fig. 3.4 and 3.5). However, relatively higher uncertainties (~20%) for the chosen source water values were observed for the Subtropical and Tropical source waters across all transects within the permanent thermocline, while uncertainties of up to 60% were observed across IO2 within the upper thermocline between 46-48 E (Fig. 3.4). No distinguishable distribution related to the uncertainty of the chosen weight was observed (Fig. 3.5).

4.5. True Oxygen Utilisation and nitrate and phosphate difference in the southwest Indian Ocean

Differences in the observed oxygen, nitrate, and phosphate concentrations relative to those expected from the fractional contributions of the various source waters were calculated from the

OMP analysis results (see Methods 3.3 for details). The results have been classified according to the largest source water contribution (i.e., datapoints are colour coded according to the water source that contributed >40% as per the OMP analysis; Fig. 4.6).

For the IO2 transect, [TOU] averaged 2.9 ± 7.6 μmol.kg^{-1} over the upper thermocline and 1.6 ± 6.9 μmol.kg^{-1} over the permanent thermocline (Fig. 4.6 (a)). The concentrations of $[NO_3^-]_{diff}$ for IO2 were weakly negative (-0.7 ± 1.2 μmol.kg^{-1} over the upper thermocline and -0.3 ± 0.9 μmol.kg^{-1} over the permanent thermocline) and showed a high degree of variability (Fig. 4.6 (b)), while the concentrations of $[PO_4^{3-}]_{diff}$ averaged -0.02 ± 0.07 μmol.kg^{-1} over the upper thermocline and -0.01 ± 0.05 μmol.kg^{-1} over the permanent thermocline and were less variable (Fig. 4.6 (c)). Negative differences of up to 20% for Frac.$[NO_3^-]_{diff}$ and Frac.$[PO_4^{3-}]_{diff}$ were calculated for the IO2 thermocline, with the magnitude of Frac.$[NO_3^-]_{diff}$ being roughly twice that of Frac.$[PO_4^{3-}]_{diff}$ for samples with larger Subtropical contributions (Fig. 4.7 (a-b)). On average, however, the Frac.$[NO_3^-]_{diff}$ and Frac.$[PO_4^{3-}]_{diff}$ were -4 ± 7% and -2 ± 5%, respectively, for the thermocline as a whole.

All three variables were more constrained across IO4, with zero-to-negative concentrations observed near the upper and lower thermocline boundaries (σ_θ <25.5 kg.m^{-3} and >26.5 kg.m^{-3}), and positive maxima of up to ~25 μmol.kg^{-1} for [TOU], ~2 μmol.kg^{-1} for $[NO_3^-]_{diff,}$ and ~1.5 μmol.kg^{-1} for $[PO_4^{3-}]_{diff}$ apparent at σ_θ = 26 kg.m^{-3} (Fig. 4.6 (d-f)). The [TOU] at the lower thermocline boundary was more negative at IO4 than IO2 (as low as -25 versus -10 μmol.kg^{-1}; Fig. 4.6 (d)), with this negative excursion in both transects associated with samples characterized by a >40% Subtropical source water contribution. The Frac.$[NO_3^-]_{diff}$ and Frac.$[PO_4^{3-}]_{diff}$ were greatest at IO4 compared to the other transects, with up to 40% of the total nitrate and 20% of the total phosphate between σ_θ = 25.6 kg.m^{-3} and 26.4 kg.m^{-3} being added between the source regions and the transect (Fig. 4.7 (c-d)). These excesses were most pronounced for the samples with a large Subtropical source water contribution.

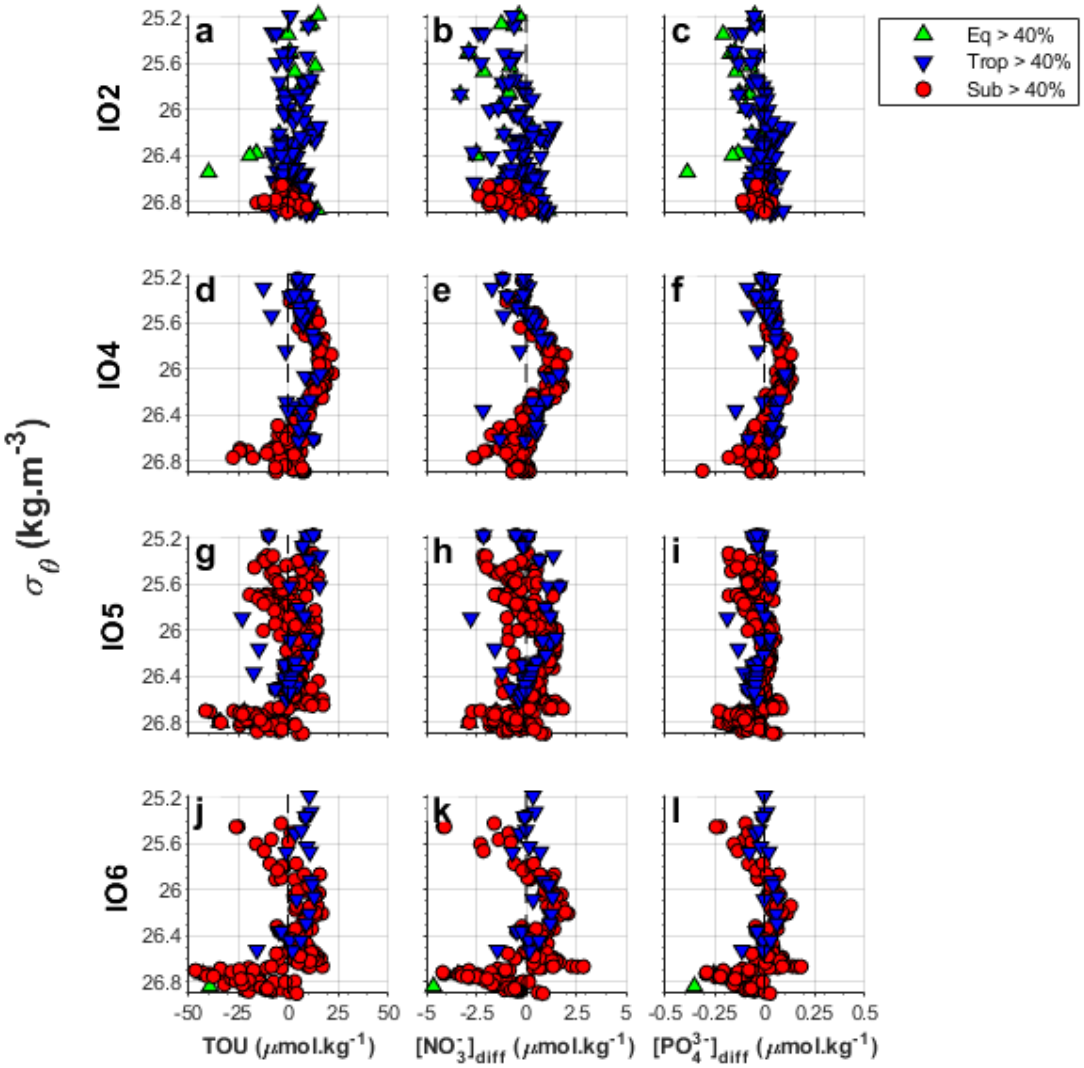

Figure 4.6 Density profiles of true oxygen utilisation ([TOU]) in µmol.kg^{-1} (left panel), nitrate difference ($[NO_3^-]_{diff}$) in µmol.kg^{-1} (centre panel), and phosphate difference ($[PO_4^{3-}]_{diff}$) in µmol.kg^{-1} (right panel) for the thermocline (σ_θ = 25.2-26.9 kg.m^{-3}) for the transects IO2 (a-c), IO4 (d-f), IO5 (g-i), and IO6 (j-l). The dashed vertical black line shows [TOU], $[NO_3^-]_{diff,}$ and $[PO_4^{3-}]_{diff}$ = 0 µmol.kg^{-1} (i.e., no change). Symbol shape and colour indicate source water contributions > 40% (see text for details).

Table 4.1 Estimates of the average [TOU], $[NO_3^-]_{diff}$, and $[PO_4^{3-}]_{diff}$ (in µmol.kg^{-1}) in the entire thermocline (σ_θ = 25.2-26.9 kg.m^{-3}) across each transect. Averages are further subdivided into entire thermocline values, values where the Subtropical fraction is >40%, and values where with the Tropical fraction is >40%.

Transect	**All OMP analysis outputs**			**Subtropical >40%**			**Tropical >40%**		
	[TOU]	$[NO_3^-]_{diff}$	$[PO_4^{3-}]_{diff}$	[TOU]	$[NO_3^-]_{diff}$	$[PO_4^{3-}]_{diff}$	[TOU]	$[NO_3^-]_{diff}$	$[PO_4^{3-}]_{diff}$
IO2	2.1 ± 7.2	-0.5 ± 1.1	-0.02 ± 0.06	-1.2 ± 5.6	-0.9 ± 0.7	-0.02 ± 0.04	3.1 ± 5.8	-0.3 ± 0.9	-0.01 ± 0.05
IO4	5.6 ± 8.5	0.09 ± 0.94	0.02 ± 0.06	5.8 ± 8.7	0.1 ± 1.0	0.02 ± 0.06	6.5 ± 5.7	0.1 ± 0.8	0.02 ± 0.06
IO5	-0.6 ± 10.5	0.06 ± 1.0	-0.03 ± 0.08	-0.4 ± 10.3	0.1 ± 1.0	-0.03 ± 0.08	2.2 ± 9.4	0.1 ± 1.1	-0.01 ± 0.16
IO6	-2.9 ± 19.7	-0.1 ± 1.5	-0.03 ± 0.10	-3.0 ± 20.0	-0.1 ± 1.5	-0.03 ± 0.1	5.4 ± 7.2	0.3 ± 0.7	-0.002 ± 0.05

Table 4.2 Estimates of the average [TOU], $[NO_3^-]_{diff}$, and $[PO_4^{3-}]_{diff}$ (in µmol.kg^{-1}) in the upper (σ_θ = 25.2-26.5 kg.m^{-3}) thermocline across each transect. Averages are further subdivided into entire thermocline values, values where the Subtropical fraction is >40%, and values where with the Tropical fraction is >40%.

Transect	**All OMP analysis outputs**			**Subtropical >40%**			**Tropical >40%**		
	[TOU]	$[NO_3^-]_{diff}$	$[PO_4^{3-}]_{diff}$	[TOU]	$[NO_3^-]_{diff}$	$[PO_4^{3-}]_{diff}$	[TOU]	$[NO_3^-]_{diff}$	$[PO_4^{3-}]_{diff}$
IO2	2.9 ± 7.6	-0.7 ± 1.2	-0.02 ± 0.07	N/A	N/A	N/A	3.3 ± 6.8	-0.5 ± 1.1	-0.01 ± 0.06
IO4	10 ± 6.3	0.5 ± 0.8	0.05 ± 0.05	11.4 ± 5.6	0.7 ± 0.7	0.06 ± 0.04	6.3 ± 6.1	0.1 ± 0.8	0.02 ± 0.05
IO5	1.8 ± 7.8	0.2 ± 0.9	-0.03 ± 0.05	2.0 ± 7.2	0.22 ± 0.9	-0.03 ± 0.05	2.6 ± 9.9	0.3 ± 1.1	-0.03 ± 0.06
IO6	4.4 ± 8.8	0.4 ± 1.2	0.04 ± 0.07	4.1 ± 9.2	0.4 ± 1.2	0.01 ± 0.07	6.5 ± 5.6	0.4 ± 0.6	0.01 ± 0.04

Table 4.3 Estimates of the average [TOU], $[NO_3^-]_{diff,}$ and $[PO_4^{3-}]_{diff}$ (in µmol.kg^{-1}) in the permanent (σ_θ = 26.5-26.9 kg.m^{-3}) across each transect. Averages are further subdivided into entire thermocline values, values where the Subtropical fraction is >40%, and values where the Tropical fraction is >40%.

Transect	All OMP analysis outputs			Subtropical >40%			Tropical >40%		
	[TOU]	$[NO_3^-]_{diff}$	$[PO_4^{3-}]_{diff}$	[TOU]	$[NO_3^-]_{diff}$	$[PO_4^{3-}]_{diff}$	[TOU]	$[NO_3^-]_{diff}$	$[PO_4^{3-}]_{diff}$
IO2	1.6 ± 6.9	-0.4 ± 0.9	-0.01 ±0 .05	-1.2 ± 5.6	-0.9 ± 0.7	-0.03 ± 0.04	2.9 ± 5	-0.1 ± 0.7	-0.01 ± 0.03
IO4	-0.3 ± 7.3	-0.5 ± 0.8	-0.02 ± 0.05	-0.4 ± 7.3	-0.5 ± 0.8	-0.02 ± 0.05	7.7 ± 3.5	-0.1 ± 0.9	0.01 ± 0.06
IO5	-4.9 ± 13	-0.2 ± 1.1	-0.03 ± 0.10	-4.9 ± 13.0	-0.2 ± 1.1	-0.04 ± 0.11	-1.5 ± 3.3	-0.4 ± 0.3	0.16 ± 0.42
IO6	-9.1 ± 24.0	-0.6 ± 1.6	-0.06 ± 0.11	-8.6 ± 24.1	-0.6 ± 1.6	-0.05 ± 0.11	-6.6 ± 12.6	-0.6 ± 1.1	-0.06 ± 0.08

The trends in [TOU], $[NO_3^-]_{diff,}$ and $[PO_4^{3-}]_{diff}$ were very similar for IO5 and IO6. On average, [TOU], $[NO_3^-]_{diff,}$ and $[PO_4^{3-}]_{diff}$ were -0.6 ± 10.5 µmol.kg^{-1}, 0.06 ± 1.0 µmol.kg$^{-1,}$ and -0.03 ± 0.08 µmol.kg^{-1}, respectively, for IO5 and -2.9 ± 19.7 µmol.kg^{-1}, -0.1 ± 1.5 µmol.kg$^{-1,}$ and -0.03 ± 0.10 µmol.kg^{-1}, respectively, for IO6 (Table 4.1). Negative differences were calculated above σ_θ = 26 kg.m^{-3} and below σ_θ = 26.7 kg.m^{-3}, typically associated with a large Subtropical source water contribution (Fig. 4.6 (g-l)). The latter shift from positive to negative values occurred abruptly and resulted in the most negative values of [TOU] (as low as -50 µmol.kg^{-1}) for the IO5 and IO6 transects, at σ_θ >26.7 kg.m^{-3} (Fig. 4.6 (g and k)). All parameters were positive below σ_θ = 25.8 kg.m^{-3} to the top of the permanent thermocline. Similar features were observed in $[NO_3^-]_{diff}$ and $[PO_4^{3-}]_{diff}$. Within the upper thermocline (σ_θ = 25.2-26 kg.m^{-3}), up to 40% of both the nitrate and phosphate was apparently lost between the source regions and the Agulhas transects, with a greater loss computed for IO5 (Fig. 4.7 (e-h)). In the upper thermocline below σ_θ = 26 kg.m^{-3}, $[NO_3^-]_{diff}$ and $[PO_4^{3-}]_{diff}$ were positive at both IO5 and IO6. For IO5, the Frac.$[NO_3^-]_{diff}$ maximum at σ_θ = 26 kg.m^{-3} (~40%) was approximately twice that of Frac.$[PO_4^{3-}]_{diff}$ (Fig. 4.7 (e) and (f)) while the fractions of total nitrate and phosphate were very similar for IO6 (Fig. 4.7 (g) and (h)).

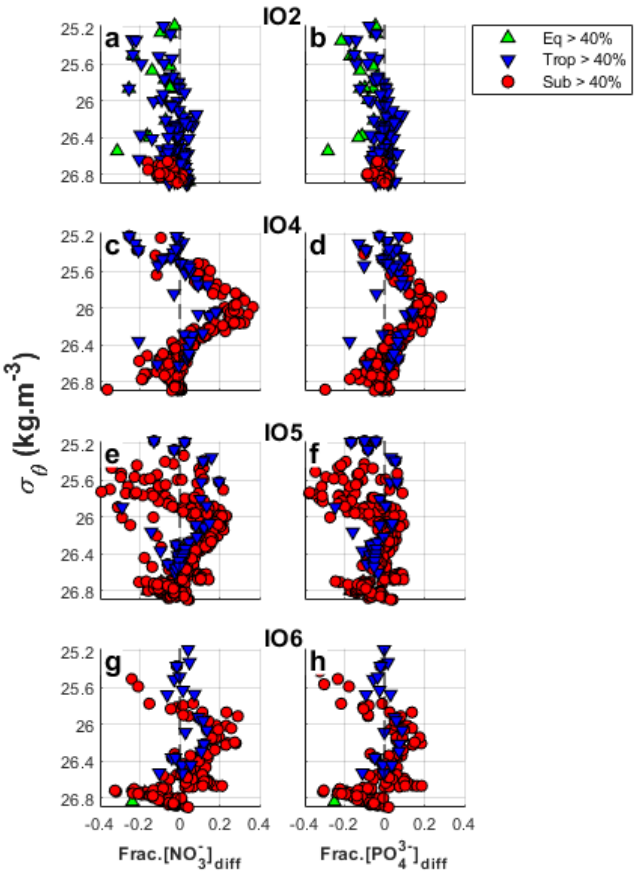

Figure 4.7 Density profiles of the fraction of nitrate (Frac.[NO_3^-]$_{diff}$; left panel) and phosphate (Frac.[PO_4^{3-}]$_{diff}$; right panel) difference in the thermocline (σ_θ = 25.2-26.9 kg.m^{-3}) for the transects IO2 (a-b), IO4 (c-d), IO5 (e-f), and IO6 (g-h) (see Methods for details). The dashed vertical black line shows Frac.[NO_3^-]$_{diff}$ and Frac.[PO_4^{3-}]$_{diff}$ = 0 (i.e., no change). Symbol shape and colour indicate source water contributions >40% (see text for details).

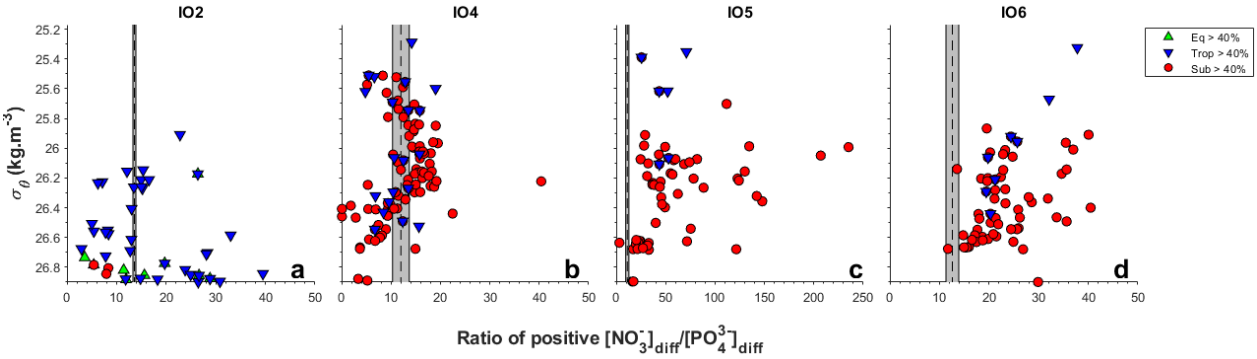

Figure 4.8 Density profiles of the ratio of [NO_3^-]$_{diff}$ to [PO_4^{3-}]$_{diff}$ in the thermocline (σ_θ = 25.2-26.9 kg.m^{-3}) for all samples with positive values of [NO_3^-]$_{diff}$ and [PO_4^{3-}]$_{diff}$ for the transects IO2 (a), IO4 (b), IO5 (c), and IO6 (d). The dashed vertical black line shows the average [NO_3^-]$_{back}$: [PO_4^{3-}]$_{back}$ ratio for each transect, with the grey box indicating the associated standard deviation. These values are as follows – IO2: 13.6 ± 0.3; IO4: 12 ± 1.7; IO5: 11.7 ± 1.6; and IO6: 12.6 ± 1.2. Symbol shape and colour indicate source water contributions >40% (see text for details). Note, the maximum value for the x-axes for IO2, IO4, and IO6 is 50, while for IO5 it is 200.

The ratios of the positive $[NO_3^-]_{diff}$ and $[PO_4^{3-}]_{diff}$ concentrations were calculated for all transects and are shown in Figure 4.8. Because only positive concentrations were used, the bulk of the data are for the mid-thermocline. The average $[NO_3^-]_{diff}$: $[PO_4^{3-}]_{diff}$ ratios for the upper and permanent thermocline are presented in Table 4.4. These were calculated by weighting the ratios computed for each sample by the measured phosphate concentration for that sample. For IO2, an average $[NO_3^-]_{diff}$: $[PO_4^{3-}]_{diff}$ ratio of 15 ± 6 was obtained for the range of σ_θ = 26-26.5 kg.m^{-3}, while for σ_θ >26.5 kg.m^{-3}, the ratios were more variable and averaged 21 ± 17 (Fig. 4.8 (a)). Within the former range, the averaged value was similar to that of the $[NO_3^-]_{back}$: $[PO_4^{3-}]_{back}$ ratio (13.6 ± 0.3; calculated using equation 3.6). The IO4 transect was unique in that ratios were attainable for the upper thermocline (up to σ_θ = 25.3 kg.m^{-3}; Fig. 4.8 (b)). Furthermore, the sample ratios exceeded the $[NO_3^-]_{back}$: $[PO_4^{3-}]_{back}$ ratio of 12 ± 1.7 between σ_θ = 25.8-26.4 kg.m^{-3} such that the averages for the upper thermocline were higher than for the permanent thermocline (13 ± 5 and 7 ± 4, respectively).

Table 4.4 Estimates of the average positive $[NO_3^-]_{diff}$ to $[PO_4^{3-}]_{diff}$ ratio in the upper (σ_θ = 25.2-26.5 kg.m^{-3}) and permanent thermocline (σ_θ = 26.5-26.9 kg.m^{-3}) across each transect.

Transect	**$[NO_3^-]_{diff}$: $[PO_4^{3-}]_{diff}$ ratio**	
	Upper thermocline (σ_θ = 25.2-26.5 kg.m^{-3})	Permanent thermocline (σ_θ = 26.5-26.9 kg.m^{-3})
IO2	15 ± 6	21 ± 17
IO4	13 ± 5	7 ± 4
IO5	67 ± 62	27 ± 16
IO6	27 ± 11	23 ± 11

IO5 was characterized by the largest variability in the $[NO_3^-]_{diff}$: $[PO_4^{3-}]_{diff}$ ratio (Fig. 4.8 (c)). Values of up to 250:1 and an average of 67 ± 62 were observed within the upper thermocline, while samples in the permanent thermocline were relatively more clustered, with an average ratio of 27 ± 16 (Table 4.4). Both Tropical- and Subtropical-sourced samples were characterized by these high $[NO_3^-]_{diff}$: $[PO_4^{3-}]_{diff}$ ratios, although the highest values were associated with the Subtropical source waters. The ratio distribution for IO6 was similar to that of IO5, although the range of values computed for IO6 was considerably narrower, with averages of 27 ± 11 and 23 ±

11 for the upper and permanent thermoclines, respectively (Fig. 4.8 (d)). For both IO5 and IO6, the sample ratios were higher than the average $[NO_3^-]_{back} : [PO_4^{3-}]_{back}$ ratios (11.7 ± 1.6 and 12.6 ± 1.3, respectively).

5. Discussion

5.1. Is this a valid approach?

In this study, an optimum multiparameter (OMP) analysis was applied to resolve thermocline water contributions to the Mozambique Channel and adjacent Agulhas Current System. This approach allowed for a quantitative assessment of the hydrography and biogeochemistry of the region, building on earlier qualitative assessments undertaken by Di Marco *et al*. (2002) and Donohue & Toole (2003). Early applications of OMP analysis evaluated changes to water mass properties relative to those set at the water-mass formation regions, and hence were applied at the basin-scale (e.g., You & Tomczak, 1992; Poole & Tomczak, 1999; Jenkins *et al*. 2015; Peters *et al*., 2018 (a)). However, the OMP analysis approach can also be applied regionally, meaning that changes to water mass properties can be diagnosed relative to (proximate) locations that are representative of the source waters to the region of interest. An example of a local application of OMP analyses is the work of Peters *et al*. (2018 (b)), who aimed to quantify the pathways of fixed nitrogen loss in the eastern tropical South Pacific using various methods including an OMP analysis.

One limitation of the regional OMP analysis approach is the subjectivity associated with the selection of source regions. While effort is made to reduce subjectivity (by means of cluster analyses, testing of the weights, and Monte Carlo simulations), a degree of subjectivity is inherent to the decision-making related to the specific study goals (You & Tomczak, 1997). Nonetheless, You & Tomczak (1992) note that while OMP analyses may not produce water mass fractions as accurately as other inverse modelling techniques despite yielding low residuals, the results can be meaningful if interpreted in the context of known oceanographic features and processes. In other words, changes should only be interpreted as relative to the predefined source regions.

In this study, regional circulation and water masses were not the sole considerations in defining the source water types as the number of source water types m could not exceed the number of mixing equations n (Tomczak, 1981). The properties, nitrate and phosphate, were intentionally excluded from the analysis (to allow for their interpretation following the diagnosis of the fractional water type contributions), such that only three water type properties (i.e., potential

temperature, salinity, and silicate concentration) and the mass conservation equation could be used to constrain the system (i.e., $n = 4$), which limited the number of source water types to three. That said, applying the *thermocline array* approach (which assumes that diapycnal mixing across the highly discretized density range is weak due to stratification within the thermocline; Jenkins et al., 2015) to a narrow density range excluded the intermediate and deep water masses, thus reducing the number of potential source water types required. The decision to define the source water types as source regions to the Mozambique Channel (instead of as water masses) provided two advantages. Firstly, the dynamical and complex thermocline structure within the channel was fully resolved as the source water types accounted for all the variability in the sample data (Fig. 2.2 and 2.3), as indicated by no unresolved water masses and low residuals. Secondly, since the various water masses that characterize a single source region were combined and treated as a single source water type, the number of source water types could be limited to three. This meant that three constraints were sufficient to set up an overdetermined system of equations. Moreover, the exclusion of nitrate and phosphate as constraints allowed for later analyses of both nutrient cycles without having to assume a constant N:P stoichiometry (e.g., the ratio in which nitrate and phosphate were added to the thermocline between the source and sample regions could be calculated; see section 5.5 below).

Two Monte Carlo analyses were conducted to test the sensitivity of the OMP analysis to the chosen source water values and the chosen weights (Fig. 3.4 and 3.5). These exercises revealed that the water mass fractions more sensitive to the chosen source water values (up to 50%) than to the chosen weights (less than 5%). The OMPA output being more sensitive to the chosen source water types than the weights was similarly observed by Peters *et al*. (2017a) in their study of the Eastern Pacific. Furthermore, the higher standard deviation percentages of the Equatorial source water appear to correlate with the residual distribution across the eastern upper thermocline of IO2 (Fig. 3.4 (i)) which further testifies to the important of the chosen source waters. Therefore, the uncertainties in the Equatorial source waters need to be taken into consideration when interpreting the resulting source water fractions across IO2 (Section 5.2.1). However, the small contribution of this source water across all the transects signifies that the interpretations of biogeochemical processes occurring in the region can be made with confidence.

5.2. Regimes of the Mozambique Channel

5.2.1. Sources to the northern Mozambique Channel

The IO2 transect, at the northern end of the Mozambique Channel, was the most heterogeneous of the four transects investigated, likely because it is located at the confluence of various western Indian Ocean flow regimes. The SEC that flows around the northern tip of Madagascar introduces waters of tropical origin to the channel entrance that occupy much (60-80%) of the upper thermocline, down to a depth of 300 m (Fig. 4.3 (b)). Elevated silicate concentrations in the upper thermocline (of up to 15 $\mu mol.kg^{-1}$; Fig. 4.2 (a)) led to the OMP analysis attributing this layer to the Tropical source water. This diagnosis is consistent with the work of Di Marco *et al*. (2002), who inferred similar flow features for the same transect.

The observation of Subtropical source water cores within the permanent thermocline of IO2 was noted by Di Marco *et al*. (2002), but not described in detail. In T-S space, the central and mode waters that occupy this density range are indistinguishable, which has led to disagreements as to the mode water's definition (Di Marco *et al*., 2002; de Ruijter *et al*., 2002; Donohue & Toole, 2003), with inferences relegated to a comment on the linearity of the T-S relationship. The high oxygen/low nutrient features clearly differentiate these Subtropical mode waters from the rest of the thermocline, a distinction that would not have been as obvious if only temperature and salinity were investigated (Fig. 4.2 (b), (f) and (j)). Additionally, the depth variation of the lower thermocline boundary (σ_θ = 26.9 $kg.m^{-3}$), which deepens by almost 200 m near the Madagascan coast, can be linked to the intrusion of higher density, higher silicate water masses into a relatively warm, low density tropical regime at the north-eastern end of the channel. The inclusion of silicate as one of the OMP analysis constraints was therefore key for differentiating the sources to the thermocline of the northern Mozambique Channel.

The meridional section of the IO2 transect offers a two-dimensional perspective on the circulation in the region, showing the westward branch of the SEC as it rounds Madagascar and its continuation as the northward-flowing EACC along the East African coast (Swallow *et al*., 1991; Di Marco *et al*., 2002). Coincident with the SEC and EACC, the OMP analysis attributes large fractions (of up to 80%) of the permanent thermocline to the Subtropical source water (Fig. 4.3 (a)). The high Subtropical fractions within the northern Mozambique Channel are consistent with the work of You & Tomczak (1992) who define Indian Central Water (ICW) as a "subtropical"

source water, and show using a model the transport of this subtropical source water into the northern Indian Ocean along the western boundary.

The coincidence of relatively high residuals (up to 4%) and Equatorial source water uncertainties (up to 50%) at the upper limit of the thermocline between 46-48 E can be further related to lower T-S values at the upper limit of the thermocline to that of the Equatorial source water. This unaccounted for water mass could be the result of the seasonality of the north-eastern Mozambique Channel, which was shown to vary in water properties throughout the year by the likes of You (1997), Di Marco *et al*. (2002) and Schouten *et al*. (2003). Since this study did not account for this seasonality and averaged according to a single cruise (i.e. WOCE IO7N from 23 April-6 June 2018), it stands to reason that additional water mass/es can be found within the region. Furthermore, studies such Resplandy *et al*. (2009) and Dilmahamod *et al*. (2016) have investigated the effects of the Seychelles-Chagos Thermocline Ridge (SCTR) on both the physical and biogeochemical properties of the upper ocean within the region. The SCTR is associated with localised open ocean upwelling, however, the extent or lack thereof are influenced at the intra and interseasonal spatial and time scales (Resplandy *et al*., 2009; Dilmahamod *et al*., 2016). The undescribed water mass near the Madagascan coastline may be the result of the variability of this feature, which suggests that these processes need to be taken into account if a more in depth study is undertaken.

5.2.2. Sources to the southern Mozambique Channel

The thermocline distribution for the IO4 transect across the southern end of the Mozambique Channel is quite different from that of IO2, in contrast to expectations based on the literature, which suggest consistent (but variable) full-depth flows from the north to the south of the channel (Di Marco *et al*., 2002; de Ruijter *et al*., 2002; Donohue & Toole, 2003; de Ruijter *et al*., 2006). Instead, the Subtropical source water dominated the entire thermocline of IO4, with a Tropical contribution near the western continental slope and patchy distributions at the upper thermocline boundary and at the mid-thermocline level (Fig. 4.3 (b) and (f)). Di Marco *et al*. (2002) suggested that the subtropical cores at the northern end of the channel evince southward flow through the channel; however, the dominance of Subtropical waters across the southern end of the Mozambique Channel suggest that two different regimes dominate either end of the channel, with

limited communication of Tropical and Equatorial water masses from the north to the south. Potential northward transport of southerly mode waters into the channel along the western boundary of Madagascar and East Africa was not clearly evident. This latter interpretation was noted by Grundlingh (1993), Di Marco *et al*. (2002), and de Ruijter *et al*. (2002), although there is some disagreement among the authors as to the nature of the transport (see section 5.3 and 5.4 below).

5.2.3. Flow pathways of Subantarctic Mode Water

An unexpected outcome of this regional OMP analysis is the ability to trace SAMW circulation in the southwest Indian Ocean's permanent thermocline and to link the source water distributions in the permanent thermocline with different pathways of SAMW. Across all four transects, Subtropical water [TOU], $[NO_3^-]_{diff}$, and $[PO_4^{3-}]_{diff}$ are negative between σ_θ = 26.5 and 26.9 kg.m^{-3} (i.e., higher oxygen and lower nitrate and phosphate concentrations than expected based on the source water contributions), with the degree to which these parameters are negative typically increasing with latitude (Fig. 4.6; Table 4.1). Negative [TOU], $[NO_3^-]_{diff}$, and $[PO_4^{3-}]_{diff}$ can result from mixing with high oxygen/low nutrient waters in the permanent thermocline, downwelling of the overlying surface waters, or upwelling of intermediate waters (specifically RSW; Talley *et al*., 2011). Another possibility is an unaccounted for water mass in the region that has the same temperature, salinity and silicate properties as the defined source waters, but higher oxygen and lower nutrient concentrations. This water could be a form of "younger" SAMW that has had less time to accumulate the signals of remineralization than the waters observed in the source region along IO7. By contrast, Tropical water in the permanent thermocline (the contribution of which is low), particularly to the south of IO2, typically has a positive [TOU], $[NO_3^-]_{diff}$, and $[PO_4^{3-}]_{diff}$ (i.e., lower oxygen and higher nitrate and phosphate concentrations than expected). Positive [TOU], $[NO_3^-]_{diff}$, and $[PO_4^{3-}]_{diff}$ can also be a result of mixing, in this case with low oxygen/high nutrient waters possibly coming from the northern basin, or from in situ remineralization processes that consume oxygen and release nutrients into the water column.

The slightly positive Tropical water [TOU], $[NO_3^-]_{diff,}$ and $[PO_4^{3-}]_{diff}$ values across the IO2 permanent thermocline (blue data in Fig. 4.6 (a-c) and Table 4.1) may be linked to the inclusion of ITF with SAMW, as ITF water is a mixture of aged waters from the western Pacific (Talley *et*

al., 2011). The circulation required to transport ITF waters to the northern end of the channel implies that the Tropical waters could also carry SEISAMW (see literature review), which has travelled a greater distance through the subtropical gyre circulation in conjunction with the SEC (and is thus ITF-influenced) relative to SAMW supplied directly by the ACC (Beal *et al*., 2006). This finding is consistent with the likes of Song *et al*. (2004) and *Beal et al*. (2006), where (ITF-influenced) SEISAMW is carried to the Agulhas system via the SEC and Mozambique Channel. The slightly negative Subtropical water [TOU], $[NO_3^-]_{diff}$, and $[PO_4^{3-}]_{diff}$ values across the IO2 permanent thermocline (red data in Fig. 4.6 (a-c) and Table 4.1) suggest that the source region selected for the Subtropical waters (i.e., 27-30°S along IO7 at 55°E) is located east of the SAMW source that enters the northern channel. This implies that SAMW within the Subtropical waters is supplied to the northern end of the channel via a northward transport between IO7N at ~55°E and Madagascar at ~50°E. A similar inference was made in the OMP analysis study by You & Tomczak (1993), which highlighted the northwards transport of their model defined *Indian Central Water* (ICW; inclusive of SAMW) along the western boundary of the Indian Ocean.

The Agulhas transects, IO5 and IO6, are characterized by more negative values of [TOU], $[NO_3^-]_{diff}$, and $[PO_4^{3-}]_{diff}$ for σ_θ = 26.5-26.9 kg.m^{-3}, and lower Tropical water contributions than the Mozambique Channel transects (Fig. 4.6 (g-l) and Table 4.1). Here, Subtropical waters are relatively higher in oxygen and lower in nutrients than expected (i.e., compared to the version found at the Subtropical source region along IO7; Fig. 3.2). This finding suggests that the mode waters in the Agulhas system could be directly supplied by SAMW formed within the SAZ (Beal *et al*., 2006), as the distance between the ACC and the Agulhas system is relatively short. This allows less time for remineralization products to accumulate, such that SAMW retains relatively high oxygen and low nitrate and phosphate concentrations compared to the mode waters first circulating through the subtropical gyre. This idea is consistent with the works of Fine (1993), Beal *et al*. (2006) and Koch-Larrouy (2010) in that the source of SAMW in the Agulhas Current System is directly supplied from the ACC. Another possible explanation for the negative values could be that the OMP analysis does not fully encapsulate the properties of the mode water found in the Agulhas region, given that the Agulhas transects are characterised by the largest residuals in the permanent thermocline (Fig. 4.5). Indeed, another mode water mass is present in the Agulhas system, STMW (see literature review); however, this water mass occurs at a lower density in the

thermocline (σ_θ = 26 kg.m^{-3}) and is far less pervasive than SAMW (Toole & Warren, 1993; Hanawa & Talley, 2001) such that it cannot account for the entire negative deviation in [TOU], $[NO_3^-]_{diff}$, and $[PO_4^{3-}]_{diff}$. It is instead more likely that a "younger" type of SAMW, supplied directly from the ACC to the Agulhas Current System (Fine, 1993; Beal *et al*., 2006), can explain the negative [TOU], $[NO_3^-]_{diff}$, and $[PO_4^{3-}]_{diff}$ computed for Subtropical waters in the permanent thermocline of IO5 and IO6.

Despite the net northward flow of SAMW from its primary formation region, the different pathways highlighted here suggest that SAMW does not move as a unified layer. Instead, three pathways are surmised within the western Indian Ocean: two pathways of "pure" SAMW that is formed within the southwestern Indian Ocean, one directly entering the Agulhas Current System and the other the northern Mozambique Channel, and ITF-influenced SEISAMW entering the northern Mozambique Channel via the SEC (Fig. 5.1). You (1997) (in their OMP analysis), Fine (1993), Song *et al*. (2004) and Beal *et al*. (2006) (based on hydrographical data) studied the various northward pathways for central and mode waters in the Indian Ocean. All confirm the basin-wide subtropical gyre circulation of "older" SEISAMW, and the hydrography-based studies confirm the more direct route for "younger" SAMW into the Agulhas Current System, which was observed in the Tropical and Subtropical waters, respectively, in this study.

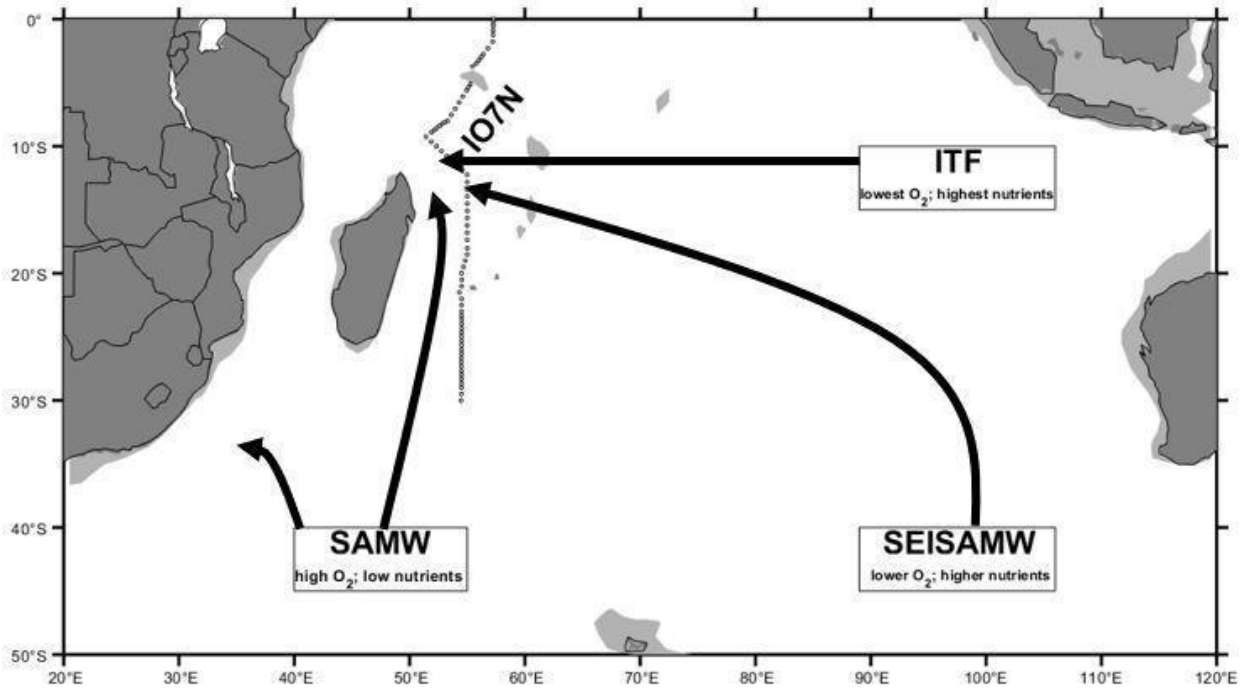

Figure 5.1 Schematic showing the hypothesised flow pathways of mode waters within the southern Indian Ocean, as well as their differentiating oxygen and nutrient properties. The sources depicted are *Subantarctic Mode Water* (SAMW), *Southeast Indian Subantarctic Mode Water* (SEISAMW), and *Indonesian Throughflow* (ITF). The IO7N transect, which was used to designate the source regions to the Mozambique Channel, is also shown.

5.3. The role of eddies in the Mozambique Channel

Flow within the Mozambique Channel is highly variable and strongly influenced by mesoscale activity in the form of southward-propagating anticyclonic eddies (Ridderinkhof & de Ruijter, 2003; Schouten *et al*., 2003; Swart *et al*., 2010). These eddies have a significant influence on the regional thermocline due to physical forcings such as surface intensification, penetrate the entire water column, and retain anomalous water masses along their propagation pathways (de Ruijter *et al*., 2002; Swart *et al*., 2010). Therefore, examining altimetry data (such as sea level anomalies, see Fig. 5.2), which can reveal eddy features expressed at the surface, is useful for linking mesoscale activity to observed variability in the thermocline.

Shoaling isopycnals and associated water properties at the southern end of the channel capture the dynamics associated with such eddies particularly well. IO4 was characterized by intensive eddy activity at the time of sampling, with both positive and negative SLA anomalies evident in the altimetry data (Fig. 5.2 (b)). The transect was dominated by a positive anomaly between 37-41°E, while small negative anomalies were observed at 36°E and 42°E. The association of the latter anomalies with cyclonic eddies is equivocal, with de Ruijter *et al*. (2002) attributing similar features to artifacts in data processing and Schouten *et al*. (2003) suggesting that a positive signal is left in the mean sea level height (MSLH) as a result of the frequent passage of anticyclonic eddies, resulting in the SLA characterising “non-anticyclonic” features as negative anomalies. However, the doming of the isopycnals at these localities denotes the presence of cyclonic eddies, which appear to affect both the physical and biogeochemical property distribution in the thermocline (IO4 column of Fig. 4.1 and 4.2). Cyclonic eddies within the channel have been noted by the likes of Tew Kai & Marsac (2010) and Halo *et al*. (2014).

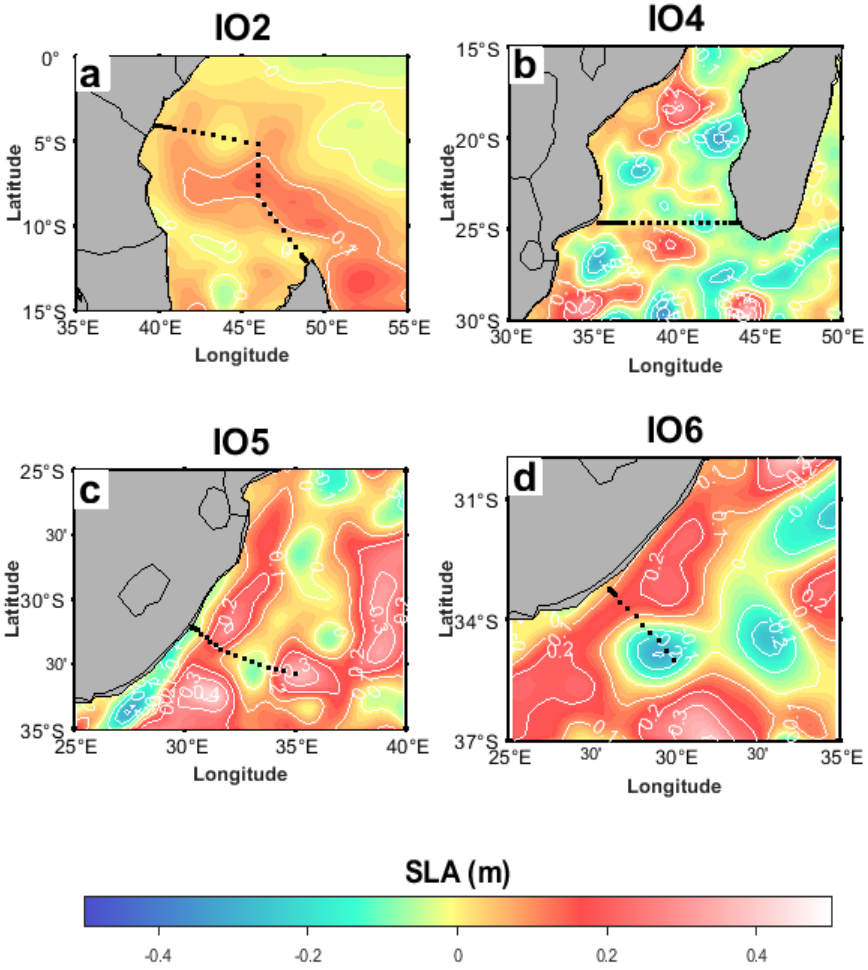

Figure 5.2 Time-mean Sea Level Anomaly (SLA; in metres) during the period of each WOCE cruise: (a) IO2 during 14-21 January 1996, (b) IO4 during 15-19 June 1995, (c) IO5 on the 24 March 2009, and (d) IO6 during 6-10 February 2008. Each transect is demarcated by the black circles. Data retrieved from AVISO (https://www.aviso.altimetry.fr/).

Ekman suction is the mechanism typically associated with cyclonic eddies, bringing nutrient-rich waters to the upper ocean and leading to enhanced productivity (McGillicuddy, 2016). While the low oxygen/high nutrient cores observed in the cyclonic eddies (Fig. 4.1 (j) and IO4 column of Fig. 4.2) are consistent with such a mechanism, the OMP analysis results suggest otherwise, with a large Tropical source water fraction (up to 60%) associated with the cyclonic eddies (Fig. 4.3 (f)). The spatial extent of the Tropical distribution evidences the retention and transport of northern water masses through the channel, a feature noted by Donohue & Toole (2003) for the same transect. Moreover, a small contribution (20%) of Equatorial water was observed at the lower thermocline boundary at 36°E (Fig. 4.4 (j)). Since this source water has the northernmost provenance of the three considered here, its intermediate water mass will be RSW (i.e., high

salinity and low oxygen/high nutrients; Fig. 3.2; green line). Upwelling of RSW as an intrusion into the permanent thermocline can be linked to the bottom-reaching depth scale of Mozambique Channel eddies, as well as their ability to retain the water masses (and thus water properties) of their formation regions (de Ruijter *et al*., 2002; Swart *et al*., 2010). Anticyclonic eddies were previously postulated to be the primary mechanism of transport in the channel, transporting anomalously warm and saline water masses southwards and thus contributing to the strong heat and salt fluxes of the Agulhas Current System (Swart *et al*., 2010). The results presented here suggest that cyclonic eddies may also play a role in Tropical water transport.

The implications of these cyclonic eddies for surface ocean productivity are important. At first glance, the dominance of the Subtropical source water across IO4 implies a high level of similarity to the source region and hence little to no change in the biogeochemical properties between source and sampled regions. However, large positive deviations in both $[NO_3^-]_{diff}$ and $[PO_4^{3-}]_{diff}$ are apparent at a density of σ_θ = 26 kg.m^{-3} (Fig. 4.6 (d-f)), indicating the addition of nutrients to the upper thermocline. Furthermore, the fractions of $[NO_3^-]_{diff}$ and $[PO_4^{3-}]_{diff}$ relative to the total nitrate and phosphate pools, of up to 40% and 20%, respectively (Fig. 4.7 (c-d)), strongly suggest enhanced productivity insofar as high rates of surface production will yield an elevated flux of OM to the subsurface that is then remineralized by heterotrophic (i.e., oxygen-consuming) bacteria to yield regenerated nutrients. The enhancement of surface productivity is likely driven by an increased nutrient supply associated with the physical forcings of the eddies, including upwelling and downwelling of the regional thermocline (Kolasinski *et al*., 2012), eddy-dipole interactions (Roberts *et al*., 2014), and the entrainment of productive coastal waters (Quartly & Srokosz, 2004; Tew-Kai & Marsac, 2009; José *et al*., 2013).

5.4. Tracing the tropics

5.4.1. Thermocline features

The distribution of Tropical waters in the Agulhas Current transects yields insights into how these waters enter the system. Although patchy, Tropical source waters contributed up to 60% (mean of ~30%) of the upper thermocline waters across the IO5 and IO6 transects, particularly near the coast at 31.25°E and 33.2°S, respectively (Fig. 4.3 (g-h) and 4.4 (c-d)). These results are consistent with the work of Beal *et al*. (2006), who found that waters along the inshore edge of the Agulhas Current core derive from the northern and equatorial Indian Ocean (Tropical origin in the present study). Beal *et al*. (2006) also found that the waters offshore of the current core predominantly derive from the subtropical Indian Ocean and Southern Ocean. While the OMP analysis results are largely consistent with this notion, large Tropical water fractions (of up to 60%) are also observed in the offshore waters (Fig. 4.3 (g-h)).

The incidences of Tropical source water offshore of the Agulhas Current appear to coincide with local sea level anomalies (SLA; Fig. 5.2 (c-d)). Across IO5 and IO6, a positive SLA (~0.1 m), was observed spanning the along-stream length of the Agulhas Current (Fig. 5.2 (c-d)). This anomaly is a permanent feature associated with the current being in geostrophic balance (Beal & Bryden, 1999). A positive SLA (>0.2 m) was also observed at 31.2°E along the IO5 transect (Fig. 5.2 (c)). This particular SLA coincides with the increased Tropical water fraction at 31.2°E (Fig. 4.3 (g)). Coincident with this positive SLA is an upwelling feature (<500 m) in the upper thermocline (likely associated with the high friction edge of an anticyclone), evident in both temperature and salinity (Fig. 4.1 (c) and (g)), as well as in the lower oxygen and higher nutrient concentrations (Fig. 4.1 (k) and the IO5 column of Fig. 4.2).

Furthermore, in IO6, a negative SLA anomaly (< -0.1 m), typically indicative of cyclonic motion and upwelling, was observed centred at 34.8°S (Fig 5.2 (d)). A coincident increase in the Tropical source water fraction at the same latitude (Fig. 4.3 (h)) and the domed isopycnals (IO6 column of Fig. 4.1) suggests that this cyclonic eddy transported Tropical waters into the Agulhas system. The coincidence of offshore Tropical waters with a negative SLA supports the existing hypothesis that Tropical waters enter the Agulhas system via eddies (Roman & Lutjeharms, 2009; Swart *et al*., 2010).

The negative Subtropical water [TOU], $[NO_3^-]_{diff,}$ and $[PO_4^{3-}]_{diff}$ values for σ_θ <26 kg.m^{-3} in IO6 (red data in Fig. 4.6 (j-l)) can be attributed to a "younger" version of STSW than that found in the Subtropical source region along IO7 since nutrients accumulate less in a younger water mass. The transition to the SAMW-dominated permanent thermocline is clearly visible as an increase in the Subtropical source water fraction below σ_θ = 26.5 kg.m^{-3} (Fig. 4.4 (c-d)). Combined with the observations from σ_θ <26 kg.m^{-3}, this results in a Tropical water mass that appears sandwiched between the subducting STSW of the subtropical gyre and the laterally-spreading SAMW in the permanent thermocline.

An interesting result of the OMP analysis is the diagnosis of Tropical source waters spread across the mid-thermocline (σ_θ = 26.5 kg.m^{-3}) of both the Agulhas Current System transects (Fig. 4.3 (g-h) and 4.4 (c-d)). No clear features were observed in the physical and biogeochemical sections of these transects coincident with these putative Tropical waters (IO5 and IO6 columns of Fig. 4.1 and 4.2).

5.4.2. Features of the northern Indian Ocean

As outlined in the literature review, *Red Sea Water* (RSW) is distinguished from *Antarctic Intermediate Water* (AAIW) by its elevated salinity and silicate concentration. For IO4 and both the Agulhas transects, the shoaling of isopycnals near the southern African coast introduces RSW into the thermocline, evident as an intrusion of Equatorial source waters (Fig. 4.3 (k-l)), reaching fractions of up to 40% (Fig. 4.4 (c-d)). Beal *et al*. (2006) observed that northern and equatorial Indian water masses (such as RSW) are found inshore of the core of the Agulhas Current, remaining separated from the offshore water masses by the high cross-stream gradient of potential vorticity and the kinematic steering of the current at intermediate depths. However, patchy distributions of Equatorial source waters were observed across the entire IO5 and IO6 transects in the present study, suggesting that RSW occurs offshore of the current as well, albeit in lesser quantities than inshore. Even though intermediate waters were not included in the OMP analysis, the signature of RSW in the thermocline is evidence of the deep-reaching nature of regional mesoscale features and their ability to mix sub-thermocline waters into the thermocline. Similar results were obtained by Roman & Lutjeharms (2007; 2009) by way of OMP analyses. These authors observed the discontinuous nature of RSW flow and commented on its association with

mesoscale features such as Mozambique Channel eddies and Agulhas Rings, noting that both anticyclonic and cyclonic eddies are responsible for its transport. The relatively small Equatorial source water fractions obtained by the OMP analysis conducted here made it difficult to derive relative changes in the biogeochemistry of these waters as any such signals were likely masked by the dominance of the Subtropical source water fraction. A separate study within the intermediate water mass range would allow for the estimation of biogeochemical changes within the RSW and AAIW water masses of the southwest Indian Ocean.

5.5. Evidence of biogeochemical changes

5.5.1. Insights from $[NO_3^-]_{diff}$: $[PO_4^{3-}]_{diff}$

The Mozambique Channel has been identified by both a modelling study (Wang *et al*., 2019) and observations (Poultoun *et al*., 2009; Groeneveld & Koranteng, 2017; Karlusich *et al*., 2021) as a region that should host N_2 fixation. However, no direct measurements of N_2 fixation have been made in these waters. An attempt to gain some insight into this process was made by calculating the ratio of positive $[NO_3^-]_{diff}$ to positive $[PO_4^-]_{diff}$ (i.e., $[NO_3^-]$]diff : $[PO_4^-]$diff) across all the transects, with values higher than the average ratio of $[NO_3^-]_{back}$ to $[PO_4^-]_{back}$ (see equation 3.4) for the respective transects indicating local additions of nitrate in excess of phosphate, which can be diagnostic for N_2 fixation (Fig. 4.8; Gruber & Sarmiento, 1997). The $[NO_3^-]_{diff}$: $[PO_4^-]_{diff}$ for IO2 (Fig. 4.8 (a)) revealed samples with ratios that were lower and higher than the background average of 13.6:1, which suggests that N_2 fixation may not contribute significantly to the northern Mozambique Channel. The $[NO_3^-]_{diff}$: $[PO_4^-]_{diff}$ in IO4 (Fig. 4.8 (b)) revealed positive excursions above the background average of 12:1, almost exclusively associated with the subtropical samples. The two Agulhas transects were characterised by the highest [NO3-]diff : [PO4-]diff ratios, particularly IO5, where ratios at times exceeded 100:1, with values as high as 240:1 (Fig. 4.8 (c)). While some Tropical waters in IO5 and IO6 coincide with $[NO_3^-]_{diff}$: $[PO_4^-]_{diff}$ in excess of the background average of 11.7:1 (and noting that these samples were not characterized by 100% Tropical waters), the majority of the high $[NO_3^-]_{diff}$: $[PO_4^-]_{diff}$ samples were associated with Subtropical waters, which suggests that the signal is generated in situ (or at least in the South Indian subtropical gyre) and not transported through the channel. Atmospheric deposition can also introduce N:P ratios much higher than those of Redfield (Jickells *et al*., 2017; Altieri *et al*. 2021),

but the magnitude of the deposition flux in the sample region and the limited subsequent water column penetration implies a minor impact of this process on thermocline biogeochemistry (Grand *et al*., 2015).

Both IO5 and IO6 host high ratios of $[NO_3^-]_{diff}$ to $[PO_4^-]_{diff}$ in the upper thermocline. Coincidently, the increase in Tropical source water within the mid-thermocline mentioned in section 5.4.1. occurs within this density range. As these waters are overwhelmingly subtropical with regard to temperature and salinity (IO5 and IO6 columns of Fig. 4.1), the only property that could cause the OMP analysis to allocate them a Tropical source water provenance is a relative increase in silicate, despite the actual source being Subtropical (Fig 4.3 (c-d)). Therefore, a potential explanation for this feature is the remineralization of organic matter with a high N:P ratio as well as elevated biogenic silica (i.e., leading to the production of silicate upon dissolution). Foster *et al*. (2011) (and further discussed more generally by Bonnet *et al*., 2016) observed and measured the rapid transfer of newly-fixed N between open ocean N_2-fixing cyanobacteria and diatoms (phytoplankton that build their shells of biogenic silica). The synergistic existence of these two phytoplankton groups could result in the remineralisation of OM with, in net, a high N:P ratio and high silica. Moreover, diatoms dominate both the inshore regions of the Agulhas Current (Barlow *et al*., 2020) and the cooler subtropical water masses south of the Mozambique Channel (Sa *et al*., 2013), likely because they prefer recently-upwelled waters that are nutrient-rich (Bruland *et al*., 2001). It is thus plausible that diazotroph-diatom coupling in Subtropical waters is (partly) responsible for the feature described in section 5.4.1 that the OMP model attributes to Tropical source waters.

From measurements of nutrient concentrations and nitrate isotopes, Harms et al. (2019) also concluded that N_2 fixation occurs in the South Indian subtropical gyre. Iron and phosphate availability are major limiting factors for N_2 fixation (Berman-Frank *et al*., 2001; Deutsch *et al*., 2007) but neither appear to be limiting across the southwest Indian Ocean (Deutsch *et al*., 2007; Grand *et al*., 2015), supporting the idea that N_2 fixation should be favoured. However, a regional study including direct measurements of N_2 fixation rates would provide more insights into the likelihood and implications of local N_2 fixation.

5.5.2. Mozambique Channel remineralization and possible sedimentary P efflux

Remineralization processes appear to dominate the thermocline biogeochemistry in the southern Mozambique Channel. An average $[NO_3^-]_{diff}$: $[PO_4^{3-}]_{diff}$ of 16-20 between σ_θ = 25.8 kg.m^{-3} and 26.2 kg.m^{-3} was observed for the IO4 transect at the southern end of the Mozambique Channel (Fig. 4.8 (b); Table 4.2), coincident with elevated concentrations of TOU, $[NO_3^-]_{diff,}$ and $[PO_4^-]_{diff}$ (Fig. 4.6 (d-f)). The overlap of these biogeochemical signatures is expected for the remineralization of "typical" marine OM (i.e., with an N:P ratio similar to that of Redfield). That this strong remineralization signal is overprinted on the regional signal of excess P relative to N (i.e., $[NO_3^-]_{diff}$: $[PO_4^-]_{diff}$ ratios <16:1 below σ_θ = 26.5 kg.m^{-3}) attests to the intensity of primary production in the southern channel surface waters, supported by nutrients that may be supplied via eddy-dipole interactions and coastal entrainment (Quartly & Srokosz, 2004; Roberts *et al*., 2014).

Above the remineralization feature in IO4 (< 26 kg.m^{-3}), the $[NO_3^-]_{diff}$: $[PO_4^-]_{diff}$ is lower than the background mean ratio for the transect of 12 ± 1.7 (Fig. 4.8 (b)), indicating a P excess in the upper thermocline that could be related to sedimentary P efflux. Further evidence for this is the fact that the fraction of $[NO_3^-]_{diff}$ is almost double that of $[PO_4^-]_{diff}$ at its peak between σ_θ = 25.8 and 26.2 kg.m^{-3} (approximately 40% versus 20%; Fig. 4.7 (c-d)), suggesting that the background phosphate is stoichiometrically decoupled from the background nitrate concentration. Jorgenson (1983) noted the global importance of coastal margins and shelf sediments in amassing OM produced by phytoplankton, with nutrients (in this case, phosphate) being preferentially retained or released as they are remineralized within the sediments (Boynton & Kemp, 1985). Conditions particular to the channel may promote sedimentary phosphate release - for instance, high rates of OM remineralization on the wide, shallow continental shelf following elevated levels of productivity in the overlying surface waters may lead to sedimentary oxygen depletion, a condition that favours phosphate release (Ingall & Jahnke, 1994). Moreover, the excess P results in N being the limiting nutrient. This condition may stimulate incidences of N_2 fixation in the Mozambique Channel (Deutsch *et al*., 2007), which, while insufficient to yield a strong N excess in the underlying thermocline (i.e., a consistently elevated $[NO_3^-]_{diff}$: $[PO_4^-]_{diff}$ ratio), may be important regionally and would be consistent with reports of diazotrophic phytoplankton proliferating in the channel (Groeneveld & Koranteng, 2017). A supply of excess P from the channel to the downstream

Agulhas Current System may also support N_2 fixation therein (Poulton, 2009).

6. Summary

The objectives of this study were, firstly, to quantitatively describe the water masses of the Mozambique Channel thermocline in terms of their respective source regions and, secondly, to investigate the biogeochemical processes and physical forcings in the surrounding waters. These objectives were achieved by way of the optimum multiparameter (OMP) analysis approach, an inverse linear regression technique used to diagnose the provenance of waters in a particular region and/or depth interval. Here, the *thermocline array* method was applied as it best-suited the stratified nature of the regional thermocline.

The approach was validated by the analysis fully resolving the source waters defined in relation to the general circulation, evidenced by low residuals obtained for all the transects included in this study. This outcome confirms that meaningful results can be attained by using source waters from regions proximate to the sample region, as opposed to from their ultimate formation (i.e., ventilation) regions. A possible exception is the Tropical source water contribution returned by the OMP analysis for the Agulhas transects IO5 and IO6. Here, the temperature and salinity conditions were typical of subtropical waters while the elevated silicate concentrations were not. This combination of input terms appears to have resulted in the (potentially inappropriate) assignment of these water as Tropical in origin.

The thermocline distributions, in terms of source water contributions, were considerably different between the northern and southern ends of the Mozambique Channel. The northern end was characterised by an overwhelmingly large Tropical contribution, highlighting the influence of the *Indonesian Throughflow* (ITF) in the region, while the southern end was predominantly Subtropical, a consequence of inputs from the southern Indian subtropical gyre. The pathways of *Subantarctic Mode Water* (SAMW) flow were also distinguishable by way of the OMP analysis, and the calculation of negative values of [TOU], $[NO_3^-]_{diff}$, and $[PO_4^{3-}]_{diff}$ in the mode water range suggests a "younger" (i.e., higher O_2, lower nutrient) source of SAMW to the southern end of the Mozambique Channel and Agulhas Current System compared to that present in the Subtropical source water region.

The inclusion of Sea Level Anomaly (SLA) data assisted the interpretation of the source water distributions across the various transects. Both anticyclonic (positive anomalies) and cyclonic

(negative anomalies) features coincided with Tropical source water contributions, suggesting that eddies of either form are responsible for the transport of tropical water masses through the Mozambique Channel and into the Agulhas Current System. The observation of Equatorial source water at the lower thermocline boundary across IO4, IO5, and IO6 was interpreted as a *Red Sea Water* (RSW) signal originating in the northern Indian Ocean.

The estimation of $[NO_3^-]_{diff}$: $[PO_4^{3-}]_{diff}$ ratios allowed for the inference of N or P excess across the transects. A remineralization signal across IO4, suggested by the Frac.$[NO_3^-]_{diff}$ distribution, was inferred based on a $[NO_3^-]_{diff}$: $[PO_4^{3-}]_{diff}$ ratio similar to that of Redfield (i.e., 16:1), which is expected for "typical" marine OM (i.e., phytoplankton growth). Furthermore, high $[NO_3^-]_{diff}$: $[PO_4^-]_{diff}$ ratios were estimated across the Agulhas transects of IO5 and IO6, signalling possible N_2 fixation in the region, in line with Gruber & Sarmiento (1997).

In sum, the findings detailed in this thesis improve our existing quantitative understanding of the hydrographical and biogeochemical dynamics of the southwestern Indian Ocean thermocline and demonstrate the utility of the OMP analysis approach in a regional context.

7. References

Anderson, L.A. and Sarmiento, J.L., 1994. Redfield ratios of remineralization determined by nutrient data analysis. *Global biogeochemical cycles*, *8*(1), pp.65-80.

Banse, K., 1987. Seasonality of phytoplankton chlorophyll in the central and northern Arabian Sea. *Deep Sea Research Part A. Oceanographic Research Papers*, *34*(5-6), pp.713-723.

Barlow, R.G., Aiken, J., Holligan, P.M., Cummings, D.G., Maritorena, S. and Hooker, S., 2002. Phytoplankton pigment and absorption characteristics along meridional transects in the Atlantic Ocean. *Deep Sea Research Part I: Oceanographic Research Papers*, *49*(4), pp.637-660.

Barlow, R., Lamont, T., Morris, T., Sessions, H. and Van Den Berg, M., 2014. Adaptation of phytoplankton communities to mesoscale eddies in the Mozambique Channel. *Deep sea research part II: Topical studies in oceanography*, *100*, pp.106-118.

Barlow, R., Lamont, T., Gibberd, M.J., Russo, C., Airs, R., Tutt, G., Britz, K. and van den Berg, M., 2020. Phytoplankton adaptation and absorption properties in an Agulhas Current ecosystem. *Deep Sea Research Part I: Oceanographic Research Papers*, *157*, p.103209.

Batten, S.D. and Crawford, W.R., 2005. The influence of coastal origin eddies on oceanic plankton distributions in the eastern Gulf of Alaska. *Deep Sea Research Part II: Topical Studies in Oceanography*, *52*(7-8), pp.991-1009.

Beal, L.M. and Bryden, H.L., 1999. The velocity and vorticity structure of the Agulhas Current at 32 S. *Journal of Geophysical Research: Oceans*, *104*(C3), pp.5151-5176.

Beal, L.M., Chereskin, T.K., Lenn, Y.D. and Elipot, S., 2006. The sources and mixing characteristics of the Agulhas Current. *Journal of physical oceanography*, *36*(11), pp.2060-2074.

Beal, L.M., De Ruijter, W.P., Biastoch, A. and Zahn, R., 2011. On the role of the Agulhas system in ocean circulation and climate. *Nature*, *472*(7344), pp.429-436.

Bonachela, J.A., Allison, S.D., Martiny, A.C. and Levin, S.A., 2013. A model for variable phytoplankton stoichiometry based on cell protein regulation. *Biogeosciences*, *10*(6), pp.4341-4356.

Broecker, W.S., Peng, T.H., 1982. Tracers in the Sea. *Lamont-Doherty Geological Observatory, Palisades, NY*, pp.690

Bruland, K.W., Rue, E.L. and Smith, G.J., 2001. Iron and macronutrients in California coastal upwelling regimes: Implications for diatom blooms. *Limnology and Oceanography*, *46*(7), pp.1661-1674.

Bryden, H.L. and Beal, L.M., 2001. Role of the Agulhas Current in Indian Ocean circulation and associated heat and freshwater fluxes. *Deep Sea Research Part I: Oceanographic Research Papers*, *48*(8), pp.1821-1845.

Currie, R.I., Fisher, A.E. and Hargreaves, P.M., 1973. Arabian sea upwelling. In *The biology of the Indian Ocean* (pp. 37-52). Springer, Berlin, Heidelberg.

de Ruijter, W.P., Ridderinkhof, H., Lutjeharms, J.R., Schouten, M.W. and Veth, C., 2002. Observations of the flow in the Mozambique Channel. *Geophysical Research Letters*, *29*(10), pp.140-1.

Deutsch, C., Sarmiento, J.L., Sigman, D.M., Gruber, N. and Dunne, J.P., 2007. Spatial coupling of nitrogen inputs and losses in the ocean. *Nature*, *445*(7124), pp.163-167.

DiMarco, S.F., Chapman, P., Nowlin Jr, W.D., Hacker, P., Donohue, K., Luther, M., Johnson, G.C. and Toole, J., 2002. Volume transport and property distributions of the Mozambique Channel. *Deep Sea Research Part II: Topical Studies in Oceanography*, *49*(7-8), pp.1481-1511.

Dilmahamod, A.F., Hermes, J.C. and Reason, C.J.C., 2016. Chlorophyll-a variability in the Seychelles–Chagos Thermocline Ridge: Analysis of a coupled biophysical model. *Journal of Marine Systems*, *154*, pp.220-232.

Donohue, K.A. and Toole, J.M., 2003. A near-synoptic survey of the Southwest Indian Ocean. *Deep Sea Research Part II: Topical Studies in Oceanography*, *50*(12-13), pp.1893-1931.

Emery, W.J. and Meincke, J., 1986. Global water masses-summary and review. *Oceanologica acta*, *9*(4), pp.383-391.

Eppley, R.W. and Peterson, B.J., 1979. Particulate organic matter flux and planktonic new production in the deep ocean. *Nature*, *282*(5740), pp.677-680.

Falkowski, P.G., Barber, R.T. and Smetacek, V., 1998. Biogeochemical controls and feedbacks on ocean primary production. *science*, *281*(5374), pp.200-206.

Ferguson, S.J., Richardson, D.J. and van Spanning, R.J., 2007. Biochemistry and molecular biology of nitrification. In *Biology of the nitrogen cycle* (pp. 209-222). Elsevier.

Field, C.B., Behrenfeld, M.J., Randerson, J.T. and Falkowski, P., 1998. Primary production of the biosphere: integrating terrestrial and oceanic components. *science*, *281*(5374), pp.237-240.

Fine, R.A., 1993. Circulation of Antarctic intermediate water in the South Indian Ocean. *Deep Sea Research Part I: Oceanographic Research Papers*, *40*(10), pp.2021-2042.

Gonçalves-Araujo, R., De Souza, M.S., Mendes, C.R.B., Tavano, V.M., Pollery, R.C. and Garcia, C.A.E., 2012. Brazil-Malvinas confluence: effects of environmental variability on phytoplankton community structure. *Journal of plankton research*, *34*(5), pp.399-415.

Glibert, P.M., Wilkerson, F.P., Dugdale, R.C., Raven, J.A., Dupont, C.L., Leavitt, P.R., Parker, A.E., Burkholder, J.M. and Kana, T.M., 2016. Pluses and minuses of ammonium and nitrate uptake and assimilation by phytoplankton and implications for productivity and community composition, with emphasis on nitrogen-enriched conditions. *Limnology and Oceanography*, *61*(1), pp.165-197.

Glover, D.M., Jenkins, W.J. and Doney, S.C., 2011. *Modeling methods for marine science*. Cambridge University Press.

Gruber, N. and Sarmiento, J.L., 1997. Global patterns of marine nitrogen fixation and denitrification. *Global Biogeochemical Cycles*, *11*(2), pp.235-266.

Gründlingh, M.L., 1985. Features of the circulation in the Mozambique Basin in 1981. *Journal of Marine Research*, *43*(4), pp.779-792.

Gründlingh, M.L., Carter, R.A. and Stanton, R.C., 1991. Circulation and water properties of the

southwest Indian Ocean, Spring 1987. *Progress in Oceanography*, *28*(4), pp.305-342.

Halo, I., Backeberg, B., Penven, P., Ansorge, I., Reason, C. and Ullgren, J.E., 2014. Eddy properties in the Mozambique Channel: A comparison between observations and two numerical ocean circulation models. Deep Sea Research Part II: Topical Studies in Oceanography, 100, pp.38-53.

Hanawa, K. and Talley, L.D., 2001. Mode waters. In *International Geophysics* (Vol. 77, pp. 373-386). Academic Press.

Harms, N.C., Lahajnar, N., Gaye, B., Rixen, T., Dähnke, K., Ankele, M., Schwarz-Schampera, U. and Emeis, K.C., 2019. Nutrient distribution and nitrogen and oxygen isotopic composition of nitrate in water masses of the subtropical southern Indian Ocean. *Biogeosciences*, *16*(13), pp.2715-2732.

Harris, T.F.W., 1972, September. Sources of the Agulhas Current in the spring of 1964. In *Deep Sea Research and Oceanographic Abstracts* (Vol. 19, No. 9, pp. 633-650). Elsevier.

Hupe, A. and Karstensen, J., 2000. Redfield stoichiometry in Arabian Sea subsurface waters. *Global Biogeochemical Cycles*, *14*(1), pp.357-372.

Ingall, E. D. and Jahnke, R. A., 1994. Evidence for enhanced phosphorus regeneration from marine sediments overlain by oxygen depleted waters, *Geochim. Cosmochim. Acta*, *58*, pp.2571–2575

Ito, T., Follows, M.J. and Boyle, E.A., 2004. Is AOU a good measure of respiration in the oceans?. *Geophysical Research Letters*, *31*(17).

Jenkins, W.J., Smethie Jr, W.M., Boyle, E.A. and Cutter, G.A., 2015. Water mass analysis for the US GEOTRACES (GA03) North Atlantic sections. *Deep Sea Research Part II: Topical Studies in Oceanography*, *116*, pp.6-20.

Karstensen, J. and Tomczak, M., 1997. Ventilation processes and water mass ages in the thermocline of the southeast Indian Ocean. *Geophysical Research Letters*, *24*(22), pp.2777-2780.

Karstensen, J. and Quadfasel, D., 2002. Water subducted into the Indian Ocean subtropical gyre.

Deep Sea Research Part II: Topical Studies in Oceanography, *49*(7-8), pp.1441-1457.

Karstensen, J. and Tomczak, M., 1998. Age determination of mixed water masses using CFC and oxygen data. *Journal of Geophysical Research: Oceans*, *103*(C9), pp.18599-18609.

Koch-Larrouy, A., Morrow, R., Penduff, T. and Juza, M., 2010. Origin and mechanism of Subantarctic Mode Water formation and transformation in the Southern Indian Ocean. *Ocean Dynamics*, *60*(3), pp.563-583.

Kolasinski, J., Kaehler, S. and Jaquemet, S., 2012. Distribution and sources of particulate organic matter in a mesoscale eddy dipole in the Mozambique Channel (south-western Indian Ocean): Insight from C and N stable isotopes. *Journal of Marine Systems*, *96*, pp.122-131.

Lamont, T., Barlow, R.G. and Brewin, R.J., 2018. Variations in Remotely-Sensed Phytoplankton Size Structure of a Cyclonic Eddy in the Southwest Indian Ocean. *Remote Sensing*, *10*(7), p.1143.

Ledwell, J.R., Watson, A.J. and Law, C.S., 1993. Evidence for slow mixing across the pycnocline from an open-ocean tracer-release experiment. *Nature*, *364*(6439), pp.701-703.

Luyten, J.R., Pedlosky, J. and Stommel, H., 1983. The ventilated thermocline. *Journal of Physical Oceanography*, *13*(2), pp.292-309.

Mackas, D.L., Denman, K.L. and Bennett, A.F., 1987. Least squares multiple tracer analysis of water mass composition. *Journal of Geophysical Research: Oceans*, *92*(C3), pp.2907-2918.

Mamayev, O., 1975. Temperature-Salinity Analysis of World Ocean Waters. *Elsevier Oceanography Series*, 174 pp.

McCarthy, M.C. and Talley, L.D., 1999. Three-dimensional isoneutral potential vorticity structure in the Indian Ocean. *Journal of Geophysical Research: Oceans*, *104*(C6), pp.13251-13267.

McClain, C.R., Signorini, S.R. and Christian, J.R., 2004. Subtropical gyre variability observed by ocean-color satellites. *Deep Sea Research Part II: Topical Studies in Oceanography*, *51*(1-3), pp.281-301.

McCreary Jr, J.P., Kohler, K.E., Hood, R.R. and Olson, D.B., 1996. A four-component ecosystem

model of biological activity in the Arabian Sea. *Progress in Oceanography*, *37*(3-4), pp.193-240.

McGillicuddy Jr, D.J., 2016. Mechanisms of physical-biological-biogeochemical interaction at the oceanic mesoscale. *Annual Review of Marine Science*, *8*, pp.125-159.

Müller, T.J., Holfort, J., Delahoyde, F. and Williams, R., 1994. Improving NBIS MK IIIB Measurements. *WHP Operations and Methods*.

Naqvi, S.W.A., Naik, H., Pratihary, A., D'souza, W., Narvekar, P.V., Jayakumar, D.A., Devol, A.H., Yoshinari, T. and Saino, T., 2006. Coastal versus open-ocean denitrification in the Arabian Sea. *Biogeosciences*, *3*(4), pp.621-633.

Nauw, J.J., Van Aken, H.M., Webb, A., Lutjeharms, J.R.E. and De Ruijter, W.P.M., 2008. Observations of the southern East Madagascar Current and undercurrent and countercurrent system. *Journal of Geophysical Research: Oceans*, *113*(C8).

Olson, D.B., Hitchcock, G.L., Fine, R.A. and Warren, B.A., 1993. Maintenance of the low-oxygen layer in the central Arabian Sea. *Deep Sea Research Part II: Topical Studies in Oceanography*, *40*(3), pp.673-685.

Peters, B.D., Lam, P.J. and Casciotti, K.L., 2018a. Nitrogen and oxygen isotope measurements of nitrate along the US GEOTRACES Eastern Pacific Zonal Transect (GP16) yield insights into nitrate supply, remineralization, and water mass transport. *Marine Chemistry*, *201*, pp.137-150.

Peters, B.D., Lam, P.J. and Casciotti, K.L., 2018b. Nitrogen and oxygen isotope measurements of nitrate along the US GEOTRACES Eastern Pacific Zonal Transect (GP16) yield insights into nitrate supply, remineralization, and water mass transport. *Marine Chemistry*, *201*, pp.137-150.

Poole, R. and Tomczak, M., 1999. Optimum multiparameter analysis of the water mass structure in the Atlantic Ocean thermocline. *Deep Sea Research Part I: Oceanographic Research Papers*, *46*(11), pp.1895-1921.

Quartly, G.D. and Srokosz, M.A., 2004. Eddies in the southern Mozambique Channel. *Deep Sea Research Part II: Topical Studies in Oceanography*, *51*(1-3), pp.69-83.

Redfield, A.C., Ketchum, B.H. and Richards, F.A., 1963. The influence of organisms on the composition of seawater. *The sea*, *2*, pp.26-77.

Resplandy, L., Vialard, J., Lévy, M., Aumont, O. and Dandonneau, Y., 2009. Seasonal and intraseasonal biogeochemical variability in the thermocline ridge of the southern tropical Indian Ocean. *Journal of Geophysical Research: Oceans*, *114*(C7).

Roberts, M.J., Ternon, J.F. and Morris, T., 2014. Interaction of dipole eddies with the western continental slope of the Mozambique Channel. *Deep Sea Research Part II: Topical Studies in Oceanography*, *100*, pp.54-67.

Roman, R.E. and Lutjeharms, J.R.E., 2007. Red sea intermediate water at the Agulhas current termination. *Deep Sea Research Part I: Oceanographic Research Papers*, *54*(8), pp.1329-1340.

Sarmiento, J. L. and Gruber, N., 2006. Ocean Biogeochemical Dynamics. *Princeton University Press: Princeton, NJ*.

Schott, F.A. and Fischer, J., 2000. Winter monsoon circulation of the northern Arabian Sea and Somali Current. *Journal of Geophysical Research: Oceans*, *105*(C3), pp.6359-6376.

Schott, F.A., Xie, S.P. and McCreary Jr, J.P., 2009. Indian Ocean circulation and climate variability. *Reviews of Geophysics*, *47*(1).

Schouten, M.W., de Ruijter, W.P., Van Leeuwen, P.J. and Lutjeharms, J.R., 2000. Translation, decay and splitting of Agulhas rings in the southeastern Atlantic Ocean. *Journal of Geophysical Research: Oceans*, *105*(C9), pp.21913-21925.

Schouten, M.W., de Ruijter, W.P., Van Leeuwen, P.J. and Ridderinkhof, H., 2003. Eddies and variability in the Mozambique Channel. *Deep Sea Research Part II: Topical Studies in Oceanography*, *50*(12-13), pp.1987-2003.

Sigman, D.M. and Hain, M.P., 2012. The biological productivity of the ocean. *Nature Education Knowledge*, *3*(6), pp.1-16.

Shenoi, S.S.C., Saji, P.K. and Almeida, A.M., 1999. Near-surface circulation and kinetic energy in the tropical Indian Ocean derived from Lagrangian drifters. *Journal of Marine Research*, *57*(6), pp.885-907.

Song, Q., Gordon, A.L. and Visbeck, M., 2004. Spreading of the Indonesian throughflow in the Indian Ocean. *Journal of Physical Oceanography*, *34*(4), pp.772-792.

Stommel, H., 1979. Determination of water mass properties of water pumped down from the Ekman layer to the geostrophic flow below. *Proceedings of the National Academy of Sciences*, *76*(7), pp.3051-3055.

Sverdrup, H.U., Johnson, M.W. and Fleming, R.H., 1942. *The Oceans: Their physics, chemistry, and general biology* (Vol. 1087). New York: Prentice-Hall.

Swallow, J., Fieux, M. and Schott, F., 1988. The boundary currents east and north of Madagascar: 1. Geostrophic currents and transports. *Journal of Geophysical Research: Oceans*, *93*(C5), pp.4951-4962.

Swart, N.C., Lutjeharms, J.R.E., Ridderinkhof, H. and De Ruijter, W.P.M., 2010. Observed characteristics of Mozambique Channel eddies. *Journal of Geophysical Research: Oceans*, *115*(C9).

Takahashi, T., Broecker, W.S. and Langer, S., 1985. Redfield ratio based on chemical data from isopycnal surfaces. *Journal of Geophysical Research: Oceans*, *90*(C4), pp.6907-6924.

Talley, L.D., 2011. *Descriptive physical oceanography: an introduction*. Academic press.

Tew-Kai, E. and Marsac, F., 2009. Patterns of variability of sea surface chlorophyll in the Mozambique Channel: a quantitative approach. *Journal of Marine Systems*, *77*(1-2), pp.77-88.

Tomczak, M., 1981. A multi-parameter extension of temperature/salinity diagram techniques for the analysis of non-isopycnal mixing. *Progress in Oceanography*, *10*(3), pp.147-171.

Tomczak, M. and Large, D.G., 1989. Optimum multiparameter analysis of mixing in the thermocline of the eastern Indian Ocean. *Journal of Geophysical Research: Oceans*, *94*(C11), pp.16141-16149.

Ullgren, J.E., van Aken, H.M., Ridderinkhof, H. and De Ruijter, W.P.M., 2012. The hydrography of the Mozambique Channel from six years of continuous temperature, salinity, and velocity

observations. *Deep Sea Research Part I: Oceanographic Research Papers*, *69*, pp.36-50.

Unesco, 1988. The acquisition, calibration and analysis of CTD data. A report of SCOR Working Group 51. Unesco Technical Papers in Marine Science, 54, 92pp.

Van Aken, H.M., Van Veldhoven, A.K., Veth, C., De Ruijter, W.P.M., Van Leeuwen, P.J., Drijfhout, S.S., Whittle, C.P. and Rouault, M., 2003. Observations of a young Agulhas ring, Astrid, during MARE in March 2000. *Deep Sea Research Part II: Topical Studies in Oceanography*, *50*(1), pp.167-195.

Vianello, P., Ansorge, I.J., Rouault, M. and Ostrowski, M., 2017. Transport and transformation of surface water masses across the Mascarene Plateau during the Northeast Monsoon season. *African Journal of Marine Science*, *39*(4), pp.453-466.

Volk, T. and Hoffert, M.I., 1985. Ocean carbon pumps: Analysis of relative strengths and efficiencies in ocean-driven atmospheric CO2 changes. *The carbon cycle and atmospheric CO2: natural variations Archean to present*, *32*, pp.99-110.

Ward, B.B., Devol, A.H., Rich, J.J., Chang, B.X., Bulow, S.E., Naik, H., Pratihary, A. and Jayakumar, A., 2009. Denitrification as the dominant nitrogen loss process in the Arabian Sea. *Nature*, *461*(7260), pp.78-81.

WOCE, 1994. WOCE Operations Manual, Part 3.1.3., WHP Operations and Methods, WOCE Report 68/91, as revised November 1994.

Williams, R.G., Marshall, J.C. and Spall, M.A., 1995. Does Stommel's mixed layer “demon” work?. *Journal of Physical Oceanography*, *25*(12), pp.3089-3102.

Williams, R.G. and Follows, M.J., 1998. Eddies make ocean deserts bloom. *Nature*, *394*(6690), pp.228-229.

Woods, J.D., 1985. The physics of thermocline ventilation. In *Elsevier oceanography series* (Vol. 40, pp. 543-590). Elsevier.

Wyrtki, K., Bennett, E.B. and Rochford, D.J., 1971. *Oceanographic atlas of the international*

Indian Ocean expedition (Vol. 531). Washington, DC: National Science Foundation.

You, Y. and Tomczak, M., 1993. Thermocline circulation and ventilation in the Indian Ocean derived from water mass analysis. *Deep Sea Research Part I: Oceanographic Research Papers*, *40*(1), pp.13-56.

You, Y., 1997. Seasonal variations of thermocline circulation and ventilation in the Indian Ocean. *Journal of Geophysical Research: Oceans*, *102*(C5), pp.10391-10422.